DESIGN AND DEVELOPMENT OF ELECTROCHEMICAL GAS SENSORS

by

ROBERT YATSHEIN CHAN-HENRY

A thesis submitted to CITY UNIVERSITY, in the Department of Chemistry, in part fulfilment of the requirements for the Degree

of

DOCTOR OF PHILOSOPHY

This investigation was mainly carried out
at CITY TECHNOLOGY LIMITED

December 1992

VOLUME 1

Linking Summary

Volume 1 : Linking Summary
Volume 2 : Carbon Monoxide Sensor Reports

DEDICATION

In memory of my late mother, Mrs Ellen (Neé Leo) CHAN-HENRY, who in her salad days, bravely ventured forth from her native

CANTON

to a strange and distant land called

SOUTH AFRICA

There, in the face of great adversity, she made her mark, raised a family of seven sons, of which I am the youngest, and in her lifetime, was destined never to return home.

Truly a pioneer -
may she rest in peace.

COMMERCIAL IN CONFIDENCE

This thesis is based on proprietary work undertaken at City Technology in collaboration with British Coal and is the subject of several patents. The thesis will therefore be lodged in the Library of City University under restricted circulation and no disclosures may be made without the express, written permission of:

BRITISH COAL CORPORATION
Ashby Road, Stanhope Bretby,
Burton-on-Trent, Staffs. DE15 0QD

Telephone: Burton (0283) 550500
Telegrams: Coalboard Burton
Fax: (0283) 550500 ext. 31118

HEADQUARTERS TECHNICAL DEPARTMENT

and

CITY TECHNOLOGY LIMITED
Walton Road
Portsmouth PO6 1SZ
England

Telephone: 44 705 325-511
Fax: 44 705 386-611

CITY TECHNOLOGY CENTRE

ACKNOWLEDGEMENTS

I should like to express my sincere and grateful thanks to Dr JA Manning - Academic Adviser (City University) and Dr ADS Tantram - External Adviser (City Technology) for their help and support.

I would especially like to acknowledge the intellectual and technical contributions of my colleagues, Dr Tantram and Dr BS Hobbs, throughout all phases of the work undertaken at City Technology.

Thanks are also due to Mr JR Finbow - Managing Director, for granting Company resources and time to compile this thesis.

I also wish to thank British Coal for their part sponsorship under Development contract no. Y135007/09/21; thanks also to the staff of British Coal, for their invaluable advice on requirements for CO monitoring in mines and for their technical cooperation in evaluating prototype sensors, both in the laboratory and in mines.

Finally, I wish to thank Professor ACC Tseung for supervision and for obtaining SERC sponsorship for my research work into CO oxidation on platinum electrodes undertaken in his laboratory at City University.

Last but by no means least, I take this opportunity to thank Miss Lisa Goodbody for the wonderfully cheerful and efficient way she coped with the typing of this thesis, often in adverse circumstances - very professional! My thanks also to Miss Elaine Milne (Millie) for preparing the CAD drawings for Volume 1.

FOREWORD

This thesis is submitted on the basis of reports prepared for the National Coal Board (now British Coal Corporation) over a period of years. The work concentrates on the development of electrochemical sensors for monitoring carbon monoxide. British Coal's prime interest was the use for incipient spontaneous combustion detection with a subsidiary interest in general safety monitoring.

Some reports concerning earlier work on oxygen sensors are relevant to the present work for two reasons: (a) some of the important concepts developed here were used in the carbon monoxide sensor, and (b) City University set up City Technology Ltd, a company which successfully exploited this novel oxygen sensor, thus providing a manufacturing and marketing base through which subsequent products could be developed. Sensors found widening commercial applications in response to urgent needs even during the early development period. A consequence was that a lot of the work was done against the background of field experience, which resulted in a better depiction of the performance requirements and raised various problems which needed urgent solution. This in its turn gave a spur to gaining the best possible fundamental understanding without which progress would have been difficult.

The other applications for carbon monoxide sensors were the subject of separate work, but wherever relevant to British Coal's interests, the findings were included in the reports. Some of the Coal Board reports date back to the early 1970's, which preceded the SI system now adopted by the Scientific Community. Consequently, the linking summary has been compiled using the same nomenclature, in order to facilitate cross referencing to the original reports. A conversion table of all units used in these reports to SI units is included in Appendix 5.

A company profile, a list of publications and a portfolio of patents are included in Appendices 1-4.

CONTENTS

CHAPTER 2 - FUNDAMENTALS AND LITERATURE REVIEW

CHAPTER 3 - SENSOR DESIGN

CHAPTER 4 - SENSOR PERFORMANCE

CHAPTER 5 - CONCLUSIONS AND FURTHER DEVELOPMENT

LIST OF FIGURES

LIST OF TABLES

GLOSSARY OF SYMBOLS

Ar	Activity Reserve
C′	Concentration
E	Electrode Potential
E_C	Cell Output Voltage
$E_{Counter}$	Counter Electrode Potential
E_o	Stardard Electrode Potential
E_{Ref}	Cell Bias Potential
$E°_{REF}$	Reference Electrode Potential
$E_{Sensing}$	Sensing Electrode Potential
F	Faraday = 96494 C mol^{-1}
i_B	Cell Baseline Current
i_L	Cell Limiting Current
k	Proportionality constant
I_C	Cell Current
n	Number of electrons per mole
P	Partial Pressure
R	Universal Gas Constant
R_G	Gain Resistor in Feedback Loop
R_L	Cell Load Resistance
T	Absolute Temperature

GLOSSARY OF ACRONYMS

BCC	British Coal Corporation - formerly National Coal Board (NCB)
BThU	British Thermal Units
CAD	Computer Aided Design
CTL	City Technology Limited
CU	City University - formerly The City University (TCU)
DHE	Dynamic Hydrogen Electrode (*)
DVM	Digital Voltmeter
EMF	Electromotive Force
GDB	Gas Diffusion Barrier
MOD	Ministry of Defence
NCB	National Coal Board - now British Coal Corporation (BCC)
NHE	Normal Hydrogen Electrode (*)
NTP	Normal Temperature and Pressure
OCV	Open Circuit Voltage
ppm	Parts Per Million
PTFE	Polytetrafluoroethylene
RARDE	Royal Armaments Research and Development Establishment
RH	Relative Humidity
SERC	Science and Engineering Research Council
SHE	Standard Hydrogen Electrode (*)
STEL	Short Term Exposure Limit
STP	Standard Temperature and Pressure
SVP	Saturated Vapour Pressure
TCU	The City University - now City University (CU)
TLV	Threshold Limit Value
TWA	Time Weighted Average
USBM	United States Bureau of Mines
wrt	with respect to
WUET	Wolfson Unit for Electrochemical Technology
YRL	Yorkshire Regional Laboratories

Note: (*) see Volume 1, App. 6

GLOSSARY OF TERMS and DEFINITIONS

1. Cross-Referencing

As a result of extensive collaboration with BCC over a number of years (1973-88) developing gas sensors for use in mines, a series of reports have been published. These are listed in chronological order and numbered from 1 to 22 in the series (see Volume 1, App. 3).

If reference is made to sections within Volume 1, the initial number in brackets will denote the volume number, thus:

(1) 2.3 - denotes Volume 1, Chapter 2, Section 3.
(1) Fig. 1 - denotes Volume 1, Figure 2, etc.

Reference to Volume 2 would be similarly annotated, but the Report Number would be included and underlined, thus:

(2) 3 4.5 - denotes Volume 2, Report No. 3, Chapter 4, Section 5.
(2) 3 Table 4 - denotes Volume 2, Report No. 3, Table 4, etc.

2. Sensor

An electrochemical transducer containing at least two electrodes, viz. a sensing electrode with access to the test gas via a diffusion barrier and a counter electrode not in contact with the test gas, which is capable of giving a coherent, galvanic response to an electrochemically active gas.

A third, reference electrode may also be included.

3. Electrode Potential (E)

The potential of an electrode in contact with an electrolyte, measured wrt another electrode in the same electrolyte, or wrt a reference electrode (see (1) App. 6).

4. Open Circuit Voltage (OCV)

The rest potential of the electrode when no external current is being drawn.

5. Over Potential (η)

The displacement from the reversible electrode potential which constitutes the driving force for the reaction to take place.

6. Open Electrode Current (i_{open})

The intrinsic current capability of the electrode, assuming no external diffusion restrictions such as capillary barriers.

7. Capillary Current

The intrinsic current capability of the capillary, assuming no other rate restrictive process ie. 100% capillary control.

8. Sensor Baseline (i_B)

Sensor output current in clean air (ie. in the absence of electrochemically active gas other than O_2).

9. Sensor Output Current (i_C)

Total sensor current in the presence of the electrochemically active gas being measured.

10. Sensor Span Current (i_{span})

$$i_{span} = i_C - i_B$$

11. Sensor Sensitivity ($)

$$\$ = \frac{i_{span}}{\text{gas concentration}}$$ eg. μA ppm^{-1}, nA ppm^{-1}

12. Activity Reserve (Ar)

$$Ar = \frac{i_{open}}{i_{span}}$$

13. i-E Curve

Current-voltage characteristic of an electrode.

14. Three-Electrode Potentiostatic Circuit

A rapid response comparator which is used to set the sensing electrode potential wrt an internal reference electrode, the output of the comparator being linked to the counter electrode of the sensor (see (1) 2.1.1 Fig. 3).

15. Two-Electrode Potentiostatic Circuit

A rapid response comparator which is used to set the sensing electrode potential wrt the counter electrode, the output and the inverting input of the comparator being linked to the counter electrode of the sensor (see (1) 2.1.3 Fig. 4).

16. Load Resistance (R_L)

Resistive element, through which the total sensor current passes, linking the sensing electrode to:

(a) ground (common) in a potentiostatic circuit.
(b) the counter electrode in a 2-electrode sensor not controlled with a potentiostat

17. Self-Powered Sensor

A 2-electrode sensor used as in 16(b) above; the voltage drop across the load resistor constitutes the voltage output signal of the sensor and therefore a control circuit is not necessary (see (1) 2.1.3 Fig. 5).

ABSTRACT

Historically, electrochemical gas sensors had suffered from several drawbacks such as poor temperature coefficient, leakage, susceptibility to shock and vibration and orientation sensitivity, which led to poor field reliability. In the present work these problems have largely been overcome by superior design, drawing on field experience in fuel cell and battery technology.

The culmination of a sensor design embodying a number of unique concepts has revolutionised electrochemical gas sensor analysis and has pioneered the way for many new and hitherto difficult applications. The main features are:

(a) A capillary diffusion-limiting barrier, based on gas-through-gas diffusion, with a theoretical temperature coefficient of 0.17% of signal per °C (at 20°C).

(b) Very active fuel cell-type Pt black electrodes with large activity reserves giving rise to low span temperature coefficients, wide dynamic measurement ranges and enhanced long-term stability.

(c) A close-wick sandwich arrangement of the electrodes conferring very good stability, to the extent that the sensors are substantially immune to shock and orientation problems. The sandwich design also enables the sensors to be very compact.

(d) Use of strong sulphuric acid electrolyte in balance with ambient relative humidity (RH) - about 65% on average in temperate climates - in conjunction with a wick dipping into an expansion reservoir, giving maintenance-free, continuous dynamic range of operation between 20% and 90% RH and very long residence times outside these limits -several weeks in zero RH and several months in 100% RH at 20°C.

(e) Extensive use of porous polytetrafluoroethylene (PTFE) membrane sealing techniques, which have dramatically improved cell integrity to the extent that leakage is virtually eliminated.

(f) Matched sensing and reference electrodes in conjunction with zero bias cell operation, which allows the sensing and reference electrodes to be shorted out when the instrument is switched off; this gives almost instant warm-up when the instrument is switched on and the cell has excellent (NULL) stability under all conditions.

(g) Since the sensor does not need to be powered-up when the instrument is switched off, there is a considerable saving on battery power in portable, hand-held instruments.

(h) Inclusion of a second sensing (auxiliary) electrode, which enables the cancellation of partially reacting cross-interfering gases such as hydrogen. The auxiliary electrode can also substantially offset baselines; this is especially beneficial in biased sensors which generate large baselines.

(i) Use of inboard chemical filters, which can remove cross interfering gases such as NO, NO_2, SO_2, Cl_2, NH_3 and C_2H_4 by chemical reaction/adsorption.

ERRATA

Page xxi	E_o	Standard Electrode Potential
Page xxv	14. . . . . (see (1) 2.1.2 Fig. 3)	
Page 10	n = Number of electrons transferred per **molecule**	
Page 26	Table 1 : $\propto$ is the Transfer Coefficient	
Pages 26, 27	Equs. (20), (22) and (24) refer to 25°C	
Page 35	Fig. 8 Key : r_D should be τ_D	
Page 79	2nd line : electron transfer	

CHAPTER 1 - OVERVIEW

1.1 LINKING SUMMARY STRUCTURE

The thesis is based on a series of 5 annual reports resulting from a joint collaboration between City Technology Limited (CTL) and British Coal Corporation (BCC) to develop an electrochemical trace level CO detector to meet BCC's needs for advanced warning of incipient spontaneous combustion in mines.

Volume 1 constitutes a Linking Summary of the work contained in the reports and Volume 2 is a bound copy of the annual progress reports, from Phase 1 through to Phase 5 of the development.

The Linking Summary is structured to take the reader step by step through the logical progression of designing and developing a trace level CO detector suitable for British Coal's needs. Thus, examination of the technical requirements identifies the design objectives listed in (1) Chapter 1, whereas reviewing the fundamentals and relevant sensor electrochemistry gives one a basic understanding of sensor technology - (1) Chapter 2.

In addition to Volume 1 being a systematic exposition of sensor design, it is also intended to be a summary of the work contained in the annual reports and therefore, where necessary, reference is made to Volume 2 for further detail. Inevitably, reference to the original reports does not always follow the chronological order of development.

1.2 BACKGROUND

Since carbon monoxide is a product of most combustion reactions, it is a wide-spread pollutant. In dense urban areas, the internal combustion engine is the largest single source of carbon monoxide pollution, where levels as high as 30-50ppm are not uncommon. This may be compared with the Threshold Limit Value (TLV) of 50ppm CO and the Short Term Exposure Limit (STEL) of 300 ppm CO[1]. [The TLV is the 8 hour exposure limit and the STEL is the 10 minute exposure limit.]

Carbon monoxide reduces the ability of the bloodstream to carry oxygen to body tissue by displacing oxygen from haemoglobin to form carboxyhaemoglobin. Continuous exposure to ambient air containing 10 ppm carbon monoxide will produce carboxyhaemoglobin levels greater than 2%, the point at which effects upon the nervous system become apparent[2].

In addition to its toxic effects, carbon monoxide is a precursor to incipient spontaneous combustion in coal mines and therefore the accurate measurement of trace levels is of vital importance in the safety of mines. For optimisation of gas, oil or coal burner efficiency and for emission control, it is essential to measure carbon monoxide, in addition to the more customary measurements of oxygen and temperature.

Because of the ubiquitous nature of carbon monoxide, it is imperative to have sensors capable of providing information on the generation and distribution of carbon monoxide in a wide variety of environments.

1.2.1 Technical Requirement

1.2.1.1 British Coal Incipient Combustion Detection

Monitoring carbon monoxide in mines is demanding. Sensors have to cope with adverse environments which have high levels of dust, extreme temperatures, at times as low as 0°C, but frequently about 35°C, accompanied by saturation moisture levels.

General background CO levels can range from 3 ppm to 10 ppm, depending on the local site conditions. Obviously, for the earliest warning of the onset of incipient spontaneous combustion, the ability to measure deviations of 1ppm from normal background is highly desirable.

Sensors require good long-term baseline and span stability as well as low temperature coefficient. It is essential for electrochemical sensors to have low (minimal) baselines, since baselines typically double with every 10°C increase in temperature (see (1) 4.3.1). For

example, an instrument which is calibrated at 20°C and tested at 40°C, using a sensor with a 2 ppm CO equivalent baseline at 20°C, will generate a null error of +6 ppm CO equivalent at 40°C (see (1) 4.4.2).

In general, sensors are required to measure 0-500 ppm CO with a resolution of 1 ppm, whilst being able to tolerate 1000 ppm CO. Mining activities can produce a host of gaseous products, which if the sensor responds to, would give erroneous CO readings and possibly cause false alarms. For example, in-situ battery charging produces hydrogen, and shot blasting and traction diesel equipment produce a host of by-products including NO, NO_2, SO_2 and CO. Incipient spontaneous combustion of coal generates CO as well as a host of unsaturated hydrocarbons such as ethylene. In addition, high levels of hydrogen, up to 1%, occur naturally under some geological conditions, such as in mines in South Africa.

All cross interferences constitute errors in true CO readings and are therefore undesirable. Most cross interfering gases only partially react on the electrode so they are activation controlled rather than diffusion controlled and consequently have high temperature coefficients of the order of 3% of signal per degree centigrade (see (2) 13 4.6).

1.2.1.2 Environmental Monitoring

The general remit for environmental monitoring is much wider than for spontaneous combustion detection in mines; temperatures can range from -40°C to +50°C and there is a much larger range of possible cross interfering gases. The usual requirement is to provide an alarm at the TLV of 50ppm so that the resolution needed is much less than for the mining application and therefore the signal to noise ratio as well as the signal to baseline ratio is much more favourable.

1.2.1.3 Flue Gas Analysis

Market forces based on increased awareness of environmental pollution and safety and efficiency[3] have provided the incentive for the development of low-cost, rugged and portable gas sensors for flue gas analysis.

Measurement of CO is needed for three purposes:

(1) To check that the appliance is safe.
(2) To check that the emissions are below the statutory requirement.
(3) To achieve the best possible fuel efficiency.

Combustion efficiency varies with stoichiometric air/fuel ratio, as shown in (1) Fig. 1.

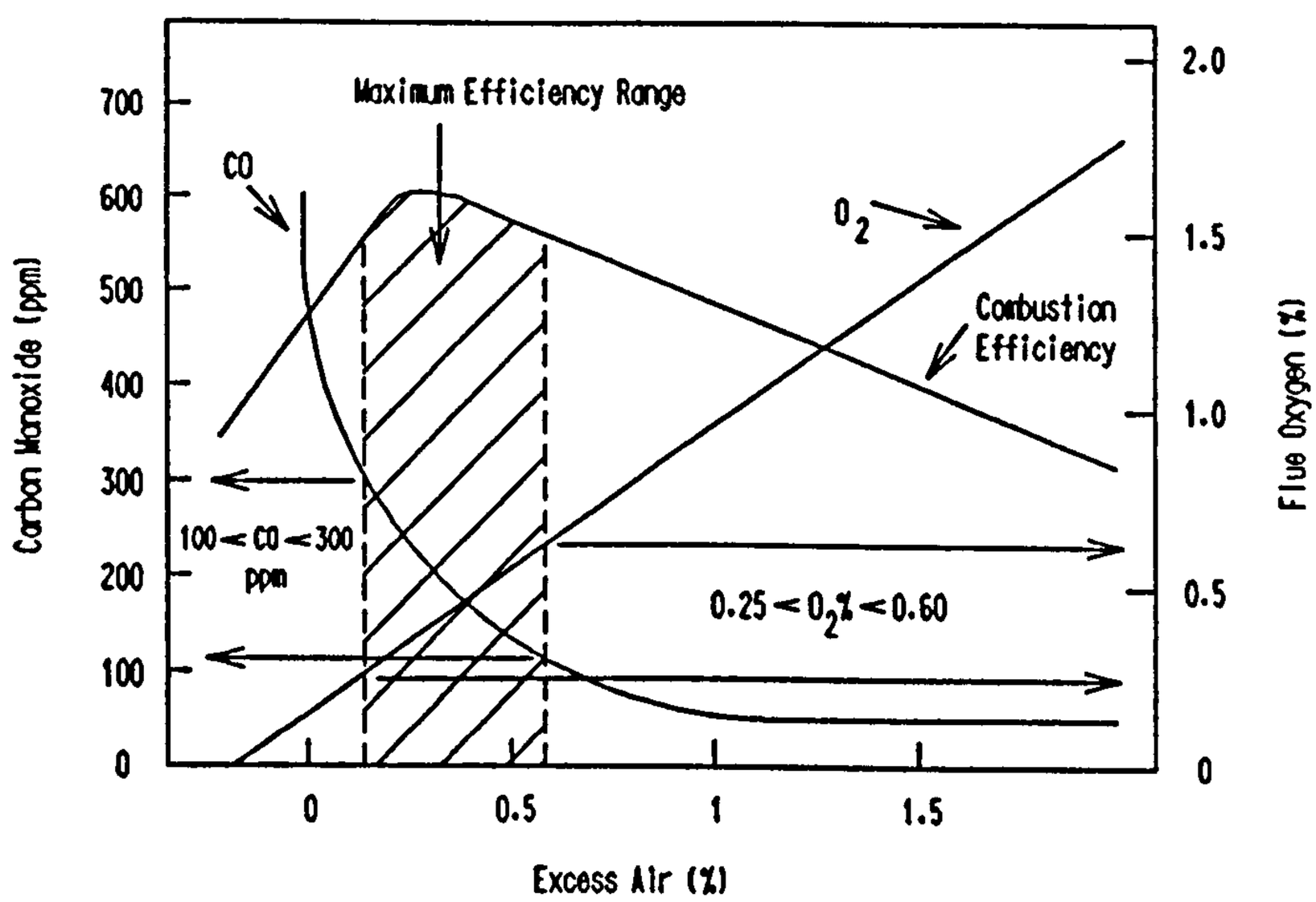

Figure 1 Variation of combustion efficiency with stoichiometric air/fuel ratio. Fuel = Natural gas [After Dalla Betta and Bynum (1989) Sensors 27]

At low excess air levels, incomplete combustion lowers efficiency, while at high air/fuel ratios, energy is wasted by heating air unnecessarily[4]. In theory, optimum combustion efficiency can be achieved by monitoring either oxygen or carbon monoxide and controlling the air/fuel ratio. In reality, neither of these components alone provides the optimal signal for easy control of combustion process efficiency. The O_2 concentration in the flue gas stream is influenced by a number of factors[5], including fuel type and British Thermal Units (BThU) value, combustion process load factor, air by-passing the combustion zone, and air leaks downstream of the combustion process but upstream of the analyzer system. To use oxygen-only analyzers for combustion control, the boiler system must be 'characterized' with portable instruments measuring both O_2 and CO at several air/fuel ratios over the entire combustion process load range[6]. This information is then used to generate a relationship expressing optimum O_2 concentration vs. boiler load for use by the combustion control system. Such a system requires a significant setup and installation cost.

Carbon monoxide concentration can be used to control air/fuel ratio, but it has several important drawbacks. The CO signal tends to vary greatly - for example, changes in boiler load cause wide swings in the CO level, necessitating the use of preprogrammed air and fuel settings until steady-state operation is obtained and CO concentration-driven control can be re-instituted. The ideal combustion control system must therefore provide both CO and O_2 concentration measurements, which must be used to control the air/fuel ratio. There are, in fact, several control strategies that use both measurements.

The first strategy uses CO measurement to offset the actual O_2 set point from the theoretical. The air/fuel ratio is continuously adjusted, based on the difference between measured O_2 concentration and the O_2 set point value; simultaneously, actual CO is measured and the average CO concentration over a timed interval is compared to the desired CO level. When this CO average deviates significantly from the desired level the O_2 set point is readjusted.

The alternative strategy uses CO as a trim control on top of primary O_2 control. When a boiler load change occurs, the O_2 sensor alone is used for adjustment of the air/fuel ratio until a new stable operating setting is reached. Typically, the controller is adjusted to make this initial condition one with slight excess air. When the process has again stabilized, the controller switches to CO control and fine tunes the settings by reducing the air/fuel ratio until CO rises to its set point range.

With the advent of microcomputers, numerous other control strategies have become possible. It is now possible to use a running CO average for primary control and look-up tables for dynamic conditions when the load is changed or process upsets occur. Look-up tables can be generated by the control system during the first weeks of operation when the combustion system is tuned and operating properly. A microprocessor-based system can also provide safety over-ride functions based on out-of-range CO and O_2 concentrations and can give diagnostic warnings of process malfunctions (e.g. when a dirty burner causes poor mixing of air and fuel and leads to high CO levels in the presence of adequate excess air). Furthermore, intelligent microprocessor-based systems can be self-teaching, identifying a 'proper operation window' in a specified time period after the process has been tuned. Diagnostic warnings can be given when the O_2 and

CO process variables stray into combinations indicative of malfunctions.

It is evident from such applications that the region of interest for boiler tuning is the range 0-1000ppm CO - see (1) Fig. 1. However, once the stoichiometric excess air ratio drops below zero, the CO concentration rises exponentially and concentrations as high as 200,000ppm CO can often be encountered in an out-of-tune flue. It is therefore essential that CO sensors for flue gas analysis are at least able to tolerate such high levels of CO, so that when the burner is re-tuned, the sensor can recover with little hysteresis to give an accurate reading round the maximum efficiency point i.e. <600ppm CO.

Low cross-interference is also of importance, because high levels of hydrogen are often found in flue gas, sometimes in the ratio 1:4 with CO. Nitric oxide can be very high - up to 1000ppm and coal-burning installations can generate up to 4000ppm SO_2 in sulphur-rich coal. Unrefined oil can also generate similar levels of SO_2.

In practice the flue gas sample is cooled before reaching the sensor, but good temperature stability is of importance, as temperatures can range from sub-zero temperature to +55°, depending on site conditions.

Since a wide dynamic range of measurement is required (10-200,000ppm CO) the sensitivity has to be low to achieve the required tolerance at high levels. This in turn puts pressure on keeping the baseline current as low as possible so that the ppm CO equivalent baseline does not shift too much with temperature.

1.3 DESIGN OBJECTIVES FOR INCIPIENT COMBUSTION DETECTOR

As a result of close collaboration with British Coal over a period of years to develop a suitable Carbon Monoxide sensor to give advanced warning of incipient spontaneous combustion in mines, the final design brief was set out as follows:

1.3.1 Service Life

Minimum of one year, preferably more than two years.

1.3.2 Temperature Range

Overall accuracy maintained within ±10% of signal over the range 0-40°C.

1.3.3 Calibration Frequency

Recalibration once every 6 months is desirable, but once every 3 months is acceptable, although there is a statutory need to check equipment fortnightly and in some applications weekly.

1.3.4 Attitude Stability

On inverting the sensor, baseline movement not more than 2ppm, preferably less than ±1ppm.

1.3.5 Shock and Vibration Sensitivity

Transient signals due to shock and vibration should not trigger the TLV alarm and in the steady-state the overall accuracy of ±10% of reading should be maintained.

1.3.6 Linear Measuring Range

The sensor output should be linear. The upper range of measurement should preferably be 500ppm CO, but an upper limit of 200ppm CO would be acceptable, if necessary.

1.3.7 Response Time

The 90% response time, measured across a load resistance of 50Ω, should be less than 40 seconds.

1.3.8 Carbon Monoxide Tolerance

On subjecting the sensor to 200ppm CO for 20 minutes, the baseline hysteresis should be less than ±2ppm CO equivalent after 5 minutes recovery in clean air.

1.3.9 Moisture Tolerance

The sensor should be able to function continuously in the relative humidity (RH) range 20% to 90% and be able to tolerate periodic excursions to 100% RH (non-condensing) intermittently.

1.3.10 Cross Interference

Cross interference should be as small as possible, preferably less than 1%, from other gases arising from various processes in mines such as:

(a) Spontaneous Combustion	-	ethylene and other unburnt hydrocarbons.
(b) Diesel traction equipment and shot blasting	-	NO, NO_2 and SO_2.
(c) Battery re-charging	-	H_2.

CHAPTER 2 - FUNDAMENTALS and LITERATURE REVIEW

2.1 ELECTROCHEMICAL GAS SENSOR FUNDAMENTALS

There are two generic methods of operating electrochemical sensors, one is POTENTIOMETRIC in which the open circuit potential of the sensing electrode, measured with respect to (wrt) an internal reference electrode, is used as the sensor signal and the other method is AMPEROMETRIC, in which the current generated on the sensing electrode, is used as the sensor signal.

Potentiometric sensors rely on the voltage response generated by the Nernstian relationship between electrode potential and gas concentration, namely:

$$\textbf{Reactants} \rightleftharpoons \textbf{Products}$$

$$\text{Thus : } E = E_o - \frac{RT}{nF} \ln \frac{[\text{Products}]}{[\text{Reactants}]} \qquad \ldots . (1)$$

where E = Electrode Potential

E_o = Standard Electrode Potential

R = Universal Gas Constant

T = Absolute Temperature

n = Number of electrons transferred per Mole

F = Faraday = 96494 C mol^{-1}

Thus, the potentiometric method measures the thermodynamic activity of a substance by relating the potential it creates at an electrode to the theoretical, thermodynamically-determined potential. The relationship between concentration and potential is logarithmic and this technique is more useful for measuring orders of magnitude than smaller changes in concentration. Further, the chemical species to be measured must exhibit 'reversible' behaviour, a characteristic of many ionic reactions but not of gases (except H_2). Gases such as CO, H_2S, O_2 do not exhibit 'reversible' electrode potentials at ambient temperature and their concentrations must be measured by amperometric methods.

The amperometric method, measuring current, measures the rate at which a species releases (oxidation) or consumes (reduction) electrons at an electrode. If the number of electrons exchanged per molecule is known, then the rate of oxidation or reduction can be calculated, eg.

$$CO + H_2O \rightarrow CO_2 + 2H^+ + 2e^- \quad \ldots . (2)$$

$$O_2 + 4H^+ + 4e^- \rightarrow 2H_2O \quad \ldots . (3)$$

$$H_2S + 4H_2O \rightarrow H_2SO_4 + 8H^+ + 8e^- \quad \ldots . (4)$$

Thus a molecule of H_2S will release 8 electrons, compared with 2 electrons from CO. If the molar concentrations are the same, then H_2S generates four times as much current as CO, assuming the electrode process is not reaction-rate limited.

The biggest advantage of amperometric sensors is the direct link between current and gas concentration expressed by Faraday's Laws of electrolytic conduction, which state[7]:

(1) In any electrolytic process the amount of chemical reaction is proportional to the quantity of electricity passed through the electrolytic conductor.

(2) The masses of different substances deposited or dissolved by the same quantity of electricity are in the proportions of their chemical equivalents.

In ideal cases these laws are exact, although this fact may be obscured in certain cells by the occurrence of side reactions.

With reference to electrochemical gas sensors, Faraday's Laws may be simply stated: "One gram - equivalent weight of gas at NTP will yield 96494 coulombs of charge".

2.1.1 Diffusion Limiting Principle

A suitable electrode in a cell can be activated by applying an anodic overpotential so that the reactant gas diffusing into the cell is fully oxidised.

Such a cell is converted to a sensor by the inclusion of the diffusion barrier at the sensing electrode[8]. The nature of this barrier is fundamentally important to the operation of the sensor and is designed to restrict access of the reactant gas so severely that it becomes completely oxidized as it arrives at the sensing electrode. Under these conditions the concentration of reacting gas at the sensing electrode approaches zero and the current becomes limited solely by the rate of gas diffusion through the barrier. The sensing-electrode is then under mass transfer control and a limiting current is observed (see (1) Fig. 2).

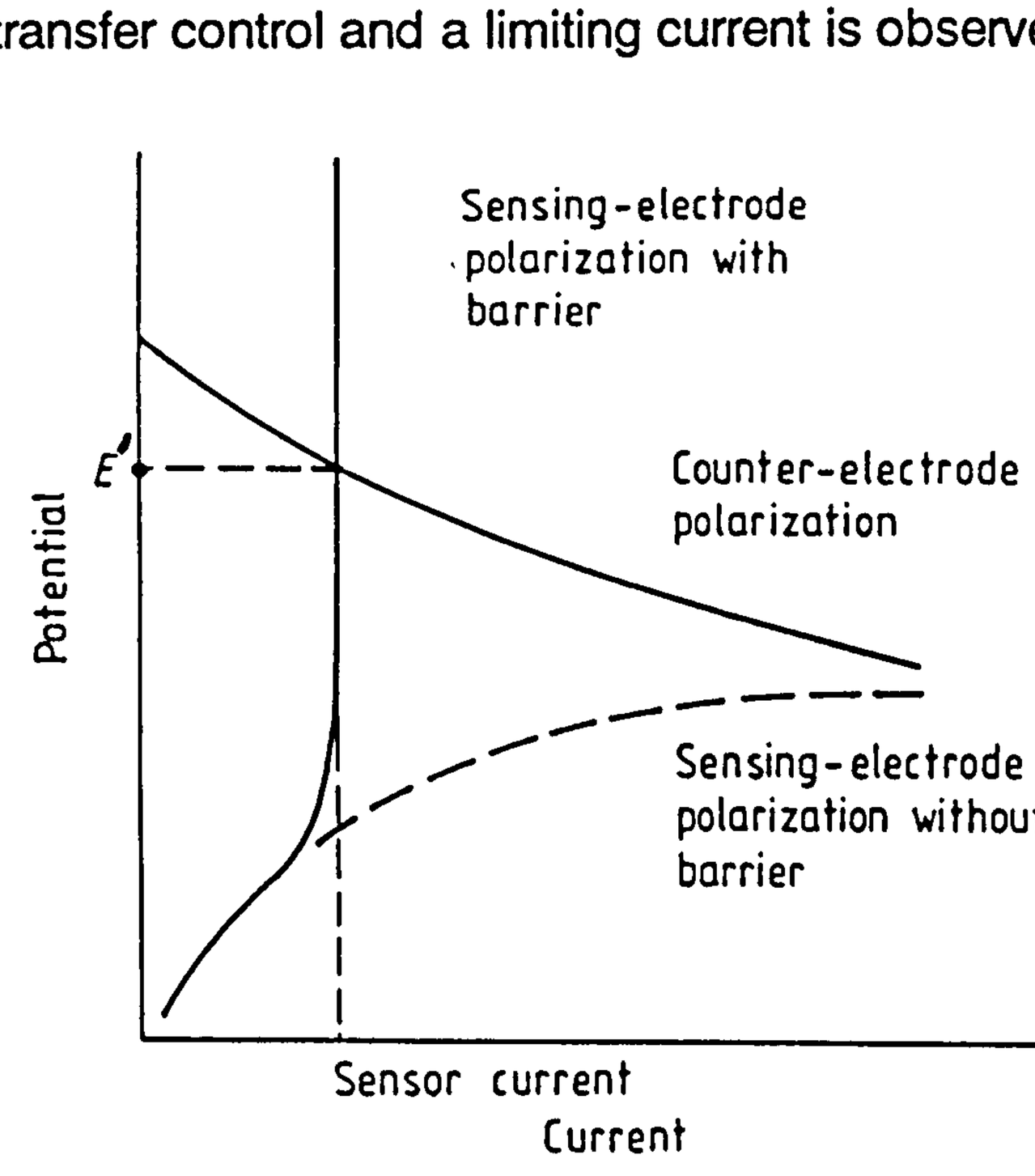

Figure 2 Schematic *I-E* polarisation characteristics for a two-electrode gas sensor. E' is the operating potential. [After Hobbs BS et al (1990) Liquid Electrolyte Fuel Cells (Adam Hilger : New York)]

The limiting current may be derived as follows:
According to Fick's first law[9], the diffusion flux of reactant gas through the barrier is directly proportional to its concentration gradient across the barrier:

$$\textbf{reactant flux} \propto C'_1 - C'_2$$

where C'_1 and C'_2 are the concentrations of reactant on the ambient air and cell sides of the barrier respectively.

However, since C'_2 approaches zero in the limiting-current condition (ie. all reactant oxidised as it arrives at the electrode), then:

$$\textbf{reactant flux} \propto C'_1$$

Also, from Faraday's law, the cell limiting current i_L is directly proportional to the diffusion flux of reactant:

$$\textbf{reactant flux (mol s}^{-1}\textbf{)} = \frac{i_L}{nF} = \textbf{constant x } C'_1$$

where i_L (A) is the cell limiting current, n is the number of electrons transferred per mole, F (= 96494 C mol^{-1}) is the Faraday, and the constant is the diffusion barrier *diffusibility* (cm^3 s^{-1}). Thus,

$$i_L = kC'_1 \qquad \ldots . (5)$$

where C'_1 (mol cm^{-3}) is the ambient concentration of reactant gas and k is a proportionality constant. There exists then a direct relationship between the reactant concentration and the sensor limiting current which constitutes the signal from the sensor.

In general, this principle may be applied to measure any gaseous substance which can be made to react electrochemically at a suitable electrode.

2.1.2 Three-Electrode Principle

The classic amperometric sensor comprises three electrodes, namely a sensing, a reference and a counter electrode. The sensor is controlled by an operational amplifier used in the so-called 'potentiostatic' mode[10] (see also (2) 13 Fig. 6.3), in which the sensing electrode potential is controlled against a stable reference electrode which draws negligible current.

The sensor is 'driven' by configuring the amplifier as a comparator, in which the sensing electrode is tied to the non-inverting input, the reference electrode to the inverting input and the counter electrode to the amplifier output (see (1) Fig. 3).

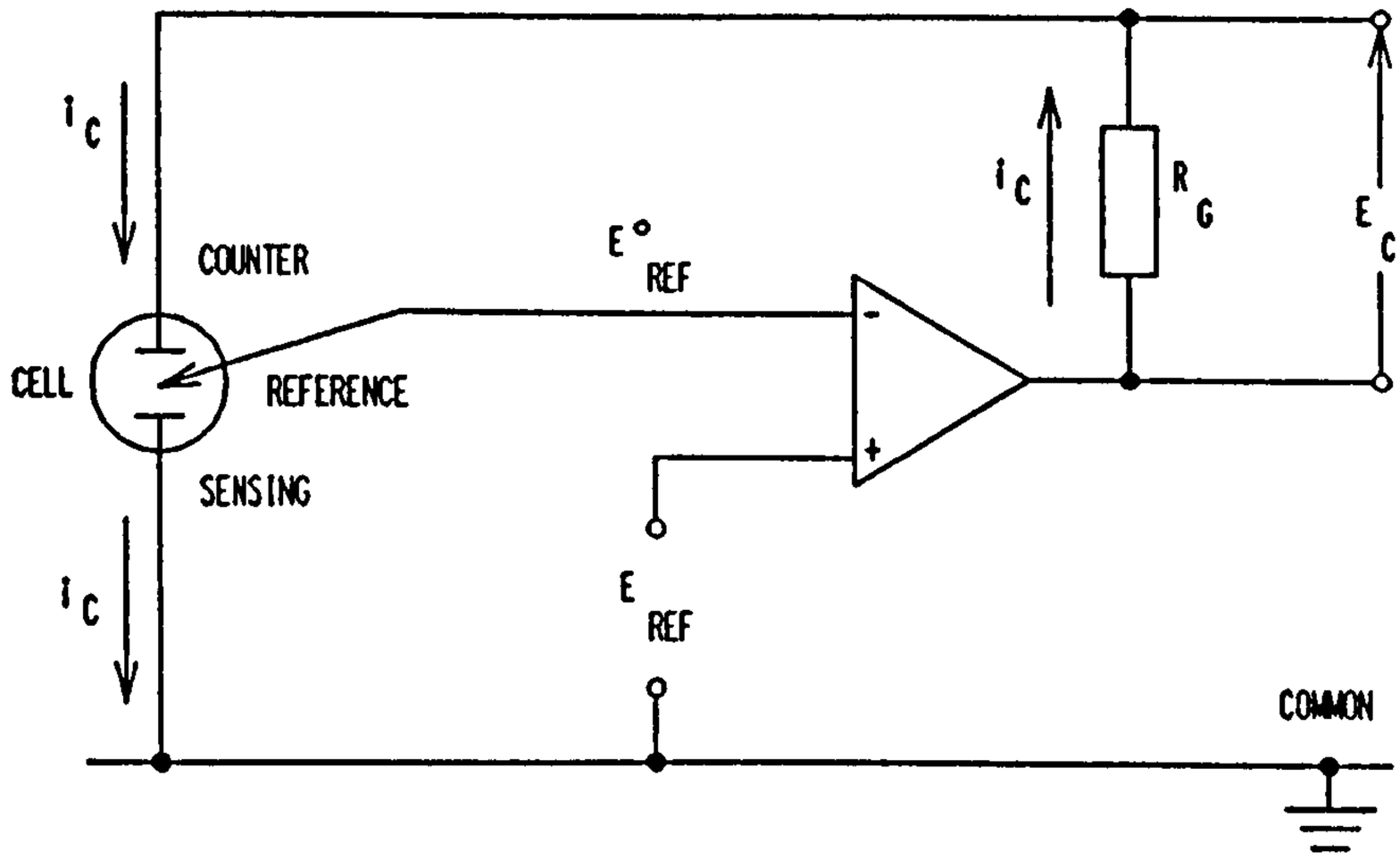

Figure 3 Potentiostatic control circuit for three-electrode sensors

The function of each electrode is best explained using CO detection as a model:

(a) Sensing Electrode - at which CO is electrochemically oxidised to CO_2 according to (1) Equ. (2).

The electrode is maintained at a fixed potential at which neither the electro-reduction of oxygen (cathodic process) nor the electro-oxidation of water (anodic process) occurs at a significant rate. Under these conditions, the CO introduced is oxidized causing a current to flow. The current is proportional to the partial pressure of carbon monoxide in the gas sample since it is limited at the electrode by a diffusion barrier (see (1) 2.2.1).

(b) Reference Electrode - to all intents and purposes, this electrode virtually operates at open circuit voltage (OCV), as no appreciable current is drawn from it because of the high input impedance of the amplifier. The operational amplifier is used as a comparator which acts to null the potential difference between the inverting input (sensing electrode) and the non-inverting input (reference electrode) by alternating the output potential (counter electrode) either positive or negative as required, thus forcing the sensing electrode to follow the reference electrode potential (see (1) Fig. 3).

(c) Counter Electrode - this electrode serves to balance the redox processes within the cell; for example, if CO is OXIDISED at the sensing electrode (see (1) Equ. (1)) then a REDUCTION reaction must be provided at the counter electrode. This can for example be O_2 reduction and then the electrode reactions are:

Sensing = $CO + H_2O \rightarrow CO_2 + 2H^+ + 2e^-$ **Equ. (2)**

Counter = $\frac{1}{2}O_2 + 2H^+ + 2e^- \rightarrow H_2O$ **. . . . (6)**

Net Cell Reaction: $CO + \frac{1}{2}O_2 \rightarrow CO_2 \uparrow$ **. . . . (7)**

and $E_c = I_C R_G$ **. . . . (8)**

Note: The sensing electrode may be controlled at different potentials with respect to the reference (E°_{Ref}) by setting E_{Ref}, in which case

$$E_{sensing} = E^\circ_{Ref} - E_{Ref} \quad \text{. . . . (9)}$$

Other examples of sensing electrode reactions involving electrochemical *oxidation* of the reactant gas are as follows:

hydrogen sulphide $H_2S + 4H_2O \rightarrow H_2SO_4 + 8H^+ + 8e^-$ **Equ. (4)**

sulphur dioxide $SO_2 + 2H_2O \rightarrow H_2SO_4 + 2H^+ + 2e^-$ **. . . (10)**

nitric oxide $NO + H_2O \rightarrow NO_2 + 2H^+ + 2e^-$ **. . . . (11)**

In these cases the normal counter electrode reaction would be oxygen reduction (see (1) Equ. (3)).

Electrochemical *reduction* of a reactant at the sensing electrode can also be applied in gas sensors. Examples are:

chlorine $Cl_2 + 2H^+ + 2e^- \rightarrow 2HCl$ **. . . . (12)**

nitrogen dioxide $NO_2 + 2H^+ + 2e^- \rightarrow NO + H_2O$ **. . . . (13)**

oxygen $O_2 + 4H^+ + 4e^- \rightarrow 2H_2O$ **Equ. (3)**

In these cases an electrochemical oxidation reaction must occur at the counter electrode eg. oxygen evolution:

$$2H_2O \rightarrow O_2 + 4H^+ + 4e^- \quad \ldots\ldots (14)$$

2.1.3 Two-Electrode Principle

The classic 3-electrode circuit may be converted to 2-electrode form by simply shorting the reference and counter electrodes (see (1) Fig. 4).

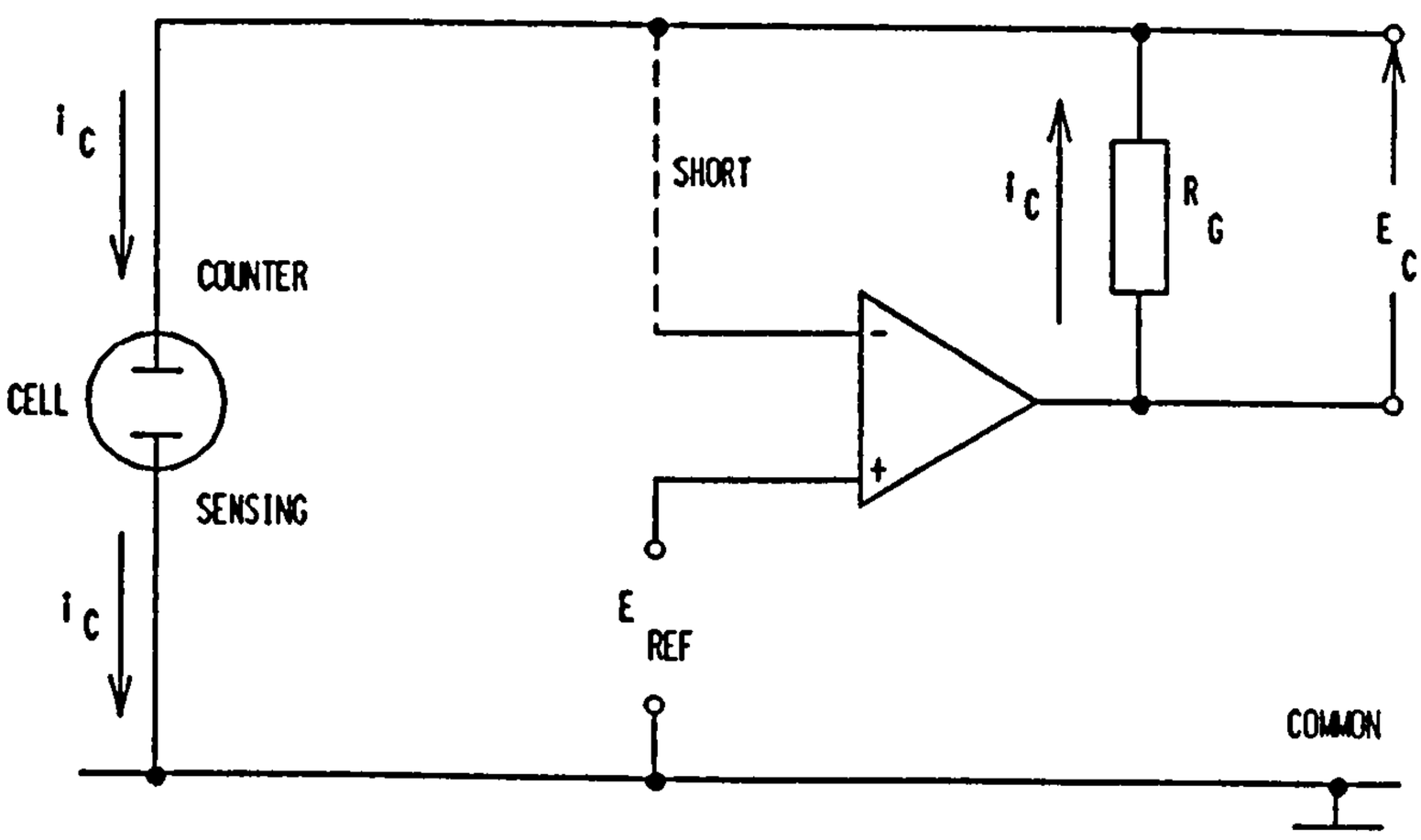

Figure 4 Potentiostatic control circuit for two-electrode sensors

In this configuration the counter electrode also serves as reference electrode (see (2) 13 6.1).

If no bias is required (E_{Ref} = 0), then the sensor can be converted to 'self-powered' mode by dispensing with the amplifier and simply using a passive load resistance R_L between sensing and counter electrodes (see (1) Fig. 5).

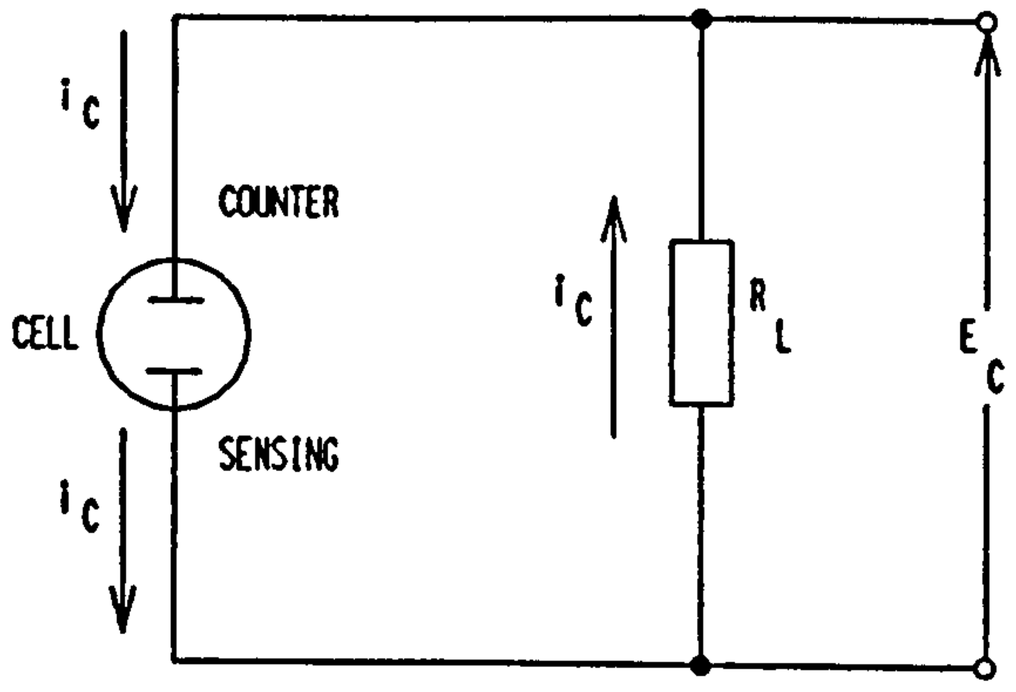

Figure 5 Two-electrode sensor with load resistor R_L

$$E_{sensing} = E_{counter} - I_C R_L \qquad \ldots\ldots (15)$$

and the cell output is given by

$$E_c = I_C R_L \qquad \ldots\ldots (16)$$

Ideally, the sensing electrode should be highly polarizable, so that it follows the potential of the counter electrode. Conversely, the counter electrode should be highly non-polarizable, so that its potential is stable under load.

2.2 ELECTROCHEMICAL GAS SENSOR REVIEW

A wide range of gas concentrations may be measured using electrochemical gas sensors. Thus commercially available systems are used to monitor near 100% oxygen in medical and gas purity applications, to around 20% for general air quality and hypoxia warning systems, a few per cent in flue gas analysis and down to a few parts per million in some process control and gas purity applications; toxic gases can be measured in the range from around 20% down to a few tenths of a part per million, the lower limit being determined by baseline (zero-gas output) and cross-interference effects.

Electrochemical sensors do not suffer from the humidity effects which are a problem with many semiconductor and solid state devices. Although cross-interferences can pose problems, as with any chemical sensor, electrochemical sensors can achieve high specificity when suitably designed and operated.

An additional advantage is that, operating on fuel cell and battery principles, they can also be constructed using well-established engineering methods to produce small compact devices with a high degree of robustness and reliability, freedom from orientation effects, intrinsically low cost and suitable for volume production. Such sensors can operate in an ambient temperature range from about -50 to +55°C without the need for external heating and therefore their power requirements are extremely low; some designs are available which are completely self-powered (see (1) 2.1.3), additional power only being required for extra-sensor functions such as alarms, recording and data transmission.

Fuel cell sensors in theory have unlimited life, but in practice, various degradation processes may occur such as attack of the seals by the acid electrolyte, loss of catalyst surface area (and hence activity) through poisoning, and solution-recrystallization reactions. These processes are generally very slow and lives of several years are typical in normal temperate environments. High temperatures, extremes of humidity and the presence of high concentrations of strongly adsorbing chemical species can reduce the working life of these sensors.

2.2.1 Commercially Available Three-Electrode CO Sensors

At the start of this work, a survey revealed that commercially available CO sensors generally used platinum electrodes contacting sulphuric acid electrolyte.

The CO sensor manufactured and marketed by Energetic Science[11-15] exemplified the early three-electrode design approach, based on an all-platinum electrode system. The electrodes were of the 'fuel cell' type[16-17] using finely divided Pt mixed with PTFE powder and bonded to porous PTFE membrane material.

The cell comprised a sensing electrode and a split reference/counter electrode, one half serving as the counter electrode and the other half as the reference electrode. Since the electrodes were made from finely divided Pt contacting sulphuric acid electrolyte, the OCV of the electrodes in clean air was of the order of 1050mV vs. the Dynamic Hydrogen Electrode[18](DHE).

The sensing electrode was biased to the reversible potential for oxygen reduction (~1250mV vs. DHE) to avoid cathodic oxygen interference on the sensing electrode and to minimise H_2 cross-interference (<1%). Carbon monoxide was aspirated through the sensing electrode compartment where it was oxidised to CO_2 (see (1) Equ. (2)) and oxygen reduction took place on the counter electrode (see (1) Equ. (3)) to complete the cell reaction.

Output sensitivity was high since the sensor did not contain an external diffusion barrier, the current being limited only by the electrolyte film in the electrode. This eased signal processing since the signal/noise ratio was good, but contributed to the following problems:

- output electrolyte film-limited (see (1) 3.3) and hence large temperature coefficient (~3% signal per °C). This required thermistor compensation of the span signal[15].

- high CO consumption rate required flow rates in excess of a litre per minute to stabilise the output and this consumed a lot of power.

- in-line chemical filters rapidly consumed and back-pressure build-up in the sampling system aggravated.

- water transfer rates enormously accelerated, especially since dilute electrolyte was used in order to improve electrode activity. This necessitated frequent topping up with distilled water, especially under low RH conditions.

Running the sensor at high anodic bias also created other problems:

- increased the sensitivity to hydrocarbon gases such as ethylene and propylene.

- caused large standing currents (~10μA) in the absence of CO - at a sensitivity of 1μA/ppm ≡ 10ppm CO baseline[19]. Since such baselines arise out of activated processes, baselines roughly double for every 10°C rise in temperature (see (1) 4.3.1), leading to baseline shifts of 40ppm CO equivalent 0-40°C. Thermistors were used to temperature compensate baselines, but bad location of the thermistor often resulted in appreciable mismatching as well as causing severe thermal lag and complex circuitry was needed to compensate baselines accurately.

- the primary control stage had to be permanently powered, otherwise a considerable warm-up time was required for baselines to settle.

Because of these drawbacks, these cells tended to be cumbersome, bulky and suffered tremendous orientation problems. Bad sealing caused extremely unreliable performance, which tainted the image of past electrochemical sensors.

2.2.2 Commercially Available Two-Electrode CO Sensors

The INTERSCAN range of sensors were based on a precious metal sensing electrode coupled to a lead dioxide counter electrode. These electrodes were housed in a large canister, with the intervening space bridged by an infill of glass wool and wetted with sulphuric acid electrolyte[20].

Since the counter electrode potential of 1500mV was high enough to evolve oxygen on the Pt sensing electrode, a cathodic bias of about 250mV was applied to control the sensing electrode at 1250mV vs. DHE to avoid interference from O_2 evolution.

The INTERSCAN sensor suffered most of the disadvantages of the Energetic Science sensor (see (1) 2.2.1) and in addition, the counter electrode further suffered from:

(1) Finite capacity of the counter electrode

Discharge reaction:

$$PbO_2 + SO^{2}_{4}{}^{-} + 4H^{+} + 2e^{-} \rightarrow PbSO_4 + 2H_2O \quad \ldots . (17)$$

(2) Self-discharge and therefore limited shelf life.

A Pt wire current collector was used on the counter electrode and the oxygen evolution overpotential on the Pt surface was sufficiently low to evolve oxygen at a small but finite rate.

Self-discharge reaction on Pt:

$$H_2O \rightarrow 2H^{+} + 2e^{-} + \tfrac{1}{2}\, O_2\uparrow \quad \ldots . (18)$$

Since self-discharge is an activated process, the rate of reaction roughly doubled per decade increase in temperature, thus limiting the service life of the sensor even further.

2.3 ELECTROCHEMISTRY REVIEW

The review of commercially available electrochemical CO sensors revealed that platinum is the only catalyst with sufficient activity to completely oxidise CO to CO_2 in acid electrolyte.

Trace level sensors are required to measure low ppm concentrations of CO in the presence of very high concentrations of oxygen (209,000ppm O_2) in ambient air. Since platinum is a polyfunctional electro-catalyst which promotes not only CO oxidation[21], but oxygen reduction[22] as well, it is remarkable that trace levels of CO can be measured without significant cross interference from oxygen. That

it can, depends, serendipitously, on there being a window of potential with a platinum electrode where oxygen reactivity is effectively zero, but CO reactivity is high.

To understand the fundamentals involved and the practical consequences that follow, one needs to look at the electrochemistry of platinum, oxygen, carbon monoxide and the intimate co-relations between them.

The logical steps determining the design of the sensor may be set out as follows:

(a) The first essential consideration is NO OXYGEN INTERFERENCE -must operate in dead region (see (1) 2.3.1) 1000-1500mV vs. DHE.

(b) In this region, platinum is partially covered with oxide (see (1)2.3.2.3). The amount of coverage increases with potential so the platinum is faradaically active. Increase in potential will produce an anodic current and a decrease in potential, a cathodic current.

(c) The above factors dictate that CO has to be oxidised on a platinum surface partially covered with oxide at potentials 1000-1500mV vs DHE. Serendipitously, these are the best conditions, since:

- bare Pt is poisoned by CO because it adsorbs strongly with high coverage. However, Gilman's Reactant Pair Mechanism for CO oxidation (see (1) 2.3.3) requires bare Pt sites which adsorb CO and adjacent platinum oxide sites to adsorb water molecules, thereby forming an activated complex which facilitates electron transfer and promotes CO oxidation.

- the requirement to operate between 1000-1500mV vs. DHE results in a high over voltage for CO oxidation, since the CO rest potential, relative to a hydrogen electrode in the same electrolyte, is given by:

$$E = -0.103 + 0.0295 \log \frac{P_{CO_2}}{P_{CO}} \quad \ldots\ldots (19)$$

Where P_{CO_2} and P_{CO} are the partial pressures of CO_2 and CO respectively (see (1) 3.3.4.1).

For a gas mixture at 1 atmosphere containing 50ppm CO, 0.03% CO_2 and balance N_2, the theoretical OCV would be - 80mV and under the operating conditions described above, the overpotential for CO oxidation would be 1080 - 1580mV vs. DHE.

These are the most relevant points affecting the operation of the sensor and are discussed in more detail under separate headings below.

2.3.1 Electrochemical Oxygen Reduction

The most relevant and important aspect of the electrochemistry of oxygen is the existence of the so-called, dead region. This is the fairly broad region of potential, around the theoretical potential, in which oxygen is electrochemically very inactive (see (1) Fig. 6).

In fire detection and safety applications, it is required to detect low ppm concentrations of CO in air, ie. in the presence of some 210,000ppm of O_2.

Platinum black electrodes of the hydrophobic fuel cell type, as used in the CO sensor, are capable of producing currents of over 100mA cm^{-2} (100,000μA cm^{-2}) when operating as air electrodes in the active region for O_2 reduction. This may be compared with the minute (low μA) currents which are all that is possible from the low ppm concentrations of CO that need to be detected.

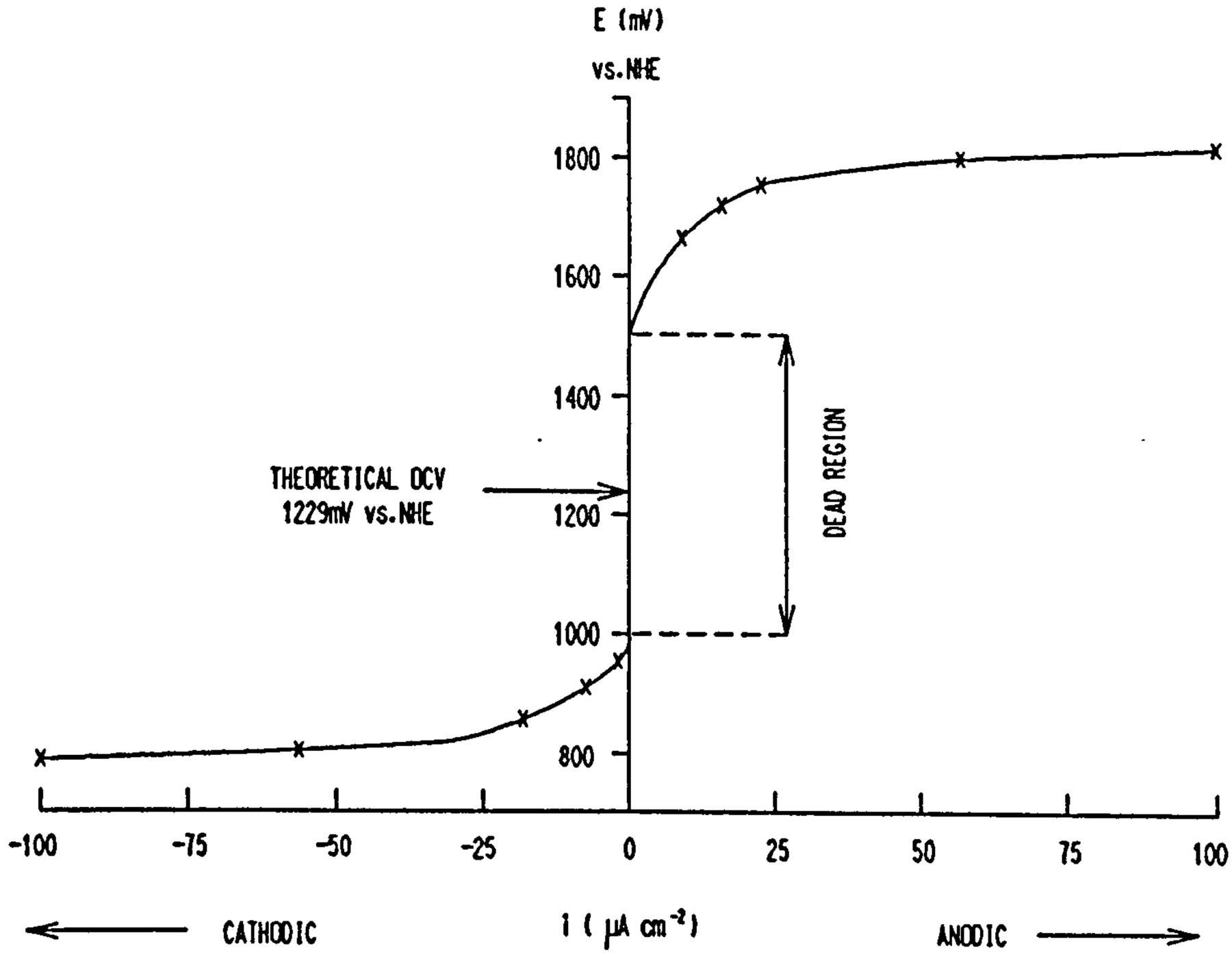

Figure 6 A plot of the anodic and cathodic overvoltage obtained galvanostatically on the same bright Pt electrode in O_2-saturated, 1M H_2SO_4 solution. The cathodic curve was obtained first, after which the anodic curve was determined. The potential was calculated from 1229mV vs DHE. [After Hoare JP (1965) J.Electrochem. Soc. 112 602, replotted on a linear scale].

These figures serve to emphasise how vital it is to maintain operation within the dead region for oxygen. The low oxygen reduction activity in the dead region may be explained as follows:

The overall electrochemical reaction for the oxygen electrode in acid solution is:

$$O_2 + 4H^+ + 4e = 2H_2O \qquad \text{Equ. (3)}$$

The accepted value of E_o calculated from thermodynamic data for pure O_2 at 1 atmosphere and O°C is 1229mV[23-27]. The electrode potential relative to a normal hydrogen electrode in the same electrolyte is given by [28]:

$$\mathbf{E = 1.229 + 0.0148 \log Po_2} \qquad \ldots . \textbf{(20)}$$

Thus the theoretical air rest potential (Po_2 = 0.20 Atm) is 1220mV. However, the measured air rest potential in acid electrolyte is found to be much lower, namely 1050mV vs. DHE.

The explanation for this discrepancy between the theoretical and measured air rest potentials probably lies in the highly irreversible nature of (1) Equ. (3) above, which requires breaking of the 0-0 bond; this bond is very strong and therefore leads to high activation polarization.

The irreversible nature of oxygen reduction is apparent from the very low exchange current densities measured in practice. (1) Table 1 gives a representative selection of i_o values. However, agreement between different workers is poor and the concentration dependence is not known.

Electrolyte	i_o A cm^{-2}	α
0.5M H_2SO_4	10^{-7}	0.36
0.5M H_2SO_4	10^{-9}	0.45
1M KOH	5×10^{-7}	0.20
5M $HClO_4$	4×10^{-8}	0.32

Table 1 Exchange Current Densities in Acid and Alkali Electrolytes.
[After Riddiford AC (1961) Electrochim. Acta 4 170]

Since the i_o for the oxygen reaction is so low (10^{-9} A cm^{-2}), many impurity reactions could become potential - determining at potentials below 1229mV. Such impurities would set up a 'mixed potential' (see (1) Ref. 22 p.32) depending on relative areas of anodic and cathodic surface sites. The existence of such sites would explain not only the failure to attain the reversible potential, but also the strong dependence of the potential on the method of electrode preparation.

An alternative theory is that a more favourable reaction pathway for O_2 reduction could be found via a peroxide intermediate (see (1) Ref. 22 p.20), which would not require breaking of the 0-0 bond:

$$O_2 + 2H^+ + 2e^- \rightleftharpoons H_2O_2 \qquad \ldots\ldots (21)$$

$$E = 0.682 - 0.0591\ pH + 0.0295 \log \frac{P_{O_2}}{[H_2O_2]} \qquad \ldots\ldots (22)$$

The peroxide intermediate can then be further reduced in a second step:

$$H_2O_2 + 2H^+ + 2e^- \rightleftharpoons 2H_2O \qquad \ldots\ldots (23)$$

$$E = 1.776 - 0.0591\ pH + 0.0295 \log [H_2O_2] \qquad \ldots\ldots (24)$$

In order for (1) Equ. (23) to proceed, a finite concentration of peroxide has to build up to drive the reaction from left to right. This peroxide concentration will then set the electrode potential according to (1) Equ. (21).

Conversely, if we calculate the peroxide concentration at the measured air rest potential (PO_2 = 0.21, 1050mV vs DHE) in acid electrolyte (pH = -1) using (1) Equ. (22) we get

$$[H_2O_2] = 7 \times 10^{-12} \qquad \ldots\ldots (25)$$

Thus, we only need the smallest amount of peroxide at the electrode to drop the air rest potential from 1,220mV to 1050mV vs DHE and this would explain the large initial polarization observed in practice.

It is important to note that other workers have found that the OCV is dependent on Pt morphology and on pre-treatment history, thus:

- clean Pt electrodes in O_2-saturated acid solution[26, 29, 30] have OCV's of 1050mV vs. DHE.
- Pt electrodes in which the surface is covered by a complete layer of adsorbed oxygen produced by anodization and heating in pure O_2 [23, 31, 32] or by treating in HNO_3[30] have OCV's is of 1229mV vs. NHE, but cathodic discharge leads to cyclic hysteresis. Thus, Lingane[33] obtained an initial OCV of 1240mV vs. NHE (in sulphuric acid) on a freshly anodised Pt electrode, but after cathodic discharge, the electrode returned to 980mV, which is the potential of the PtO - Pt couple and oxygen reduction only started at 700mV. Lingane claimed that in acid solution the first discharge removed most of the anodic oxide film and subsequent discharges utilised only dissolved O_2 from solution, since direct cathodic oxygen reduction is probably much slower on the heavily oxidised surface than on almost bare metal and the current density increases rapidly at cathodic potentials at which the oxide film becomes unstable. The effect, noted by Lingane and others, that a freshly anodised and reduced surface is active to oxygen reduction has at least three explanations:

(1) As Lingane believed, it may be necessary for the surface to be oxidised to some extent before it adsorbs oxygen and gives cathodic current.
(2) Anodization-cathodization may remove adsorbed impurities or anions, which only slowly readsorb.
(3) Reduction of an anodized surface may produce particularly active surface sites (crystal defects, for example) on the platinum, which anneal out on standing.

The abnormal activity of an anodized-reduced surface is maintained even when the electrode is taken to vigorous hydrogen evolution, and it has not been demonstrated that a surface oxide layer can withstand such treatment.

Gas diffusion electrodes containing high surface area platinum black give immediate activity with hydrogen or oxygen, and in reasonably pure solutions they do not require activation by anodic-cathodic cycling nor does such cycling increase performance. An electrode of this type which has been used for many days as a hydrogen electrode can be immediately used as an oxygen electrode. This suggests that inactivity of bright platinum electrodes is due to impurities and lack of active surface sites rather than the absence of an oxide film. Massively anodized-reduced surfaces are probably abnormal surfaces and results cannot be directly compared with steady-state operation of fuel cell electrodes.

The impact on sensor design of these characteristics can be summarised as follows:

- on bright Pt, the dead region (see (1) Fig. 6) extends from 1000-1580mV. These limits will be narrowed slightly for the more active Pt black fuel cell electrodes, namely 1050-1450mV vs DHE.
- the lower limit round 1050mV vs. DHE is the one of prime importance, representing the air rest potential of the Pt electrode. This can vary a little with Pt black morphology and with electrode preparation and loading.
- It is essential to operate the sensing electrode within the dead region to avoid oxygen reduction cross interference and yet the Pt black counter electrode has to work off oxygen reduction, ie. outside the dead region. This problem is overcome by making the Pt loading on the counter electrode heavier than that on the sensing electrode (see (1) 3.5.4).

2.3.2 Platinum Electrochemistry

As discussed in (1) 2.3.1, trace CO sensors based on Pt/H_2SO_4 must work within the 'dead' region for oxygen, namely 1000-1500mV vs DHE. In this region platinum, although stable in bulk, can undergo surface reactions and in this sense is Faradaically active, adsorbing oxygen in the form of an electronically conducting film about a monolayer thick (see (1) Ref. 22, p.39).

2.3.2.1 Triangular Sweep Technique

Information about the nature of the adsorbed oxygen layer on Pt may be obtained using a triangular wave potential sweep method, an excellent technique for studying quickly and qualitatively the potential regions of a given electrochemical system in which various components of the system are adsorbed. Randles[34] and Sevcik[35] independently were the first to give the theory behind this method.

Early work using this technique concerned the study of electrode processes controlled by mass transfer steps and is summarised by Vogel[36]. As the electrode reaction proceeds in a solution containing an excess of inert electrolyte, the concentration of reactants at the electrode surface decreases and diffusion processes set in. During the potential sweep, the thickness of the diffusion layer increases (lowering the diffusion current), but the concentration gradient across the diffusion layer also increases (increasing the diffusion current). The opposing effects of these two processes on the diffusion current produce a peak in the current. Randles[34,37] has shown that the peak value of the diffusion current may be related to the concentration of the reactant in the bulk of solution.

Will and Knorr[38] first used the output of a triangular sweep generator to control the reference potential of a potentiostat having a fast response time. In this way a potentiostatically

controlled voltage sweep is presented to the cell, and *E-i* curves containing information about electrode processes involving chemisorption may be obtained, provided the experimental conditions are chosen in this case to minimize the effects of mass transfer (eg. strongly stirred solutions). Under these conditions, a current peak corresponds to the existence of a Faradaic process, and so the potential range over which the given electrode process takes place may be determined.

The cyclic scan shown in (1) Fig. 7 is typical of the curves obtained by this method on bright Pt[39-42] for acid solutions, in which oxygen adsorption begins at about 800mV and oxygen evolution above 1500mV.

Below 400mV the hydrogen adsorption peaks are observed, and between 400 and 800mV is the low current double layer region. During the cathodic sweep the oxygen reduction peak is displaced from the oxygen adsorption peak toward less noble potentials, which indicates that an activation energy hump must be surmounted before reduction can take place. In contrast to oxygen adsorption, it is seen that hydrogen adsorption occurs reversibly; the adsorption and reduction peaks occur at the same potential.

Böld and Breiter[39] and Burshtein and co-workers[41] found that for fast sweeps $Q_a = Q_c$. Where Q_a and Q_c are the charge under the anodic and cathodic curves respectively. The value of Q is determined by integration under current peaks since the sweep rate is constant and known. A correction to the charge due to double layer charging currents must be made and is usually obtained from the low current double layer region.

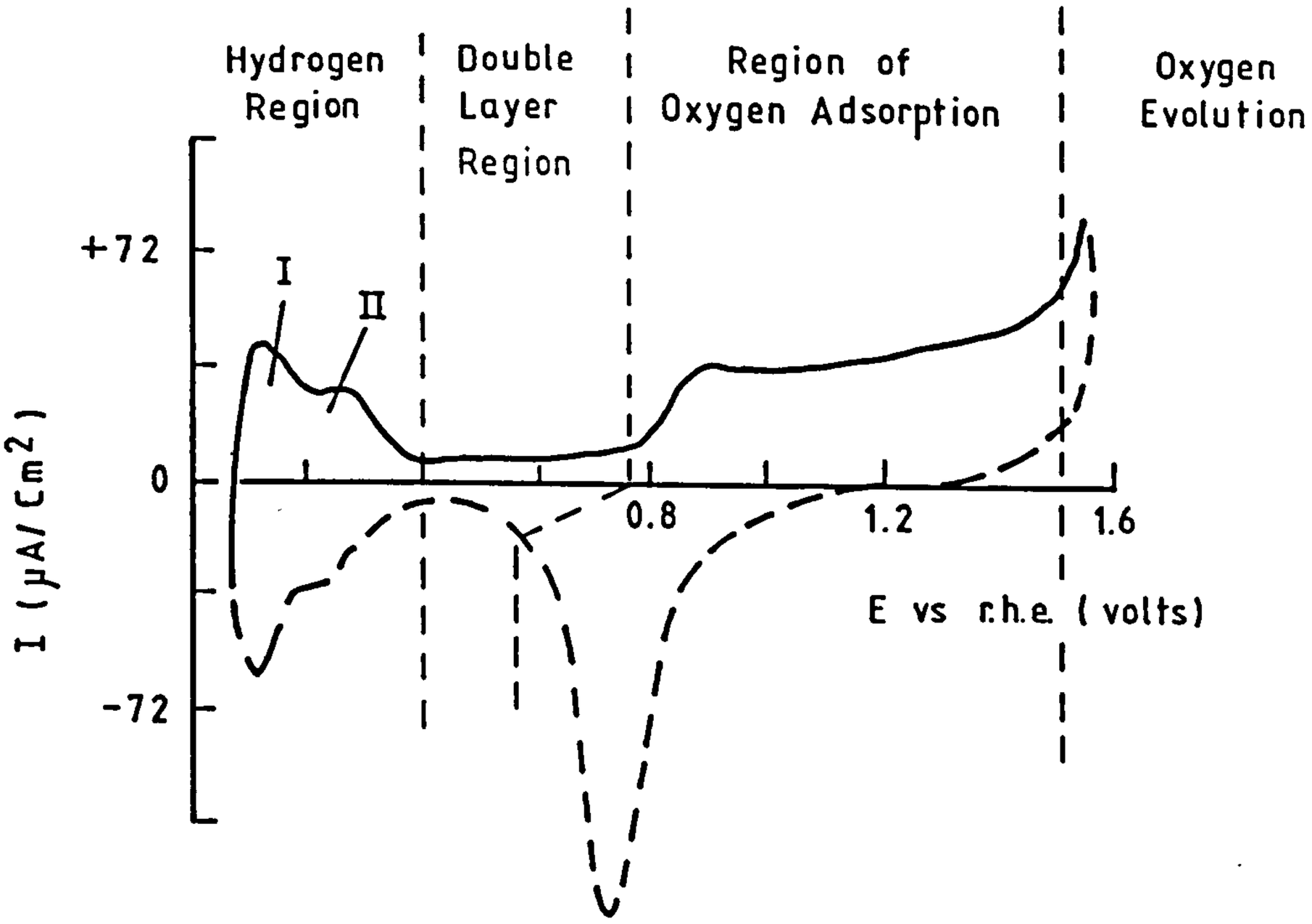

Figure 7 Current potential curve for a smooth platinum electrode in 0.5M sulphuric acid (30°C). The potential was scanned linearly between 0.05 and 1.55V at a speed of 30mV/sec:- the solid line indicates the anodic sweep and the broken line the cathodic sweep [After Will FG and Knorr CA (1960) Zeitschrift für Elektrochemie 64 258]

For slow sweep speeds, Böld and Breiter observed $Q_a > Q_c$ because, as they suggest, oxygen enters the Pt metal on the anodic scan. Burshtein recorded that the value found for Q_c is larger for a single sweep than for repetitive sweeps.

It has been observed[38-40] that the adsorbed oxygen layer builds up with anodic polarization to a point (about a monolayer thick) and then no further. Such behaviour would be expected if the layer of adsorbed oxygen was electronically conducting.

2.3.2.2 Oxide Theory

Both Lorenz and Spielmann[43-47] and Grube[48] measured the potentials of the metal-metal oxides electrodes constructed from

the chemically prepared oxides. A summary of the results obtained by these investigators is presented in (1) Table 2. A definite potential was not obtained for a $Pt/Pt(OH)_2$ electrode[48] which is to be expected[47] since $Pt(OH)_2$ is very unstable.

Electrode Couple	Lorenz & Spielmann [45-47]	Grube[48]	Nagel & Dietz[49]	Latimer[50] de Bethune[51]	Hoare[52]
Pt/Pt-O					0.88V
Pt/PtO		0.9V			
$Pt/Pt(OH)_2$			0.98V	0.98V	
$Pt/PtO.2H_2O$	0.95V	1.04V			
$Pt/PtO_2.2H_2O$	0.96V				
$Pt/PtO_2.3H_2O$	0.98V				
$Pt/PtO_2.4H_2O$		1.06V			
Pt/PtO_3		1.5V			
Pt/PtO_4		>1.6V			
Pt/Pt_3O_4			1.11V		
$Pt(OH)_2/PtO_2$			1.1V	1.1V	

Table 2 Standard Potential for Various Platinum Oxide Couples in Acid Solutions as Reported in the Literature

However, many of the early investigators[53-57] subscribe to some form of the oxide theory. Foerster[53] observed that the potential of a Pt electrode anodized to 1.5V fell under open-circuit conditions without hesitation through the potential values of 1.23, 1.1 and 1.06V. From his investigations, he concluded that the various potentials observed on open circuit were the result of different combinations or ratios of an ill-defined oxide, PtO_x [approximating to PtO or $Pt(OH)_2$], and PtO_2. Above 1.23V the potentials may be due to higher oxides such as PtO_3 or PtO_4 as suggested by Grube[48], but Foerster considered these to be very

unstable, decomposing to mixtures of PtO_x and PtO_2. It was observed by Klemenc[54] that the rest potential varied with the partial pressure of oxygen, $P\ O_2$, but the Pt/O_2 potential was produced by PtO_2 in equilibrium with the $P\ O_2$ above the solution. At high $P\ O_2$ up to about 100psi, Tamman and Runge[57] found large hysteresis effects with changes in $P\ O_2$, yet they came to the same conclusions as Foerster about the potential-determining species on the electrode at high potentials. Some investigators[40, 49, 58-62] hold that at potentials below about one volt the adsorbed oxygen is in the form of PtO and that above this, it is in the form of a mixture of PtO and PtO_2. Anson and Lingane[58] concluded from their experimental work of oxidising Pt electrodes and then chemically stripping the 'oxides', that two oxides were present, namely PtO and PtO_2, in a ratio of 6:1. Apparently this ratio did not alter, even at more anodic potentials when more oxide was formed, which is rather surprising, since one would expect the concentration of PtO_2 to increase at the expense of PtO.

Other investigators[29, 30, 39, 52, 63-69] favour the concept that the oxygen exists on the Pt surface as adsorbed oxygen atoms, Pt-O. On oxygen-free surfaces, Bockris et al[67,70] observed that a square root relationship exists between the partial pressure of oxygen and the amount of oxygen adsorbed on the Pt surface as determined from cathodic stripping techniques. This indicates that oxygen is adsorbed as atoms by a dissociative adsorption process.

2.3.2.3 Oxide Coverage

It is not just the nature, but also the degree of surface coverage with oxide, that is of importance to sensor design, because any movement in sensing electrode potential will generate an oxide rearrangement current. This in turn will cause hysteresis in the dynamic performance, as the counter electrode polarizes under load (see (1) 2.4).

Oxide coverage on bright Pt has been studied by Gilman[71] by means of rigorous pretreatment and applying fast 'potentiodynamic' sequences to adsorb and subsequently to strip the oxide under controlled conditions (see (1) Fig. 8).

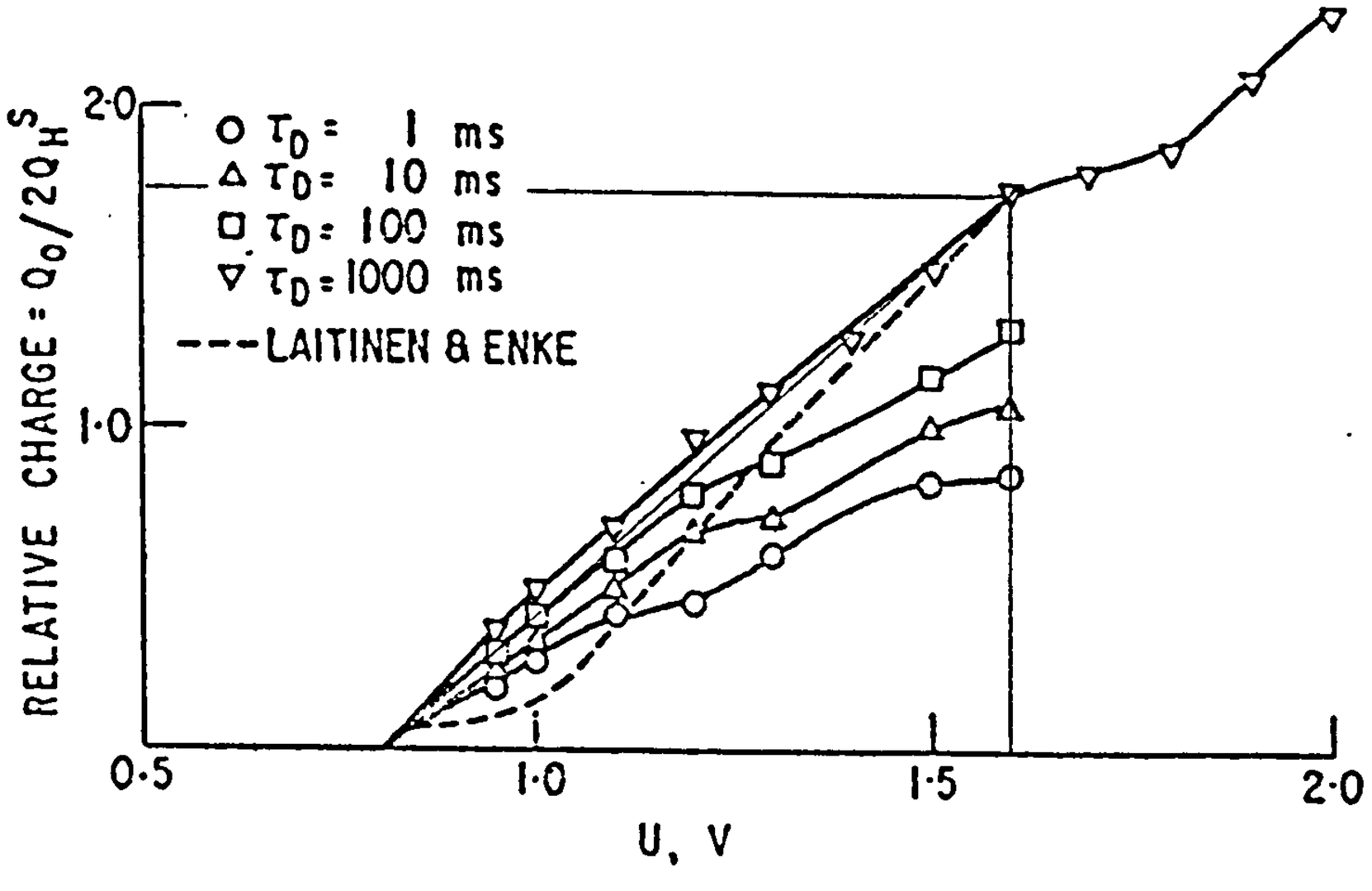

Figure 8 Relative charge for platinum surface oxidation measured at constant potential (step sequence of figure 2(e) used for $0.8 \leq U \leq 1.6V$; sequence 2(g) used for $1.6 \leq U \leq 2.0V$. r_D is the oxidation time at constant potential).
[After Gilman S (1964) Electrochemica Acta 9 1025]

Gilman assumed $Q_o = 2Q^S_H = 2 \times 210\mu$ C cm^{-2}

Where Q_o = surface oxide charge on Pt

Q^S_H = charge equivalent to monolayer surface coverage with H_2 on Pt.

Using the mean values found by Gilman at an adsorption time of 1000ms and that of Laitinen and Enke[60] - see (1) Fig. 8:

$$\text{Slope} = \frac{\partial(Q_o / 2Q^s_H)}{\partial V} = \frac{1.72}{0.78} = 2.21\ v^{-1}$$

$$\text{or} \quad \frac{\partial Q_o}{\partial V} = \frac{2.21 \times 2 \times 210}{1000} = 0.928 \mu C\ cm^{-2}\ mv^{-1}$$

Since this is on bright Pt, the fuel cell sensing electrode will have a surface roughness of about 1000, therefore:

$$\left(\frac{\partial Q_o}{\partial V}\right)_{sensor} = 928 \mu C\ mv^{-1}$$

It is evident therefore that oxide rearrangement, as a result of quite small potential changes, can result in significant interference to the CO signal. The consequences of this are considered in more detail in (1) 2.4.

2.3.3 Electrochemical Carbon Monoxide Oxidation

Since trace level CO monitoring takes place largely against a background of ambient air, the Pt sensing electrode OCV is 1050mV vs. DHE, ie. in the oxygen adsorption region (see (1) Fig. 7 and (1) 2.3.2). However, most of the published literature on CO oxidation concerned its poisoning effect on low-temperature fuel cell H_2 anodes[72] operating at much lower potentials[73], viz 100mV vs. DHE.

In fuel cell applications, H_2 is produced by catalytic cracking of hydrocarbons to generate 'reformer gas' for direct utilisation as anode feedstock[74]. However, due to the shift reaction, a small amount of CO(~1%) is produced as an impurity, which rapidly poisons the anode, causing the operating potential to rise and hence causing the fuel cell power to drop off rapidly. In other applications, CO itself was considered as anode feedstock for fuel cells[75-76].

Hence interest in CO oxidation in fuel cell applications led to a number

of mechanistic studies by Gilman using potentiostatic pulse techniques[21, 77-79] whilst others used galvanostatic stripping[80-82] and potentiodynamic sweeps at various speeds[83-87].

In 1964 Gilman proposed the 'reactant pair ' mechanism for CO oxidation[21]. Gilman's work was based on adsorbing dissolved CO at low anodic potential (400mV vs. DHE) onto bright Pt pre-cleaned by a series of anodic pulses at 1500mV vs. DHE to oxidise adsorbed organic impurities. This was followed by cathodic stripping of the Pt oxide to prepare a clean surface for CO adsorption.

The 'reactant pair' mechanism postulated that CO was strongly adsorbed on bare platinum sites and that water was adsorbed on adjacent platinum oxide sites to form an activated complex of the type:

$$\begin{array}{ccc} (CO) & (H_2O) & \\ | & | & \\ Pt & PtO_x & \end{array} \rightarrow \begin{array}{ccc} (CO) & \ldots\ldots & (H_2O) \\ | & & | \\ Pt & & PtO_x \end{array} + e^-$$

(activated complex)

$$\rightarrow \begin{array}{ccc} (CO) & \text{----} & (OH) \\ | & & | \\ Pt & & PtO_x \end{array} + e^- + H^+ \rightarrow CO_2 + 2e^- + 2H^+ \quad \ldots\ldots (26)$$

in which the activated complex facilitated the electron transfer step in the oxidation of CO to CO_2.

Gilman's 'dual-site' mechanism was confirmed in a different way by the work of Brummer[88], who studied the reaction of CO oxidation on three compound electrodes:

(a) platinum, platinum
(b) platinum, tantalum carbide
(c) gold, tantalum carbide

In each of the above systems the first material of the two named was a solid electrode and the second a powder electrode, dispersed in the electrolyte. The two reactants in the oxidation, carbon monoxide and water, were adsorbed separately on either the solid or the dispersed electrode, in order to regulate their relative concentrations. The steady state rates of oxidation were thereby increased, sometimes by several orders of magnitude.

Tantalum carbide was chosen because it does not adsorb carbon monoxide, but is very hard and therefore has a very high surface energy, thereby making it a strong adsorbent for water.

Additional evidence for the involvement of Pt oxide was found in the work of Brett et al[89] who studied CO oxidation on bright Pt and supported Pt using potentiodynamic sweep techniques (see (1) Fig.9). In the anodic sweep (0.4-1.3V vs. DHE), there was no oxidation current from 0.4V to 0.9V. The CO oxidation current increased sharply at 0.91V (start of PtO_x formation) and thereafter decreased linearly with potential. In the cathodic sweep the oxide current was less than on the anodic sweep in the range 1.3 - 0.9V; it was slightly greater in the range 0.9 - 0.7V and zero from 0.7 to 0.2V.

The need for portable analytical devices for monitoring CO led to the development of electrochemical sensors based on Pt fuel cell electrodes[90] and metallised membrane electrodes[91-94].

More recently, mechanistic studies of CO oxidation on smooth Pt electrodes by McCallum and Pletcher[95] led to the development of Pt and Au metallised electrodes[96] for use in CO sensors, from which they concluded that both types of electrode behaved similarly towards CO oxidation. However, they noted that both Pt and Au metallised electrodes are rapidly poisoned by CO oxidation intermediate products. This is not surprising, since such metallised electrodes have very low surface area compared to fuel cell-type electrodes.

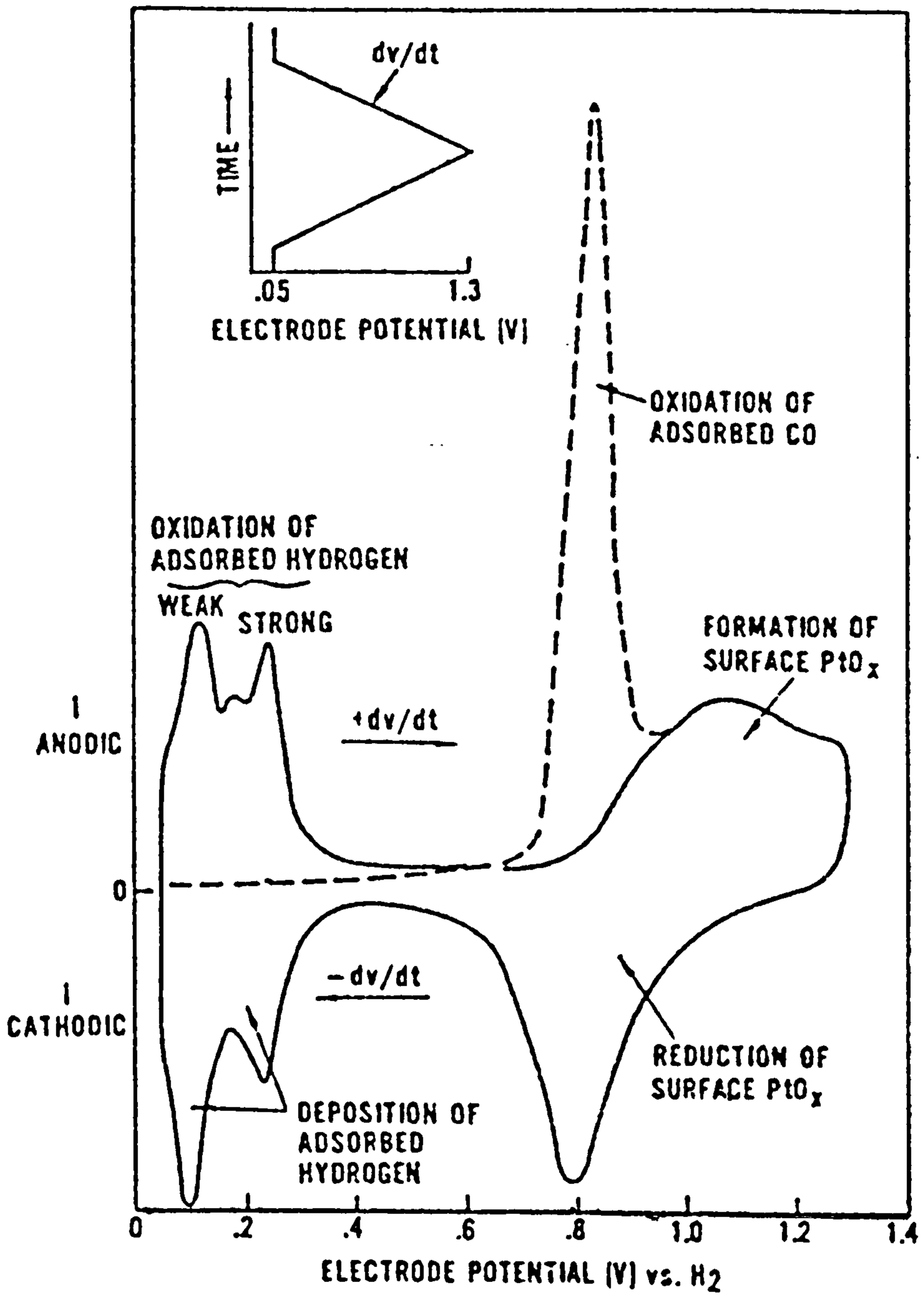

Figure 9 Potentiodynamic sweep of platinum under anaerobic conditions. Solid line 20% H_2SO_4, N_2. Broked line 20% H_2SO_4, CO, 30 min, N_2 10 min, 24°C. [After Brett J et al (1973) Journal of Catalysis 29 160]

Of most relevance to studying CO oxidation under realistic sensor conditions ie. using fuel cell Pt electrodes/H_2SO_4 electrolyte operating in ambient air and at high anodic potential to avoid oxygen reduction (see (1) 2.3.1) is the work of Blurton & Sedlak[19], who studied CO oxidation

under potentiostatic control, mapping out the j-v curve under quasi steady state conditions measuring one point per day. This is thought to more closely approximate to the genuine steady state where the influence of surface platinum oxide on carbon monoxide could be taken into account. These results in conjunction with studies of oxide formation on platinum electrodes[97-100] identified PtOH as the most active electrocatalytic species for CO oxidation.

This may be summarised as follows:

Stage 1 : Reversible electrosorption of OH^- species on Pt

Pt ⇌ PtOH **$0.72V \leq E \leq 0.9V$** **. . . . (27)**

Stage II: Rearrangement of surface PtOH species

PtOH → OHPt **$0.90V < E \leq 1.1V$** **. . . . (28)**

Stage III: Conversion of OHPt Species to PtO

OHPt → PtO **$1.1V < E \leq 1.5V$** **. . . . (29)**

As the surface is oxidised at successively higher potentials or is held for longer times at a given potential the irreversibility of the reaction of rearranged PtOH and formation of the PtO species is increased.

The increase in carbon monoxide oxidation current in the range 0.8 - 1V (see (1) Fig. 10) parallels the increase in reversibly bound OH species on the Pt surface (see (1) Equ. (27)).

Between 1.0 and 1.1V there is a sharp decrease in current (see (1) Fig. 10, curve (a)) corresponding to the rearrangement in the surface layer (see (1) Equ. (28)). At more anodic potentials the continuing decrease in current with increasing potential is in accordance with the diminished availability of PtOH groups (see (1) Equ. (29)).

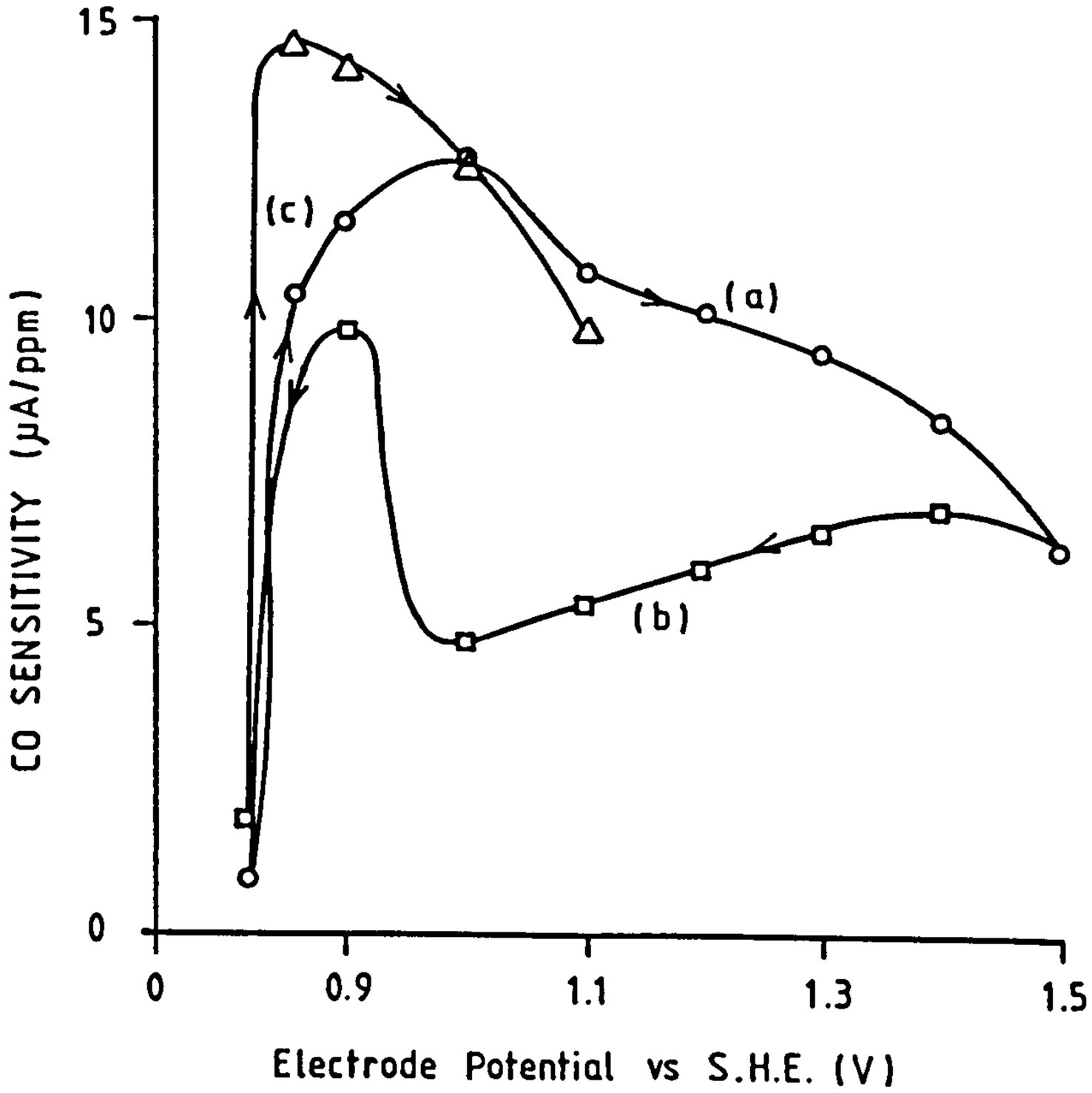

Figure 10 CO oxidation current as a function of Pt electrode potential. ○ Potential increased from 0.8 to 1.5V; □ potential decreased from 1.5 to 0.8V; Δ potential increased from 0.8 to 1.1V. [After Blurton KF and Sedlak JM (1974) J.Electrochem. Soc. 121 1315]

On decreasing the potential from 1.4 to 1.0V (see (1) Fig. 10, curve (b)) the current decreased linearly with potential due to the retention of PtO which was formed at 1.5V together with the decreasing over voltage for the reaction. At 0.9V the current increased sharply due to the reformation of electro-adsorbed PtOH (see (1) Equ. (27)) and on further decrease of the potential to 0.8V, the CO oxidation current dropped to a low level in accordance with a decrease of surface PtOH concentration.

On the subsequent increase of potential (see (1) Fig. 10, curve (c)), very high currents were observed at 0.85 and 0.9V due to extensive surface coverage with PtOH. On increasing the potential beyond the reversible PtOH formation (see (1) Equ. (27)), the CO oxidation current decreased

markedly due to the rearrangement of electrosorbed OH^- (see (1) Equ. (28).

Blurton and Sedlak[19] concluded:

(A) oxidised Pt electrodes are more active for CO electro-oxidation than unoxidised Pt.

(B) PtOH is the preferred catalytic site and PtO is catalytically active to a lesser extent.

(C) The oxidation of the Pt surface in the potential range 0.8 to 1.0V is reversible while that in the range 1.0 to 1.5V is irreversible.

(D) The Pt electrode does not attain a steady state at 1.2V until it has been under potentiostatic control for some 35 days.

2.4 Two-Electrode Dynamic Oxide Balance

Since two-electrode sensors combine the function of both reference and counter in one electrode (see (1) 2.1.3), polarization of the counter electrode will cause the sensing electrode potential to shift by an equivalent amount. This movement of the sensing electrode potential will elicit a Faradaic response due to oxygen reduction/Pt oxide surface re-arrangement (see (1) 2.3.1, 2.3.2 and especially oxide charge calculation in (1) 2.3.2.3).

It is therefore possible to qualitatively postulate the dynamic response of a two-electrode CO sensor using Pt electrodes (see (2) 12 2):

Case 1 : Sensor anode operating above the OCV

If the anode potential is V_o in clean air and drops to V_{co} (see (1) Fig. 11) when the sensor is exposed to CO, due to polarization of the cathode (ie. non-ideal counter), then a spurious cathodic transient current will be generated due to oxide reduction (see (1) Equ. (30)), which would subtract from the CO oxidation current:

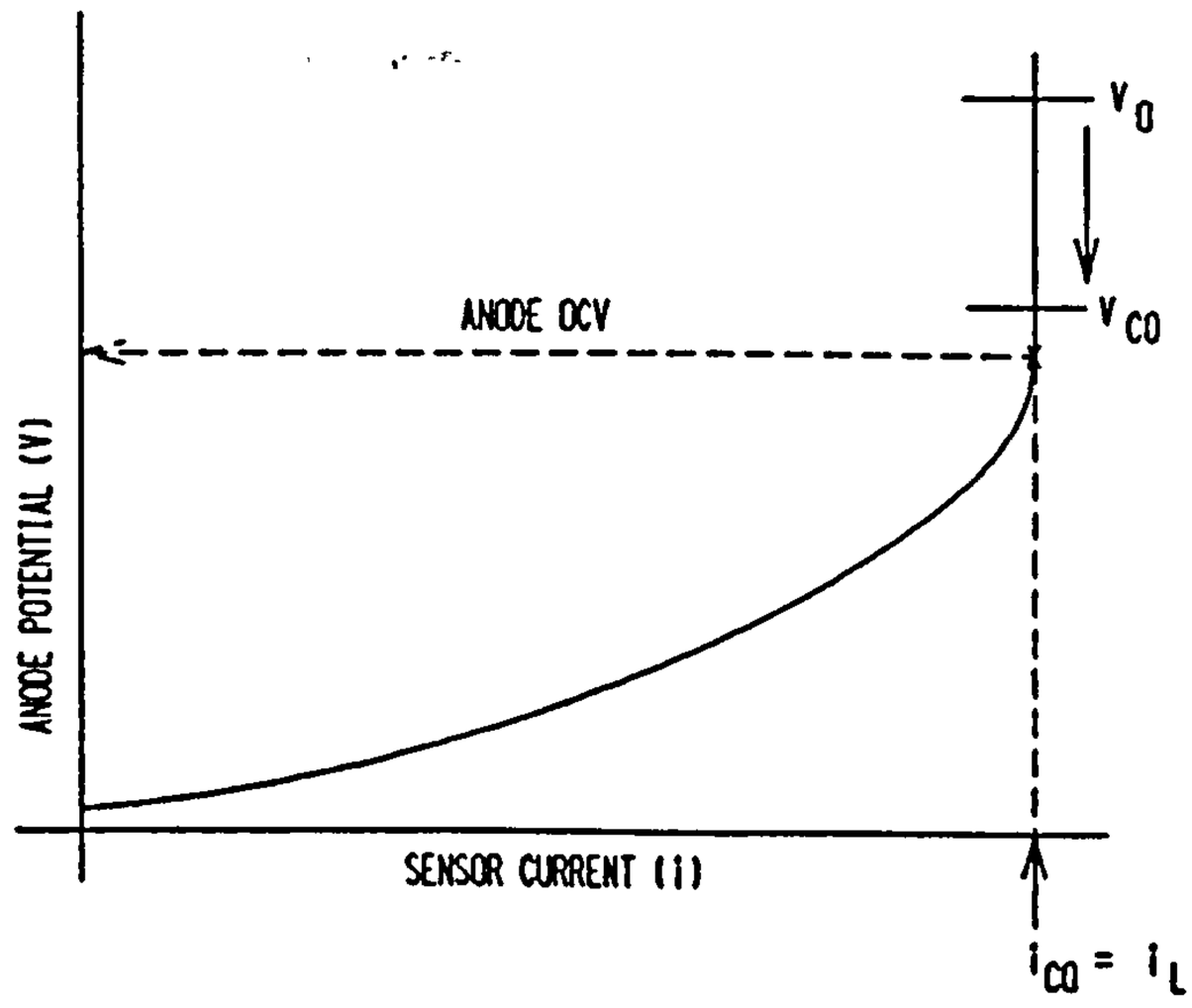

Figure 11 Schematic diagram showing anode polarization under load. [After CTL Report No. 81/31/006, (2) 12 p.7]

$$PtO + 2H^+ + 2e^- \rightarrow Pt + H_2O \quad \ldots\ (30)$$

This results in a low initial response (see (1) Fig. 12), but as the Pt oxide dissolution current dies down, the sensor output 'creeps' to its full signal and on recovery positive baseline hysteresis occurs because the anode surface is re-oxidised to equilibrium coverage as the cathode depolarises.

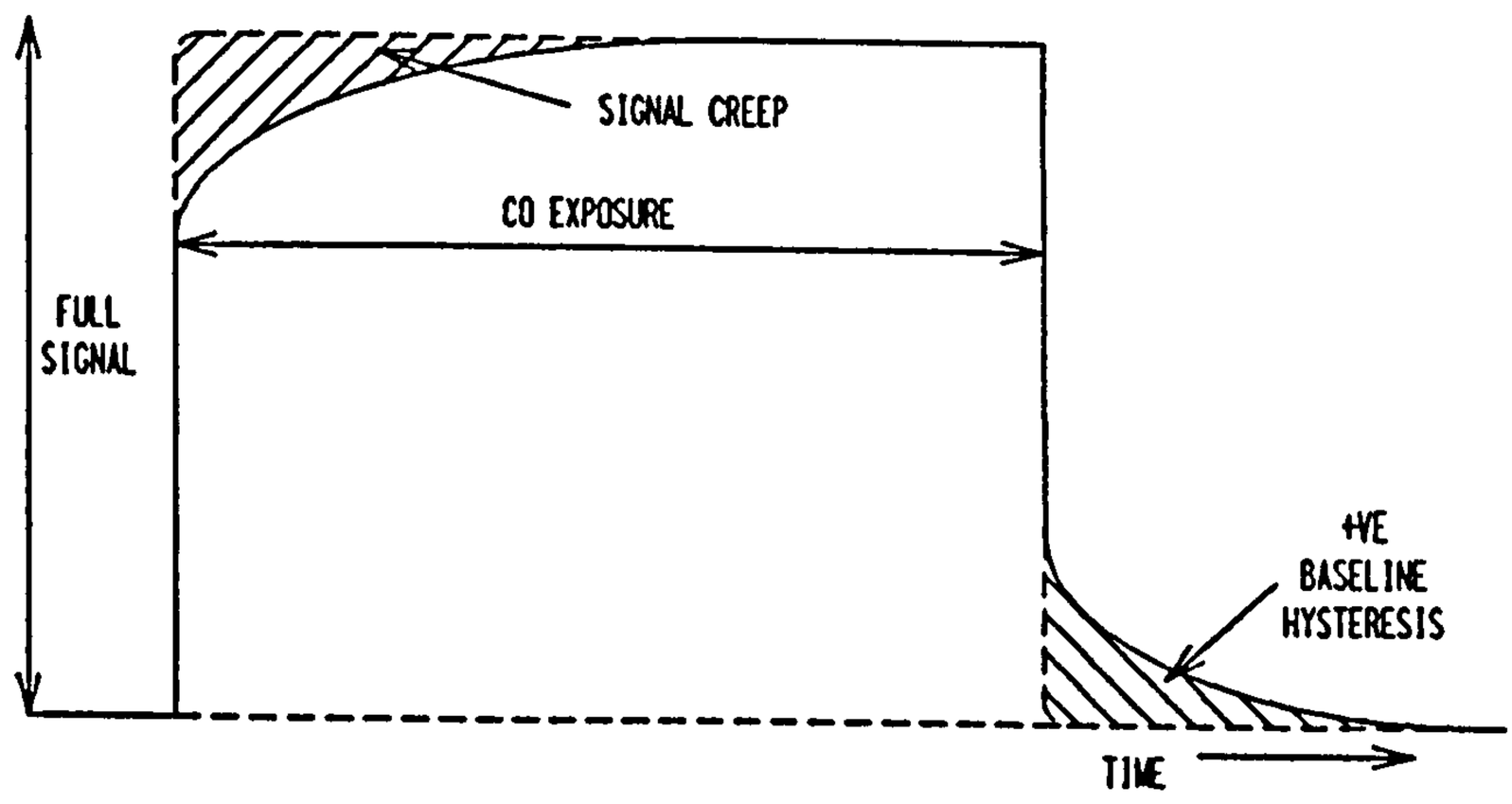

Figure 12 Schematic diagram showing sensor response to CO and baseline hysteresis on recovery. [After CTL Report No. 81/31/006, (2) 12 p.8]

Signal 'creep' may be summarised as follows:

	Anode		Cathode	
Transient Signal	$S = i_{CO} - i_{PtO}$ (a)	=	i_{O_2} (c) + i_{PtO} (c)	. . (31)
Steady State Signal	$S = i_{CO}$	=	i_{O_2} (c)	. . . . (32)

Case 2 : Sensor anode polarising below the OCV

Sensors which are over exposed to carbon monoxide will exhibit Case 1 'creep' behaviour initially, but as the anode polarises below the OCV under excessive load (see (1) Fig. 13), oxygen reduction will set in on

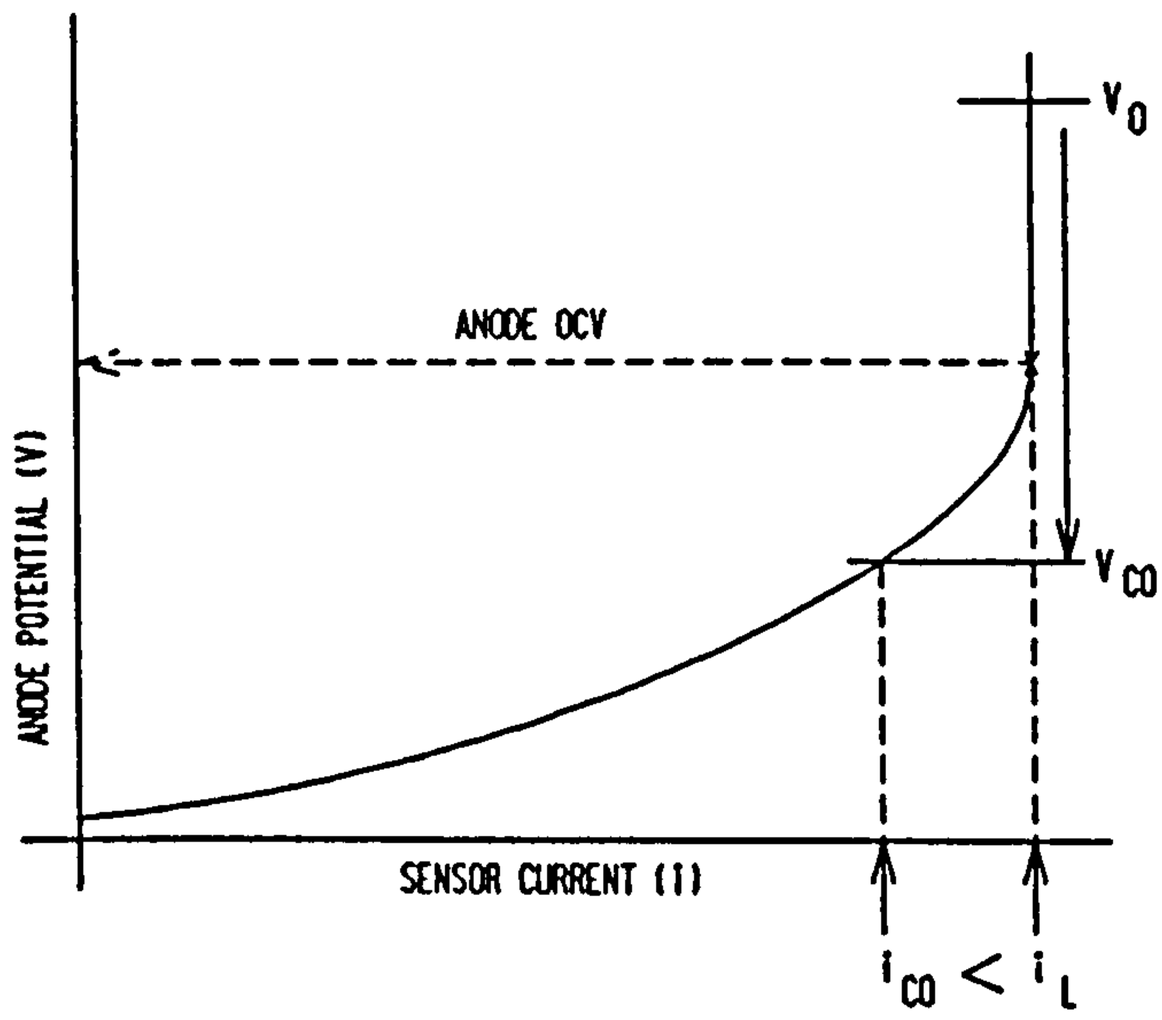

Figure 13 Schematic diagram showing sensing electrode coming out of the 'current-limiting' mode due to cathode polarization under load. [After CTL Report No. 81/31/006, (2) 12 p.4]

the sensing electrode and the transient response can be described by:

Anode		Cathode	
$S = i_{CO} - i_{PtO}$ (a) - i_{O_2} (a)	=	i_{O_2} (c) + i_{PtO} (c)	. . . . (33)

With time, i_{CO} remains constant, both i_{PtO} (a) and i_{PtO} (c) decay to zero and both i_{O_2} (a) and i_{O_2} (c) increase to a final steady state value. At the steady state:

$S = i_{CO} - i_{O_2}$ (a)	=	i_{O_2} (c)	. . . . (34)

The i_{O_2} values apply at the steady state potential (V_{CO}).

As the sensing electrode potential polarises from V_o to V_{CO} during the exposure, the sensor signal will decay expontially, approaching its steady state value when V_{CO} is reached (see (1) Fig. 14).
This leads to a response curve of the type:

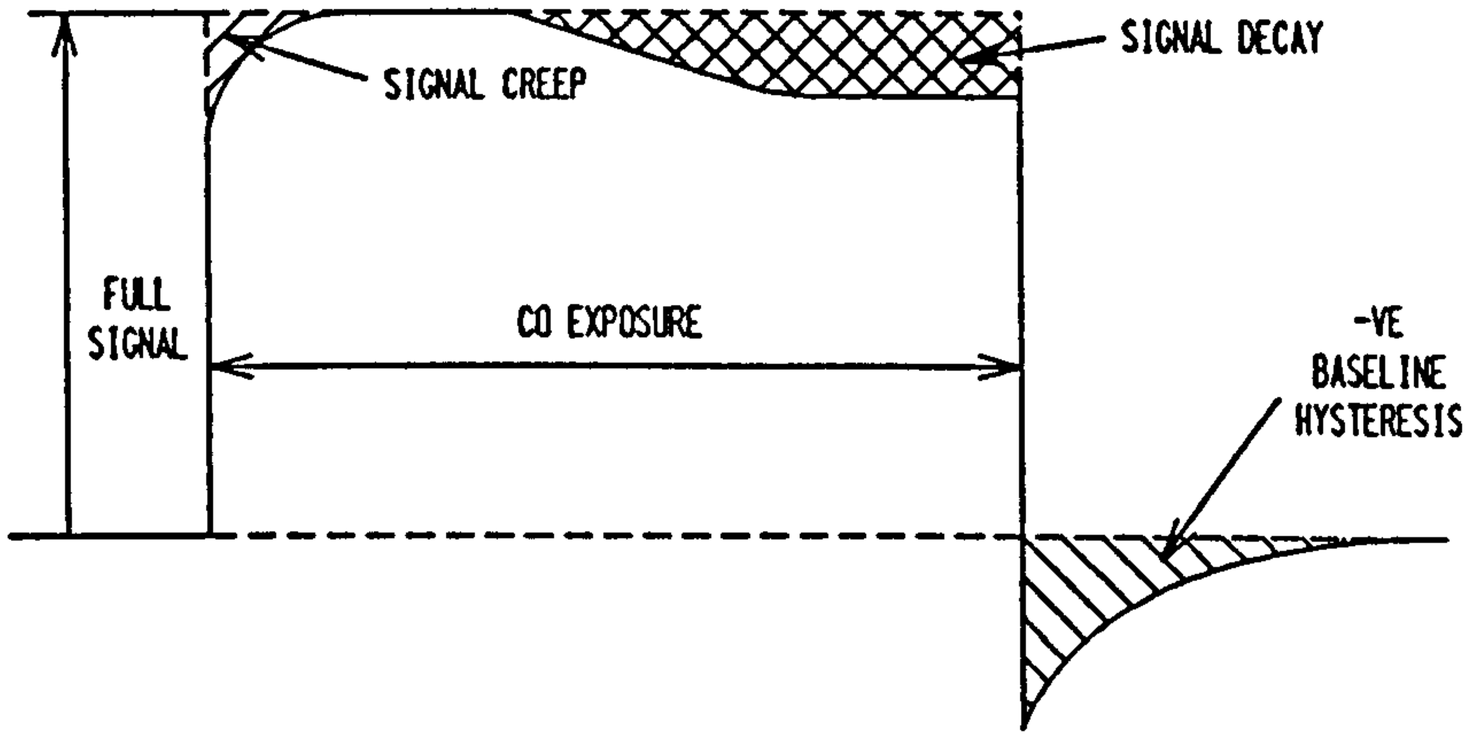

Figure 14 Schematic diagram showing sensor response under extreme overload to CO. [After CTL Report No.81/31/006, (2) 12 p.11]

On recovery, the Pt surfaces are re-oxidised:

$$\underline{\text{Anode}} \qquad \underline{\text{Cathode}}$$

$$S = i_{Pt}(a) - i_{O_2}(a) = i_{O_2}(c) - i_{Pt}(c) \qquad \ldots\ldots (35)$$

All these currents decay to zero with time, or at least revert back to the net baseline current.

2.5 Diffusion and Diffusion Barrier

Early sensors such as those described by Oswin and co-workers[11-15] (see (1) 2.2.1) were simply minifuel cells with no separate additional barrier. The diffusion-limiting step was diffusion in solution through the electrolyte film around the electrode catalyst (see (1) 2.6 and Fig. 21), which constituted the diffusion barrier and resulted in a high temperature

coefficient with an exponential response. Such sensors had large sensitivities and needed to be operated in a pumped system.

The use of a separate, more restricted diffusion barrier enabled sensors to be made which could operate in the diffusion mode, without the need for a pumped gas supply. Solid non-porous membranes were first used for this purpose[101], involving a process of solid state diffusion of the reactant gas, dissolved in solid solution in the polymer. The outputs at a fixed temperature of sensors utilizing such membranes are linearly related to reactant gas partial pressure[102], thus:

$$i_L = \text{constant} \times p_i \qquad \ldots . (36)$$

where i_L (amps) is the sensor limiting current and p_i is the partial pressure of the reactant gas in the environment being sensed. The proportionality constant, or membrane diffusibility, is a function of the nature, thickness and area of the membrane at a given temperature (see (1) Ref. 22 p.191).

In practice, these membranes have fairly low diffusibilities and need to be very thin to achieve practical sensor sensitivities. Such thin films can give handling difficulties due to static, fragility, etc, and problems with cracks, pinholes and other defects. The process of solid state diffusion has an inherently high exponential temperature coefficient and sensor outputs can vary with temperature[103] by as much as 3-4% $°C^{-1}$ at or near 20°C. The principal advantage of the solid membrane barrier is that it furnishes a true partial pressure measurement which is linear over the complete concentration range 0-100%; this can be important in some applications, eg. in deep diving where large pressure changes are experienced and a true partial pressure measurement is essential for physiological reasons. However, these requirements are not necessary in the majority of ambient-pressure-monitoring application and the benefits of a gas diffusion (capillary) barrier (GDB) as used in CTL sensors[104] far outweigh those of solid membranes (see (1) Ref. 8 p.167).

2.5.1 Gas Diffusion Barrier

The gas diffusion barrier can take the form of a porous plastic, metal or ceramic membrane, or simply a single capillary hole. If the pore diameter is much greater than the mean free path of the gas molecules undergoing diffusion, then the effects of wall collisions with the pores of capillaries are relatively insignificant to the process. Under these conditions, intermolecular collisions dominate the diffusion process, resulting in a sensor output which has a considerably lower temperature coefficient and provides a volume fraction, rather than a partial pressure measurement. This can be illustrated by considering the case of a capillary diffusion barrier sensor:

$$\text{reactant flux (mol}^{-1}) = \frac{i_L}{nF} = \text{constant x } (C'_1 - C'_2). \qquad \ldots . (37)$$

The constant in (1) Equ. (37) is the diffusion barrier diffusibility D' which for a porous barrier is given by the following relationship:

$$D' \ (\text{m}^3\text{s}^{-1}) = \frac{\text{barrier diffusion area (m}^2\text{) x porosity x } D_0(\text{m}^2\text{s}^{-1})}{\text{barrier diffusion thickness (m) x tortuosity}} \qquad \ldots . (38)$$

where D_0 is the diffusion coefficient of reactant gas through the background (carrier) gas at fixed temperature (273K) and pressure (1atm). Tortuosity is the ratio of mean pore length to barrier thickness; for a simple capillary, both porosity and tortuosity will be equal to unity.

For a simple capillary barrier, at a temperature of 273K and a pressure of 1 atm, (1) Equ. (38) becomes:

$$D' = \frac{\Pi d^2}{4L} D_0 \qquad \ldots . (39)$$

where d (m) is the capillary diameter and L(m) is the capillary length.

According to the kinetic theory of gases[105], D_0 varies in direct proportion to the $^3/_2$ root of absolute temperature and in inverse proportion to the total pressure, therefore

$$D' \text{ (at } T\text{(K) and P (atm) total pressure)} = \frac{\Pi d^2}{4L} D_0 \left(\frac{T}{273}\right)^{3/2} \frac{1}{P} \quad \ldots . (40)$$

Considering the concentration gradient across the barrier in (1) Equ. (37), at temperature T(K) and partial pressure p_1 and p_2 (atm).

$$C'_1 - C'_2 \text{ (mol m}^{-3}) = \frac{(p_1 - p_2)\ 273 \times 10^3}{22.4T} \quad \ldots . (41)$$

This derives from the molar volume of an ideal gas, occupying 22.4 l at 273K and 1 atm pressure.

However, p_2 tends to zero in a limiting-current condition, therefore

$$C'_1 - C'_2 = \frac{p_1 \times 273 \times 10^3}{22.4T} \quad \ldots . (42)$$

Substituting (1) Equs. (40) and (41) into (1) Equ. (37) gives:

$$\text{reactant flux (mol s}^{-1}) = \frac{I}{nF} = \frac{\Pi\ d^2}{4L} D_0 \frac{1}{P} \left(\frac{T}{273}\right)^{3/2} \frac{p_1 \times 273 \times 10^3}{22.4T} \quad \ldots . (43)$$

$$\text{cell current (A)} = \frac{2.05 \times 10^5\ D_0 T^{1/2} n d^2 p_1}{LP} \quad \ldots . (44)$$

(1) Equ. (44) predicts the following:

2.5.1.1 Capillary Temperature Coefficient

The signal will have a $T^{½}$ dependence on temperature, equivalent to 0.17% $°C^{-1}$ near 20°C or about one twentieth of that of a solid membrane, or other activated diffusion barrier. When considering wider temperature excursions, the differences in temperature sensitivity become even more marked because of the exponential response of the activated diffusion barrier. For example between 0 and 40°C, an activated diffusion barrier gives a signal change of the order of 300-400%, compared with about 10% with gaseous barriers.

2.5.1.2 v/v Measurement

The ratio p_1/P is the volume fraction (Boyle's law), so the sensor signal measures volume fraction rather than partial pressure. This produces a signal which is essentially independent of barometric pressure.

2.5.1.3 'Carrier' Gas Effect

The diffusion coefficient D_0 of the reactant gas, diffusing through a gas phase barrier, varies inversely with the square root of the mean molecular weight of the background gas filling the pores, or capillary, of the diffusion barrier[105]. Most applications are concerned with ambient air monitoring where the background gas is essentially nitrogen and remains constant. However, where the composition of the background gas does change, such that its mean molecular weight alters significantly, then recalibration of the sensor in this environment will be necessary.

2.5.1.4 Linearity

Since reactant gas is being consumed at the sensing electrode, a pressure difference will tend to develop across the barrier which will have the effect of drawing in additional gas by bulk flow, over and above that coming in by diffusion, and provide an enhanced signal over that predicted by (1) Equ. (44). Macropores offer

relatively little resistance to bulk flow and in practice the pressure difference is very small. If we take an oxygen sensor in pure dry air at 1 atm as an example, we see that the partial pressure of nitrogen in-board of the barrier will be close to 1 while out-board it is 0.79. Nitrogen will therefore be diffusing back. Since there is no net flux of nitrogen, the bulk flow of air must be such that the input of nitrogen exactly balances its back diffusion. This enables the total mass transport of oxygen to be calculated[105] and leads to the law

$$S = K \ln (1 - C'') \quad \ldots . (45)$$

where S is the sensor signal expressed as a fractional concentration, C'' is the actual fractional concentration of reactant and K is a constant whose value depends on the calibration point. For example, for an oxygen sensor calibrated at 21% oxygen, $C'' = S = 0.21$ and $K = 0.891$.

For low concentrations, below a few per cent of reactant gas, the bulkflow is imperceptible and sensor outputs are highly linear with respect to reactant concentration (see (1) Fig. 15).

At concentrations above a few per cent, sensors become increasingly non-linear. (1) Fig. 16 shows the output of a capillary barrier oxygen sensor with oxygen concentration between 0 and 25%. The figure shows the error resulting in assuming a linear response over the concentration range on calibrating in air at 20.9% oxygen. Above 25% oxygen, the deviations from linearity become much more significant. Since the bulk flow effect follows a clearly defined logarithmic law, it can be compensated electronically using a suitable linearizing logarithmic amplifier.

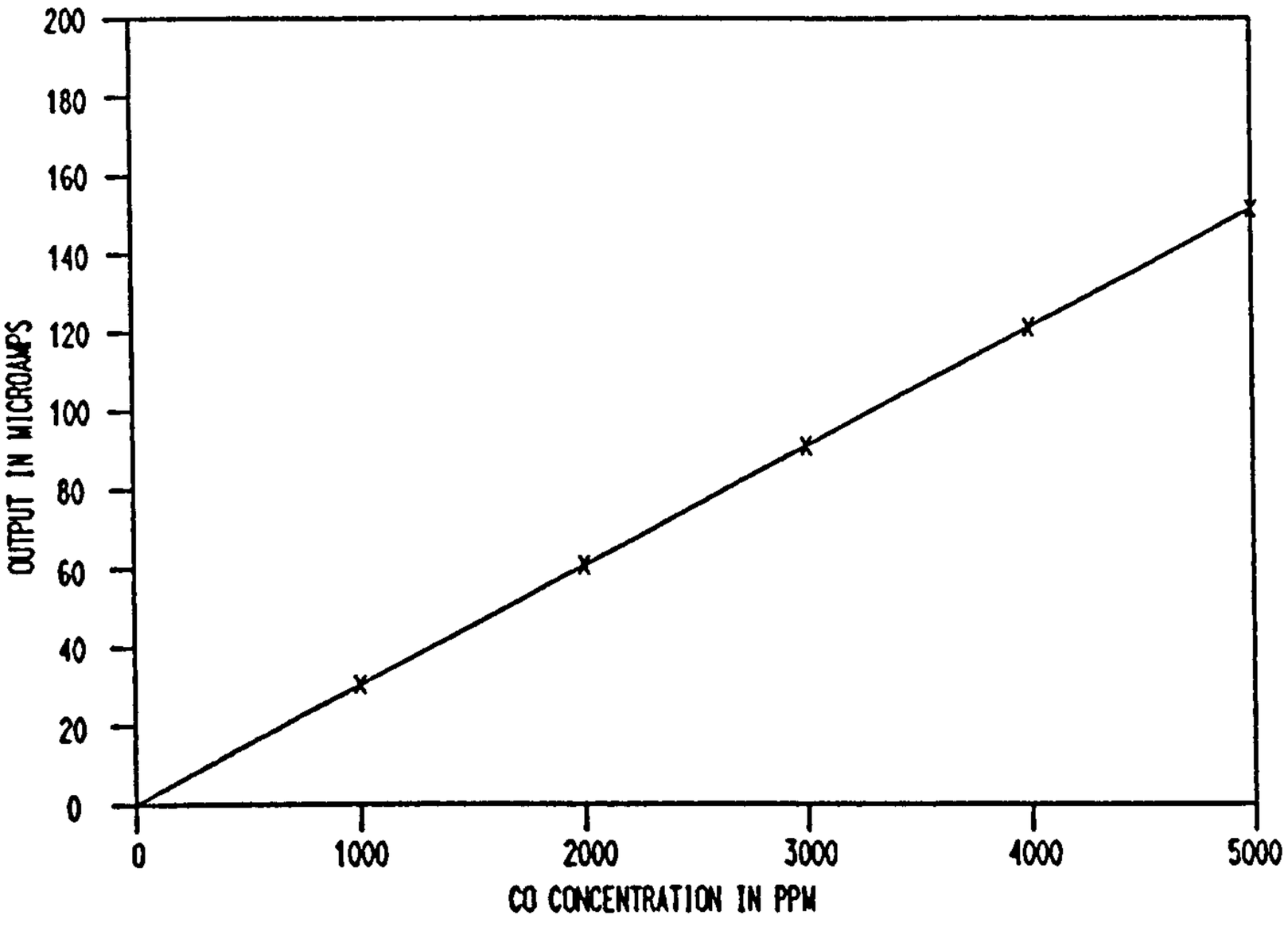

Figure 15 Output signal as a function of concentration of a capillary barrier sensor for 0-5000ppm carbon monoxide.
[After (1) Ref. 8 p.172]

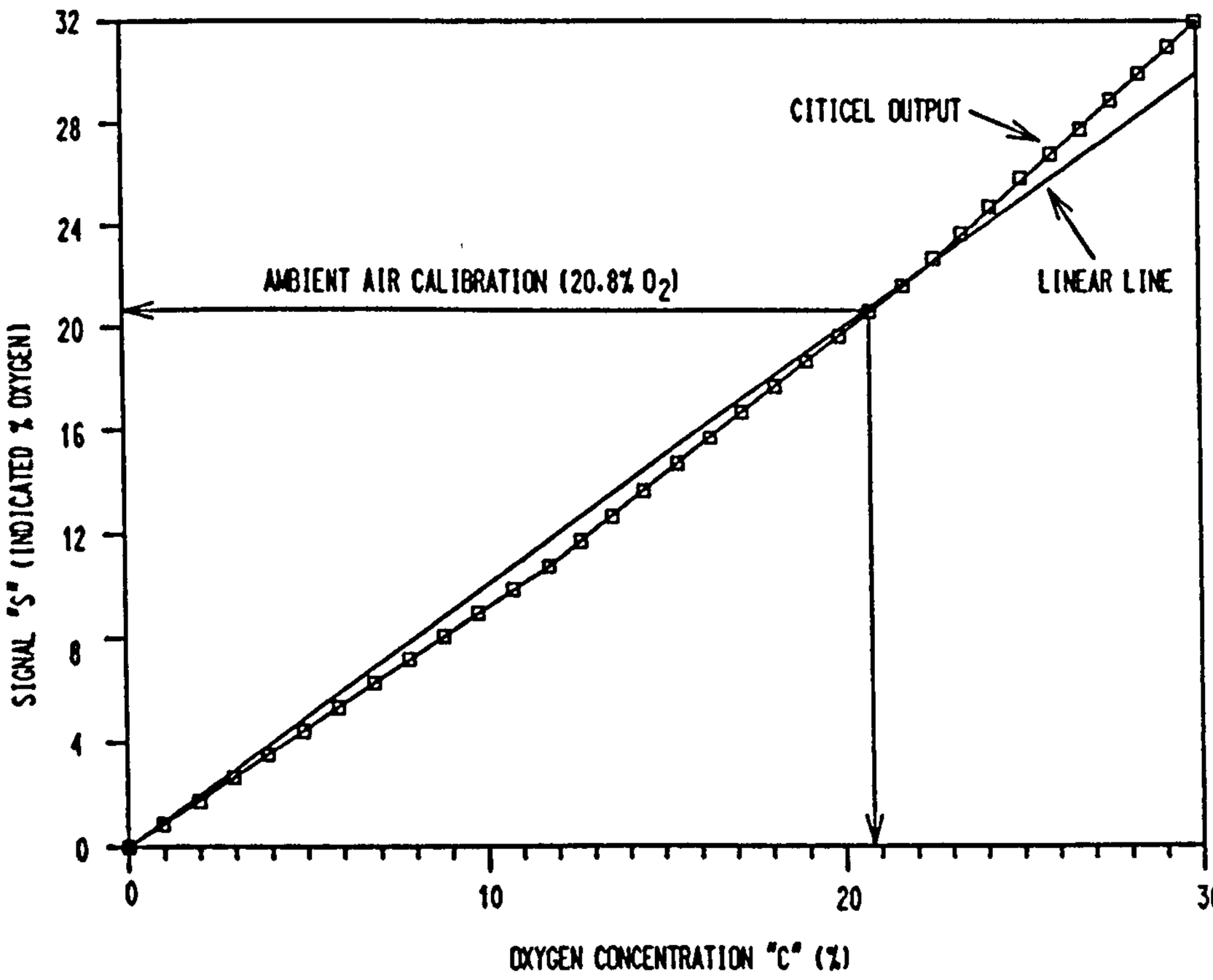

Figure 16 Output signal as a function of concentration of a capillary barrier sensor for 0-30% oxygen : □ = sensor output[After Ref. 8 p.173]

2.5.2 Pressure Transients

Additional bulk flow effects arise with porous and capillary barriers when the sensors are subjected to sudden sharp pressure pulses. This results in gas being forced into the sensor through the barrier, producing a current transient. These transients rapidly decay to zero as the normal diffusion conditions are re-established once the pressure change or pulse is over. However, such transients may trigger false alarms and steps need to be taken to avoid them where an application involves sudden pressure changes. Current transients resulting from pressure pulses can be dampened by using a protective porous membrane in front of the main diffusion barrier; this membrane is chosen to be highly diffusive, relative to the main barrier, but of sufficiently small pore size to restrict bulk flow of gas significantly. This membrane performs the additional function of protecting the sensor from draughts and ingress of dirt or dust particles, moisture condensation etc, which may block the main capillary or porous barrier.

When using diaphragm pumps, in aspirated gas-handling systems, pressure oscillations introduced into the gas sampling stream can produce false, enhanced signals with capillary or porous barrier sensors which are also flow dependent, as the pressure pulses will change with pump speed and flow rate. This may be overcome by suitable design of the gas sampling system. Thus the gas supply line to the sensor may contain an expansion chamber with a small bleed hole to dampen the gas flow to the sensor; a flow restrictor, upstream from the sensor, will also help dampen such pressure oscillations. An additional effective measure is to ensure that back pressure downstream of the sensor is very low, such that the gas stream has an essentially unrestricted flow to ambient air. However, it is important that the exhaust outlet is of suitable dimensions to prevent back diffusion from ambient air, diluting the gas stream and lowering the gas concentration being measured.

2.5.3 Electrode Activity Reserve Concept

Ideally, if the electrode is infinitely active, the gaseous capillary barrier will be fully in control of the sensor signal and will exhibit a $t^{1/2}$ temperature dependence giving a temperature coefficient of 0.17% signal per °C at 20°C. In practice, however, electrodes have finite activity and therefore the capillary is not the sole barrier to diffusion, some of the control residing within the electrolyte film, as shown schematically in (1) Fig. 17.

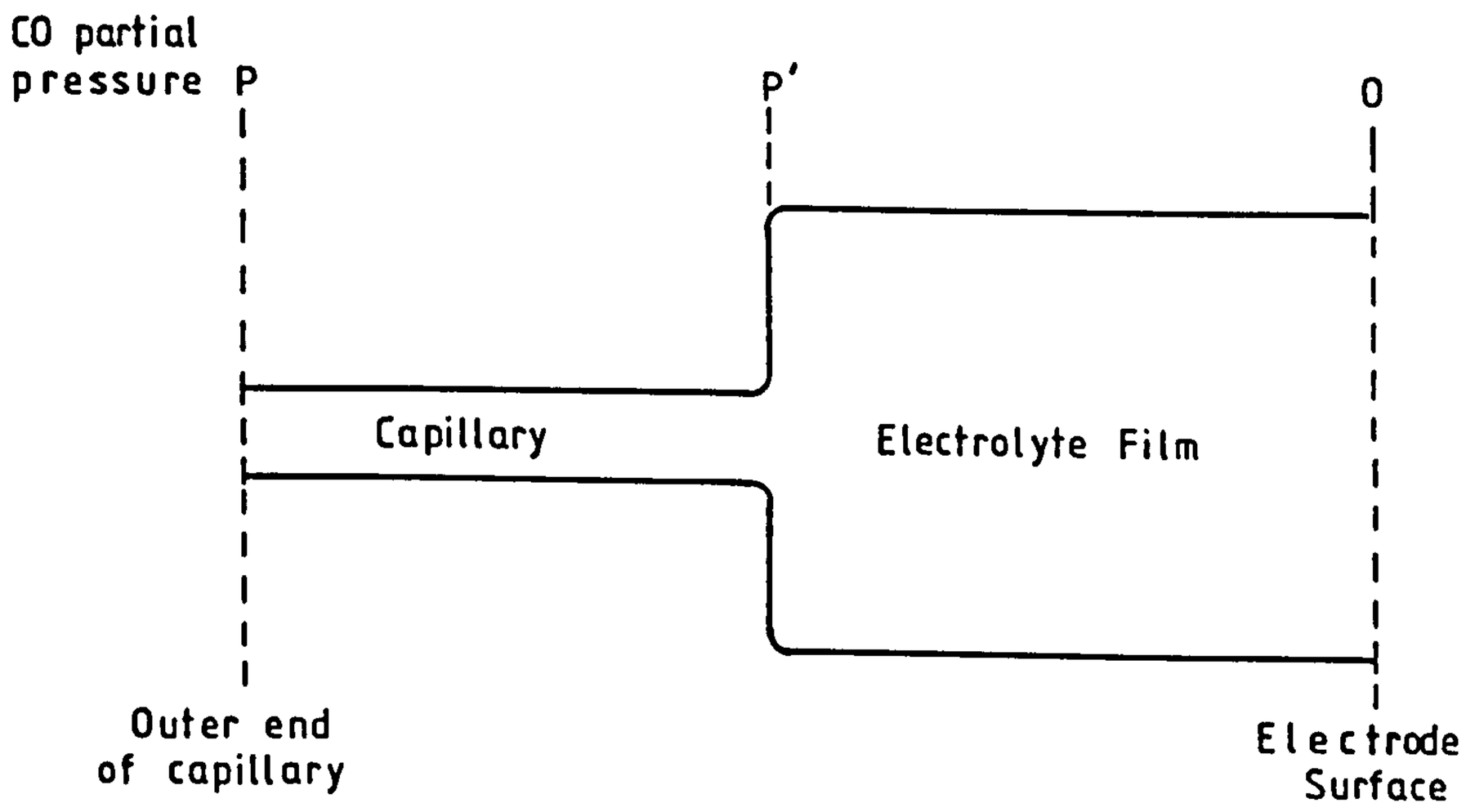

Figure 17 Relative diffusion resistance barriers [After CTL Report No. 82/09/007, (2) 13 App.3]

Finite electrode activity will affect sensor performance as follows:

(a) depress the true capillary signal

(b) increase the sensor temperature coefficient. The temperature dependence of diffusion through electrolyte or electron transfer kinetics or other electrode reaction activated processes is exponential (2-3% of signal per °C at 20°C) and will be higher at low temperature and lower at high temperature. The sensor characteristics will therefore depend on the relative contributions of these two diffusion resistances (see (2) 13 App.3):

The flux of CO through the capillary expressed as a current (i_s) is given by:

$$i_s = k_c (P - P') \quad \ldots\ldots (46)$$

where P and P' are the CO partial pressures outside and inboard of the capillary respectively and the proportionality constant k_c includes the diffusion constant, geometric factors and conversion factor from mass flow to current.

Similarly for the electrolyte film:

$$i_s = k_e P' \quad \ldots\ldots (47)$$

Substituting in (1) Equ. (46) for $P' = \frac{i_s}{k_e}$ from (1) Equ. (47):

$$i_s = k_c \left(P - \frac{i_s}{k_e} \right)$$

Rearranging:

$$i_s = \left(\frac{k_c k_e}{k_c + k_e} \right) P \quad \ldots\ldots (48)$$

For the capillary on its own:

$$i_c = k_c P \text{ hence } k_c = \frac{i_c}{P}$$

For the electrolyte film on its own:

$$i_e = k_e P \text{ hence } k_e = \frac{i_e}{P}$$

Substituting in (1) Equ. (48) gives:

$$i_e = \frac{i_c i_e}{i_c + i_e} \quad \ldots\ldots (49)$$

It is convenient to express the sensing electrode activity in terms of an activity reserve (Ar) factor, defined as:

$$Ar = \frac{i_e}{i_c} \quad \ldots\ldots (50)$$

i.e. the ratio of the current capability of the electrode on its own (open electrode current) to the current with 100% capillary limitation.

Substituting for $i_e = Ar\, i_c$ in (1) Equ. (49) gives:

$$i_s = \frac{i_c Ar}{1 + Ar} \quad \text{and } i_s \rightarrow i_c \text{ as } Ar \rightarrow \infty \quad \ldots\ldots (51)$$

2.5.3.1 Activity Reserve Effect on Sensor Drift

The effect of activity reserve (Ar) on long-term sensor drift may be calculated as follows:

If the initial signal is i_s at activity reserve Ar and the signal decays to i_s' after six months when the activity reserve has, say halved,

then the percentage signal decay after six months may be calculated by substituting the values into (1) Equ. (51) to give:

$$\text{Stability} = \frac{i_s'}{i_s} \times 100 = \frac{1+Ar}{Ar} \times \frac{Ar/_2}{1+Ar/_2} \times 100 \quad \ldots\ldots (52)$$

At Ar = 5 Stability = 85.7%

At Ar = 10 Stability = 91.7%

The relationship is shown in (1) Fig. 18(x) where it is seen that even at an activity reserve of 20, there is a measurable element of electrode control in the sensor signal.

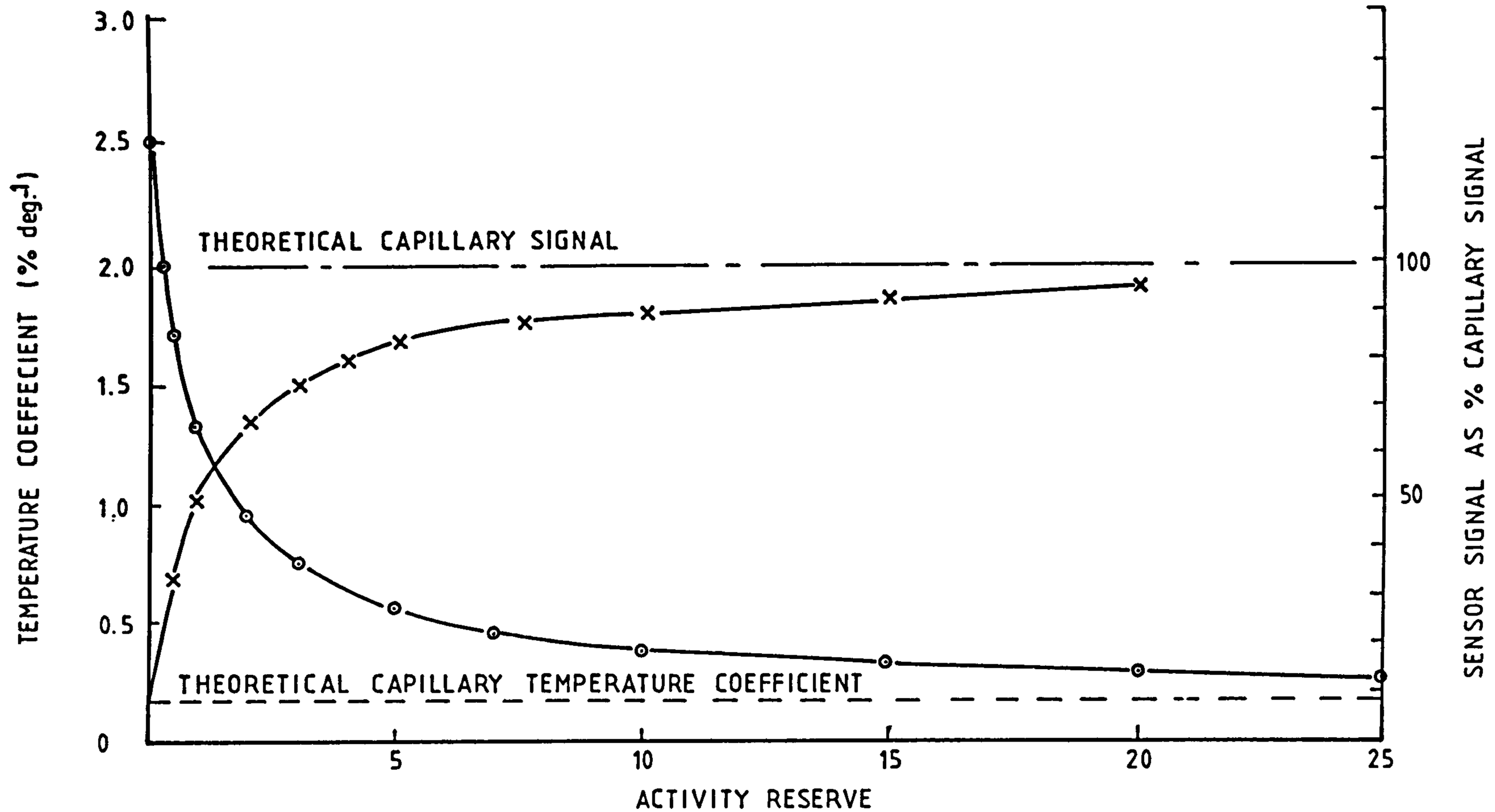

Figure 18 Relationship between 'Activity Reserve' and sensor signal and temperature coefficient.

O = Sensor Temperature Coefficient ($\propto_E$ = 2.5% degree) X = Proportion of Capillary Control of Sensor Signal

[After CTL Report No. 82/09/007, (2)13 Fig. A.3]

2.5.3.2 Activity Reserve Effect on Sensor Temperature Coefficient

The effect on temperature coefficient may be derived as follows:

If the activity reserve is Ar then the relative contributions to the signal are Ar from the capillary, compared to 1 from the electrode. An amount Ar is subject to the capillary temperature coefficient ($\propto_c$) and an amount 1 to the electrode temperature coefficient; $\propto_s$ will be the resulting mean, so:

$$\propto_s = \frac{Ar\propto_c + \propto_e}{Ar + 1} \qquad \ldots\ldots (53)$$

Rearranging: $$\propto_s = \frac{Ar}{Ar+1}\left(\propto_c + \frac{\propto_e}{Ar}\right) \qquad \ldots\ldots (54)$$

The theoretical capillary temperature coefficient ($\propto_c$) is 0.17% per degree and measured values of $\propto_e$ for CO oxidation on platinum electrodes are about 2.5% per degree centigrade. Substitution of these values into (1) Equ. (54) and its solution produces the relationship shown in (1) Fig. 18 (⊙).

Note: The above is a simplified treatment to illustrate the order of magnitude of the effects. Two points should be noted:

(1) The capillary diffusion is actually proportional to P/P_t, where P is the partial pressure and P_t is the total pressure, since the diffusion constant is proportional to $1/P_t$. The electrolyte film diffusion will be proportional to P and independent of P_t. A strict treatment should take this into account. At very high values of Ar (capillary dominated signal) the sensor will be a true concentration (volume %) sensor, with zero pressure coefficient. At low values of Ar there is an element of partial pressure response, which will result in a finite pressure coefficient when treated as a concentration sensor.

(2) The treatment has implied that temperature coefficients are substantially independent of temperature. The deviation from this assumption is not large for the capillary, which follows a $T^{½}$ law, but is much greater for the electrolyte film, which follows an exponential law.

The effect of this is that with low values of Ar the resulting temperature coefficients, expressed as % signal, per °C, will be increased at lower temperatures as illustrated in (1) Fig.

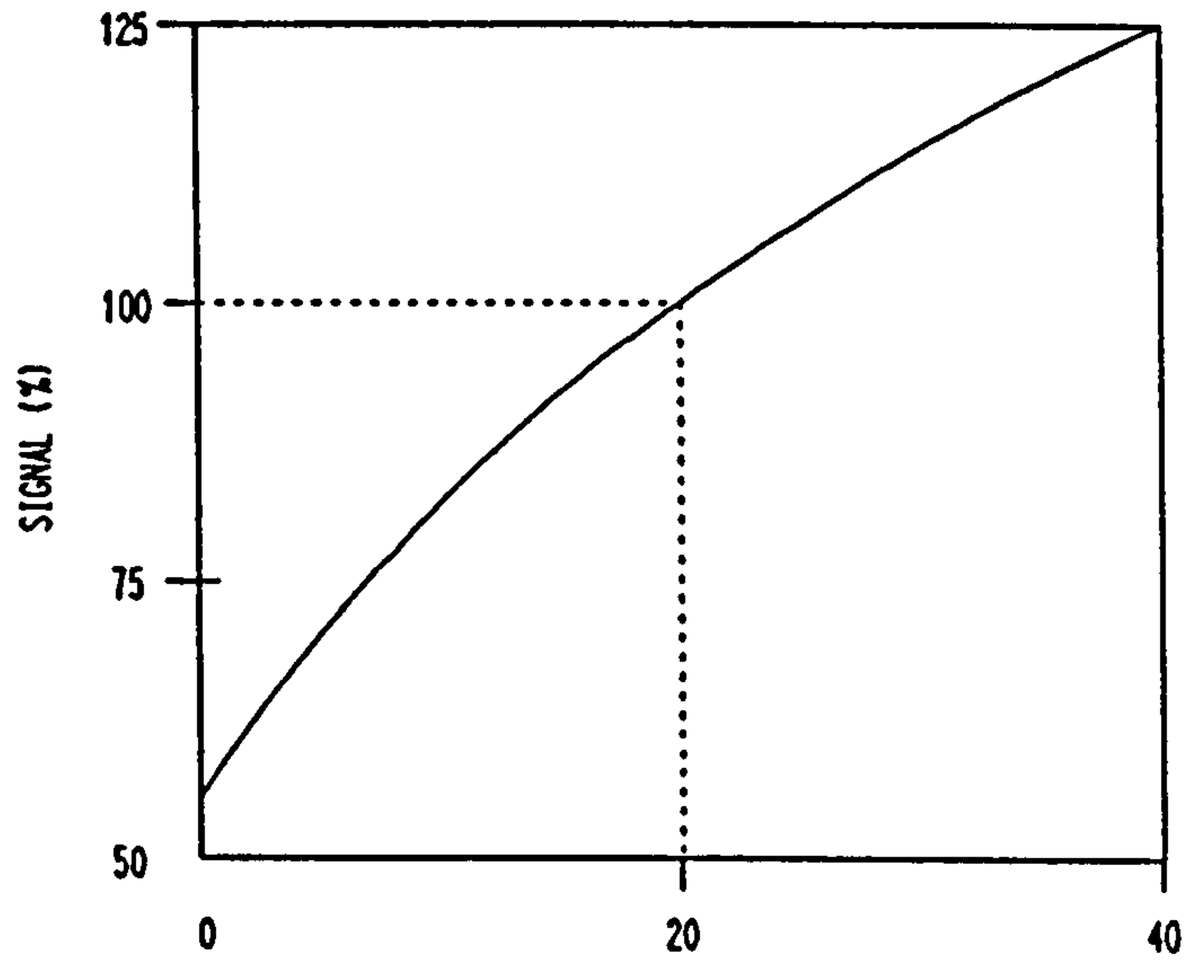

Figure 19 Schematic curve showing exponential dependence of signal on temperature
[After CTL Report No. 82/09/007, (2) 13 p.120]

2.6 FUEL CELL ELECTRODE TECHNOLOGY

2.6.1 Hydrophobic Fuel Cell Electrode Structure

Fuel cell electrodes are essentially made by mixing finely-divided electrocatalyst material with a Teflon (PTFE) binder which creates hydrophobic channels, providing effective gas penetration of the catalyst agglomerates which are filled with electrolyte (see (1) Fig. 20).

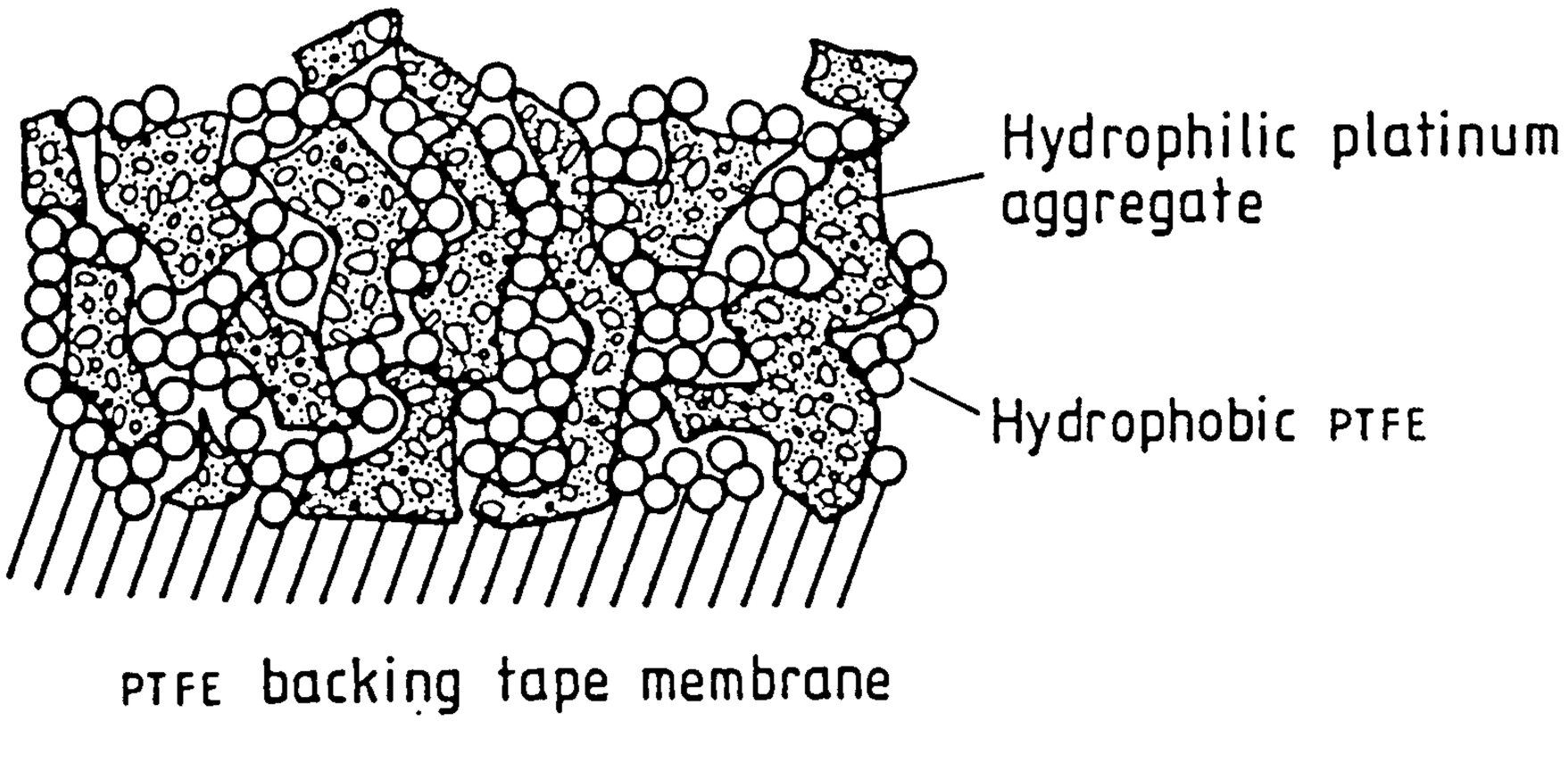

Figure 20 Two dimensional schematic representation of PTFE bonded gas diffusion electrode [After Ref. 8 Fig. 6.7]

This Teflon bonded electrode[106,107] represents a very efficient structure which allows extensive utilization of the catalyst, so that high current densities may be drawn at very low polarization. The actual sites within the fuel cell structure where electron transfer takes place, exist at the so-called 'three-phase interface' where catalyst surface, thinly wetted electrolyte film and gaseous reactant co-exist (see (1) Fig. 21).

According to the double-porosity model[108,109], it is thought that the catalyst forms porous, electronically conductive agglomerates which under working conditions are completely flooded with electrolyte. These catalyst agglomerates are held together by the Teflon binder which also creates hydrophobic gas channels. When current is drawn from the electrode, reactant gas diffuses through the hydrophobic channels, dissolves in the electrolyte contained in the agglomerates and reacts on available sites on the catalyst particles. The number of sites available depends on the rate of diffusion and on the rate of reaction at sites located near the surface of the agglomerate.

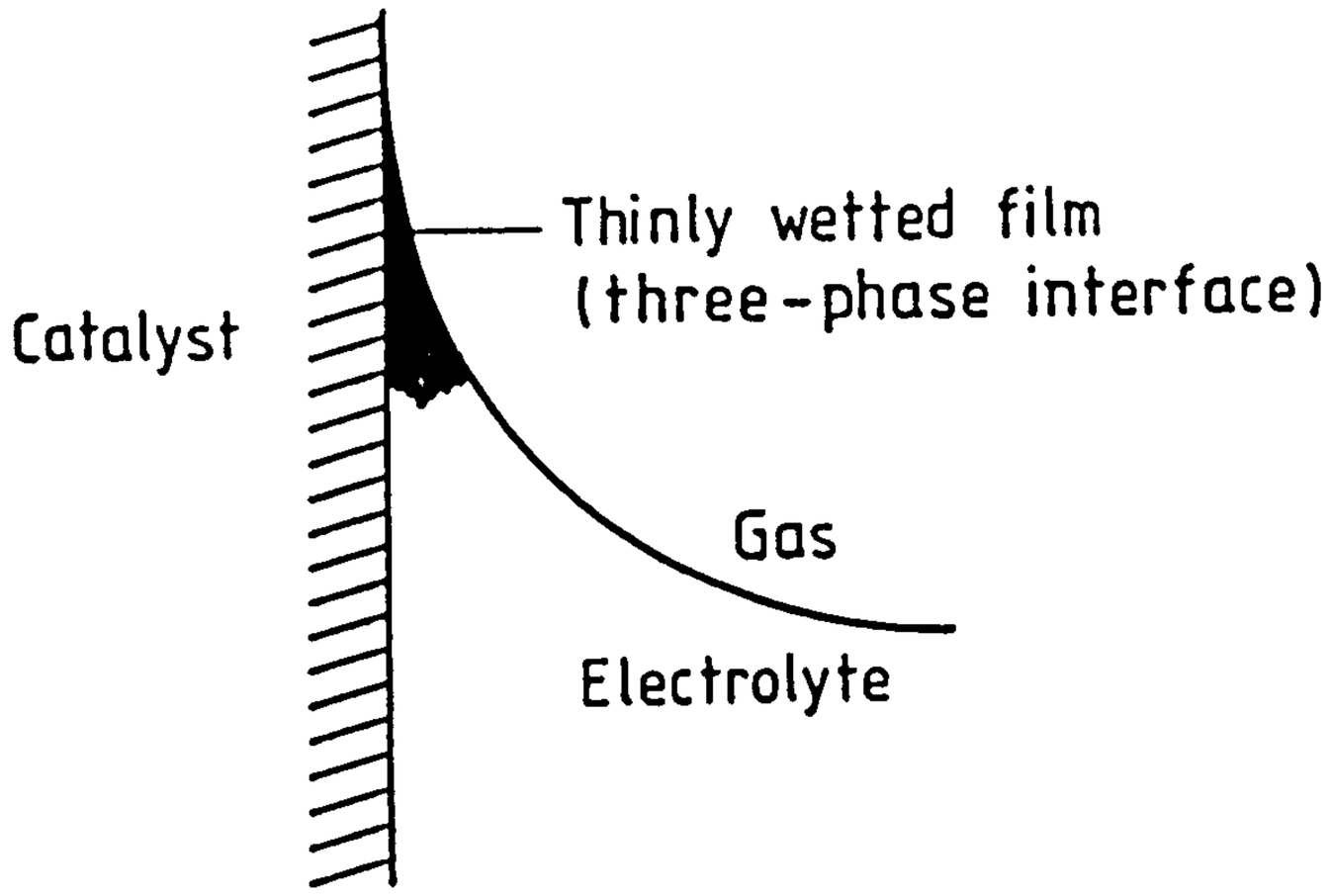

Figure 21 Schematic diagram of 3-phase interface.
[After Ref. 8 Fig. 6.6]

If all the catalyst particles are in good electronic contact with the external circuit and there is good ionic contact with the electrolyte, then efficient utilization of the catalyst surface will depend on mass transfer rates within the agglomerate.

2.6.2 Electrode Activity

The term 'electrode activity' has been used to denote the current generating capability of the electrode. There are two factors concerned with this (a) The catalytic activity of the catalyst which affects the kinetics of the actual electrochemical reaction. (b) The diffusibility of the electrode which affects the rate of mass transfer of the reactant eg. CO to the catalyst sites.

Factor (a) will be a function of the nature of the catalyst and its surface area. Other things being equal, activity should increase with surface area.

Factor (b) is a function of the path length and area available. Diffusion through the electrolyte should be the dominant factor, since rates of diffusion through solution are many orders of magnitude slower than through the gas phase. This diffusibility will be a function of the aggregate size of the catalyst agglomerates and will maximise with minimum agglomerate size.

Hence, diffusibility is the dominant factor determining the electrode activity. Increasing the surface area of the platinum beyond a certain point actually results in a reduction of electrode activity. This is because the aggregate size increases due to the higher bonding forces deriving from the higher surface energy.

This point was elegantly demonstrated with graphite catalyst by Tantram & Tseung[16] who showed that the maximum activity corresponded with the minimum aggregate size and at an intermediate value of the surface area (see (1) Fig. 22).

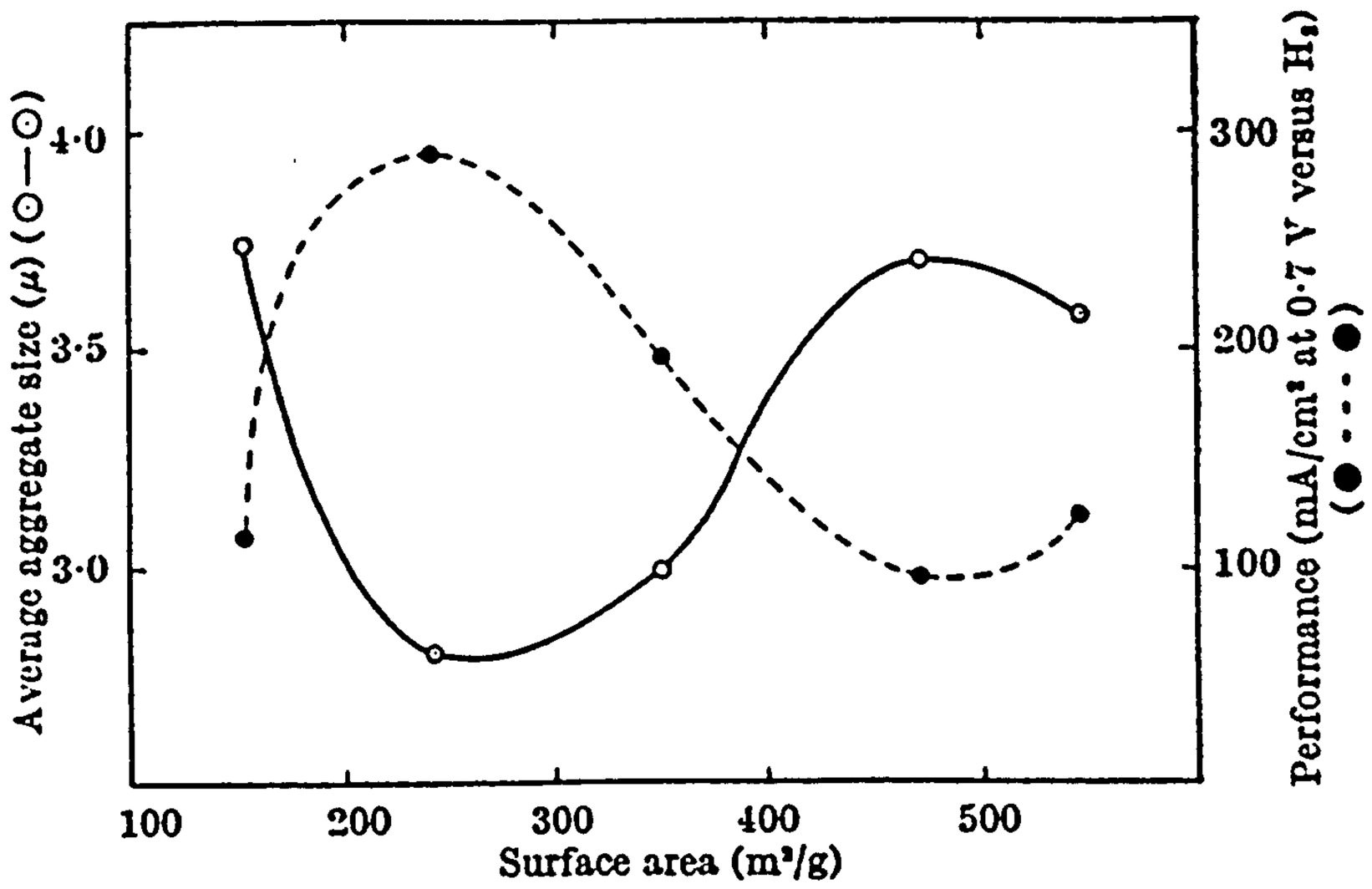

Figure 22 Variation of aggregate size with surface area compared with variation of performance with surface area [After Tantram ADS and Tseung ACC (1969) Nature 221 167]

2.6.3 Effect of Teflon Content on Electrode Performance

It has been established by Giner[110] et al that the electrode activity for hydrogen oxidation on platinum passes through a broad maximum over the range 15-50% Teflon. At both extremes the activity is found to drop off very quickly; at 15% the electrode is too hydrophilic, so that there are very long gas diffusion paths within the electrolyte and at 50% Teflon, the electrode is too hydrophobic so that there is poor electrolyte contact. Within the range of 20-40% Teflon, practically 100% of catalyst is known

to be wetted by the electrolyte and the electrode activity passes through a broad maximum.

Watanabe[111] et al also realised that it is important for low overpotential, high current density fuel cell electrodes to have a fine structure such that:

(1) most of the Pt clusters are flooded with electrolyte.
(2) reactant gas is transported to the clusters via the shortest pathway.

Watanabe et al confirmed Giner's finding that performance peaked at about 30% PTFE content for O_2 reduction, at a catalyst utilisation of ~75% (see (1) Fig. 23).

Electrode activity is also a function of the electro-catalyst surface area, the performance varying with the grade of platinum at fixed Teflon content. This is thought to be due to variations in microporosity (fraction

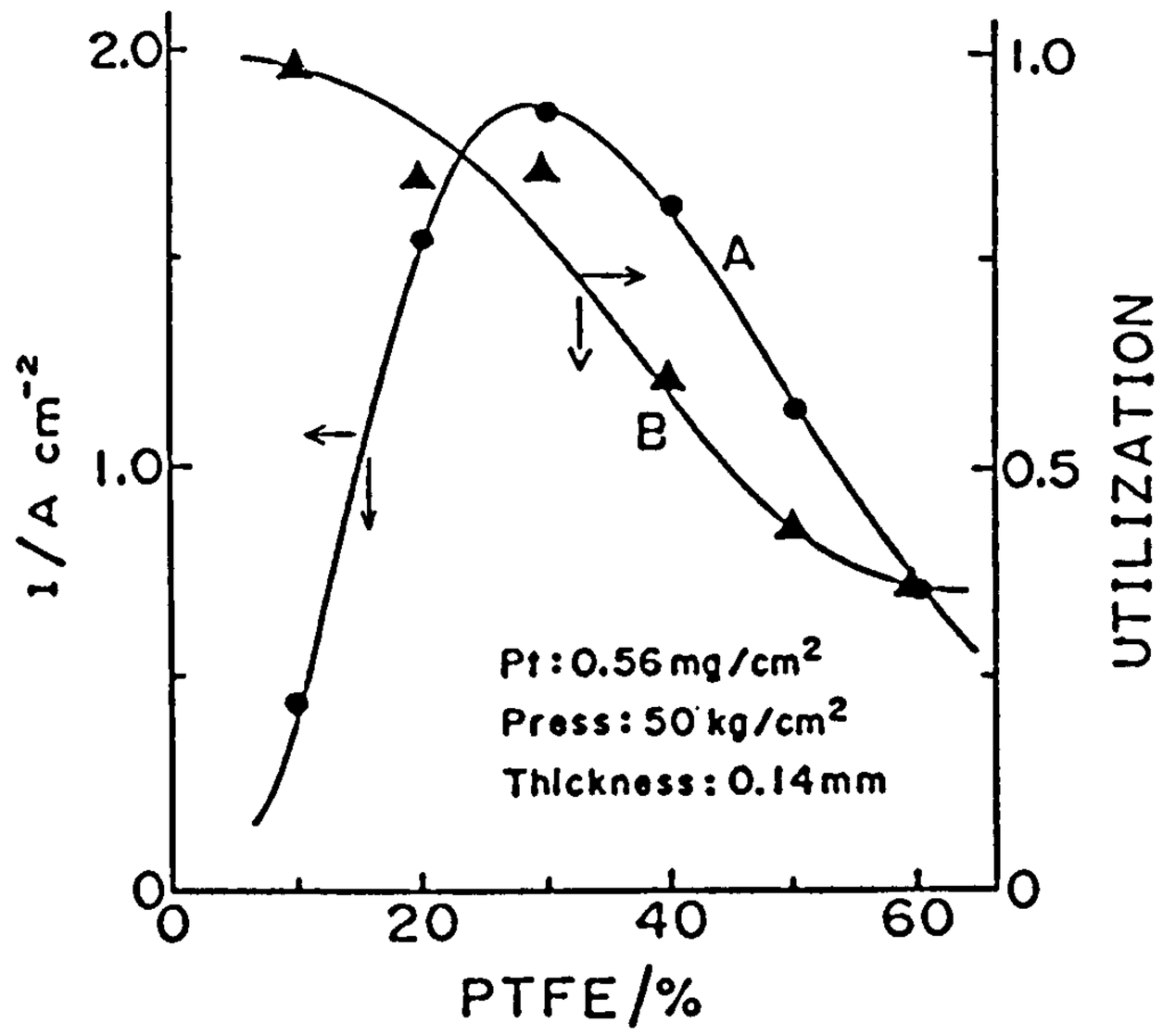

Figure 23 The effects of PTFE content on cathode performance (O_2) and the utilisation of platinum clusters. Thickness of reaction layer: 0.14mm; cool press: 50kg cm^{-2} [After Watanabe M et al (1985) J. Electroanal. Chem. 182 193]

of flooded agglomerate occupied by the electrolyte) and macroporosity (fraction of electrode not filled by the flooded agglomerate). For example, comparing different types of platinum black at 30% Teflon[110] it can be seen that microporosity varies from 80% to 90%, while macroporosity varies from 50 to 72%.

Agglomerate size is also an important characteristic of the Teflon-bonded electrode since it determines in part the radial utilization of the catalyst within the agglomerate[17,104].

CHAPTER 3 - SENSOR DESIGN

3.1 INTRODUCTION

The review of commercially available CO sensors and the statement of design objectives identified a number of problems which needed innovative solutions in order to meet the target specification for the design of a trace-level CO sensor for BCC's needs. It is worth listing these innovative solutions before discussing sensor design in depth.

Problem	Innovative Solution	Reference	
		Vol. 1	Vol. 2
(1) Leakage - seal integrity	'Sandwich' construction of electrode stack: (a) enables current collectors to be sealed between layers of porous PTFE tape, which forms a very effective electrolyte seal. (b) minimises the number of electrolyte sealing points, which benefits seal integrity.	3.5.1	10 6.1.2 12 3 13 2.1
(2) Leakage - internal pressurisation due to applied pressure, changes in temperature or changes in RH resulting in water uptake/loss	Gas vent in cover slip; hole made small enough to severely limit gas diffusion into reservoir, but not inhibit bulk flow.	3.5.14	13 2.2 14 3
(3) Controlled O_2 access to counter electrode	Unique 'sandwich' construction of electrode stack controls O_2 supply to counter electrode with negligible CO access: (a) O_2 feed via diffusion barrier and electrode tape peripheries. (b) O_2 feed via radial diffusion along counter electrode tape backing.	3.5.1.5	11 2.2 14 2.3 14 3

Problem	Innovative Solution	Reference	
		Vol. 1	Vol. 2
(4) Electrolyte water loss requiring frequent replenishment with distilled water	Use of 5M H_2SO_4 (in equilibrium at 63%RH) in conjunction with wick threaded through hole in counter electrode to link electrolyte expansion reservoir with electrode stack, gives maintenance-free continuous operation 20-90%RH and long residence time outside these limits.	3.5.1.7 4.11	10 6.2.6 11 4.1 11 4.3 12 5 13 5.1
(5) Orientation/shock stability	'Close-wicked' sandwich construction of electrode stack sealed with compression 'O'-ring demobilises the electrolyte within the electrode envelope, preventing gas bubbles tracking across the electrode face.	3.5.1	10 6.2.5 11 5.7 14 2.1
(6) Calibration drift	Use of very active fuel cell electrodes combined with gas diffusion barrier to limit open electrode signal more than 15 fold. This confers good long-term span stability.	2.5.3 3.5.3	10 4.3 10 6.1.3 10 6.1.4 11 3 13 App.3
(7) Span temperature sensitivity	Solution (6) gives low temperature coefficient - theoretically 0.17% of signal per °C at 20°C, but in practice a little higher.	3.5.4.1	10 6.2.4 13 4.5 13 5.2 13 App.3
(8) Signal pressure sensitivity	Solution (6) also gives low pressure coefficient ie. concentration measurement rather than partial pressure measurement.	3.5.4.1	14 4.5

Problem	Innovative Solution	Reference	
		Vol. 1	Vol. 2
(9) Baseline stability (a) 2-electrode (YRL) design	Use of similar 'matched pair' sensing and counter electrodes results in baselines typically less than 1ppm CO equivalent at 20°C.	3.5.3 3.5.4	10 2 12 8.1 13 4.2
(b) 3-electrode (CTL) design	Use of a third, reference electrode similar to the sensing electrode and run at zero bias results in baselines typically less than 1.5ppm CO equivalent at 20°C.	3.6	12 8.2 13 7 14 2.4
(10) Cross Interference (a) Inboard filter	Use of an inboard filter placed between capillary and electrode to remove interfering species by either chemical reaction or by physical adsorption.	3.5.1.9.2	13 5.3.2 13 App.2 14 6
(b) Auxiliary electrode	By transmitting partially reacting species to a second sensing (auxiliary) electrode and subtracting (ie. nulling) the cross-interfering signal.	3.7	(*)
(11) Size	The close-wicked sandwich construction with electrolyte expansion reservoir and vent is inherently compact, has good integrity and is amenable to production.	3.5.1	10 6 11 2 12 3 13 2 14 2

* Patents EP126 623, US 4,587,003

3.2 LABORATORY EQUIPMENT

Most of the experimental work was carried out using the following laboratory equipment:

THREE ELECTRODE POTENTIOSTAT	Ministat model 251 Thompson Electronics Ltd Newcastle Upon Tyne
DIGITAL VOLTMETER	Dana Laboratories Inc. Irvine CA USA Model 4600 S/N 505799
FLAT BED CHART RECORDER	Gould Electronics Ltd Model SC 272 Input Impedance 1MΩ (constant) Accuracy ±0.3% at 296 k Linearity ±0.25%
GAS BLENDER	H Wõstoff O.H.G. Bochum, Germany Type NA18/2 No. 14011 220V, 50Hz
ENVIRONMENTAL CABINET	Ringway Climatic Ltd London, UK Model RSS1008 Type SC10B 220V, 50Hz
MODIFIED CHROMATOGRAPH OVEN (Electrode curing up to 300°C)	Phillips Eindhoven, Holland Pye Unicam Type GLC2469 220V, 50Hz

FLOW METERS 0-100cm^3min^{-1} 0-500cm^3min^{-1} 0-1000cm^3min^{-1}	Platon Flowbits Ltd Platon Park, Viables Basingstoke, Hants RG22 4PS England
DYNAMIC HYDROGEN ELECTRODE (DHE)	See Appendix 5
GAS MIXTURES CO in 21% oxygen, balance N_2 supplied in aluminium cylinders at nominal values 50, 200 and 500ppm CO.	Rank Hilger Ltd BOC Ltd (Special Gases) 24 Deer Park Road London SW19 3UF
PLATINUM BLACK JM std. black ~$10m^2g^{-1}$ JM Fuel Cell grade ~$35m^2g$-1	Johnson Matthey Chemicals Orchard Road Royston, Hertfordshire SG8 5HE
Engelhard No. 4 ~$20m^2$ g^{-1}	Engelhard Sales Ltd Engineering Materials Group Valley Road, Cinderford Gloucestershire GL14 2PB
PTFE SUSPENSION	Whitford Plastics Ltd 10 Christleton Court Manor Park Runcorn, Cheshire WA7 1SU Grade ICI GP1
POROUS PTFE TAPE Thickness 7 thou water initiation pressure ~ 30psi	WL Gore & Associates (UK) Ltd West Pitkerro Ind. Est. Dundee Water Tayside DD5 3RX

3.3 EXPLORATORY WORK ON YRL SENSOR

At the start of the development programme, British Coal's Yorkshire Regional Laboratories (YRL) had successfully demonstrated that a commercially available three-electrode Ecolyser sensor could be modified to run as a simpler two-electrode trace level CO sensor although the linear measuring range was limited to 50ppm. This was achieved by shorting the counter and reference electrodes together to form the 2-electrode counter and linking this with the sensing electrode via a fixed load resistance (47Ω) to convert the cell current to a voltage output signal (see (2) 10 2.1.1). By replacing the plastic moulding containing channels[15] for pumping the test gas across the electrode face with a bronze sinter, the YRL cell was converted to a passive sampler, relying on carbon monoxide to reach the sensor by natural diffusion rather than having to pump the CO across the electrode face.

Comparison of the modified YRL cell and a similar modified Ecolyser run in 'pumped' mode gave similar sensitivities (see (2) 10 2.1), showing that the bronze sinter on the YRL cell was not diffusion limiting and that the limiting barrier was within the electrode itself, so for convenience the 'pumped' cell was used to study the YRL 2-electrode design.

All electrode potentials were referred to an external DHE reference electrode dipping into the cell via a luggin capillary (see (1) Fig. 24).

Baselines were established by purging with 'zero' cylinder air obtained from Rank Hilger. Span signals were obtained by purging with a nominal 50ppm CO/Air mixture at various flow rates up to 250cm^3min^{-1} to check for flow sensitivity.

Steady-state potentiostatic i-E curves were obtained by controlling the sensing electrode against the third, reference electrode within the cell.

Analysis of the Ecolyser electrolyte revealed that it contained 30cm^3 of 3.2M H_2SO_4, so this electrolyte was mostly used for the initial work. Some exploratory work was done with 4M NaOH and 4M potassium acetate/acetic acid mixtures,

which were found to be inactive for CO oxidation using Pt electrodes; gold showed good activity but was unsuitable because of massive CO_2 cross interference (see (2) 10 2.3 (B)).

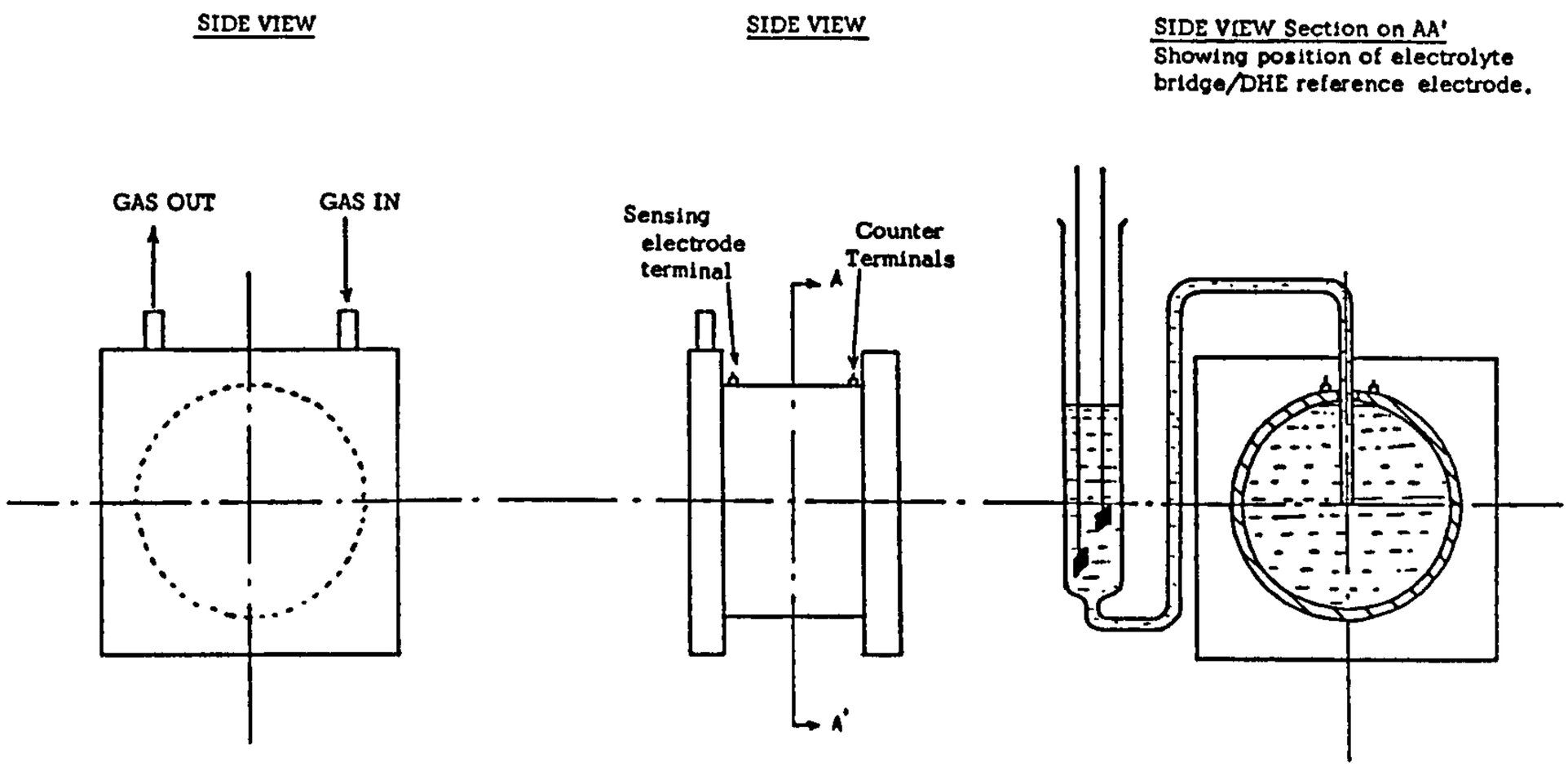

Figure 24 Diagram of Ecolyser Test Arrangement

[After CTL Report No. 79/31/002, (2) 10 Fig. 2.1]

3.3.1 Two-Electrode Dynamic Response

The Ecolyser sensor was used in its original purge configuration but otherwise run in the YRL 2-electrode mode with 47Ω load resistor.

During a 10 day period, baselines registered zero mV when purged with compressed air at flow rates between 0 and 200cm^3min^{-1}. With a resolution of 10μV on the DVM, this implied baselines less than 0.2μA (0.2ppm CO equivalent).

Initially, the cell potential rose to 1032mV after 24 hours and settled at 1050±50mV after 48 hours. Exposure to 49ppm CO/Air caused electrons to flow from sensing to counter electrode, indicating oxidation at the sensing and reduction at the counter electrode. The output generally stabilised within 10 to 30 seconds, as shown in (1) Fig. 25 and was fairly insensitive to flow rate above 80cm^3min^{-1}, producing 1μA/ppm CO or 0.2$\mu A/cm^2$/ppm CO for a working area of 5cm^2.

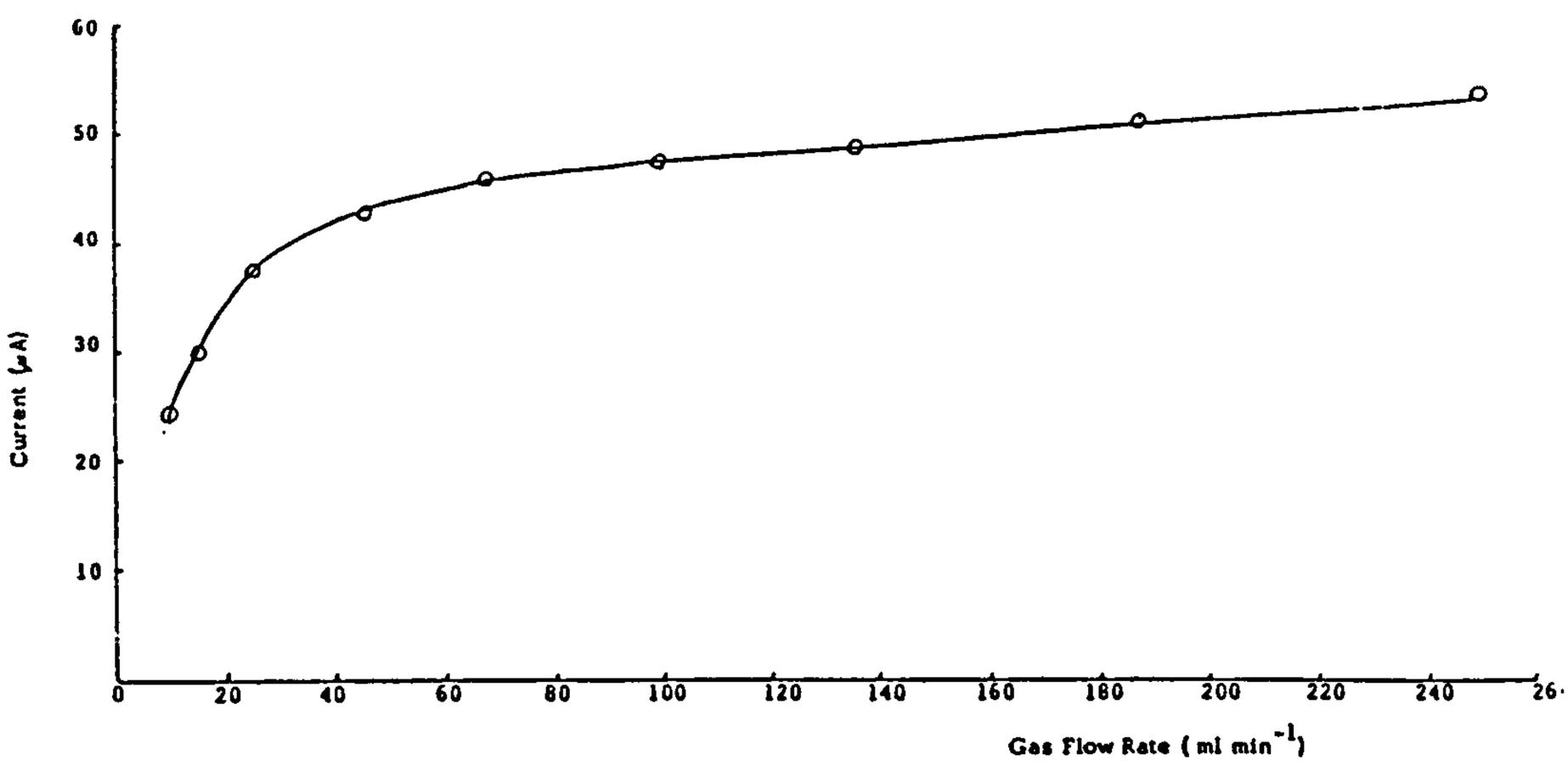

Figure 25 Output of Ecolyser Cell on a fixed load as a function of gas flow rate. Load resistor : 47Ω, temperature : 20°C, gas : 49.2ppm CO/Air, electrolyte : 3.4M H_2SO_4. [After CTL Report No. 79/31/002, (2) 10 Fig. 2.2]

The operating potential of the sensing electrode when exposed to CO (49.2ppm CO/Air, 100cm^{3}min^{-1}, 18°C) was 930mV vs DHE and the counter electrode potential was 1mV more anodic.

The change in output was followed with ambient temperature and indicated an underlying temperature coefficient of 3 to 4% of signal per °C, as shown in (1) Fig. 26.

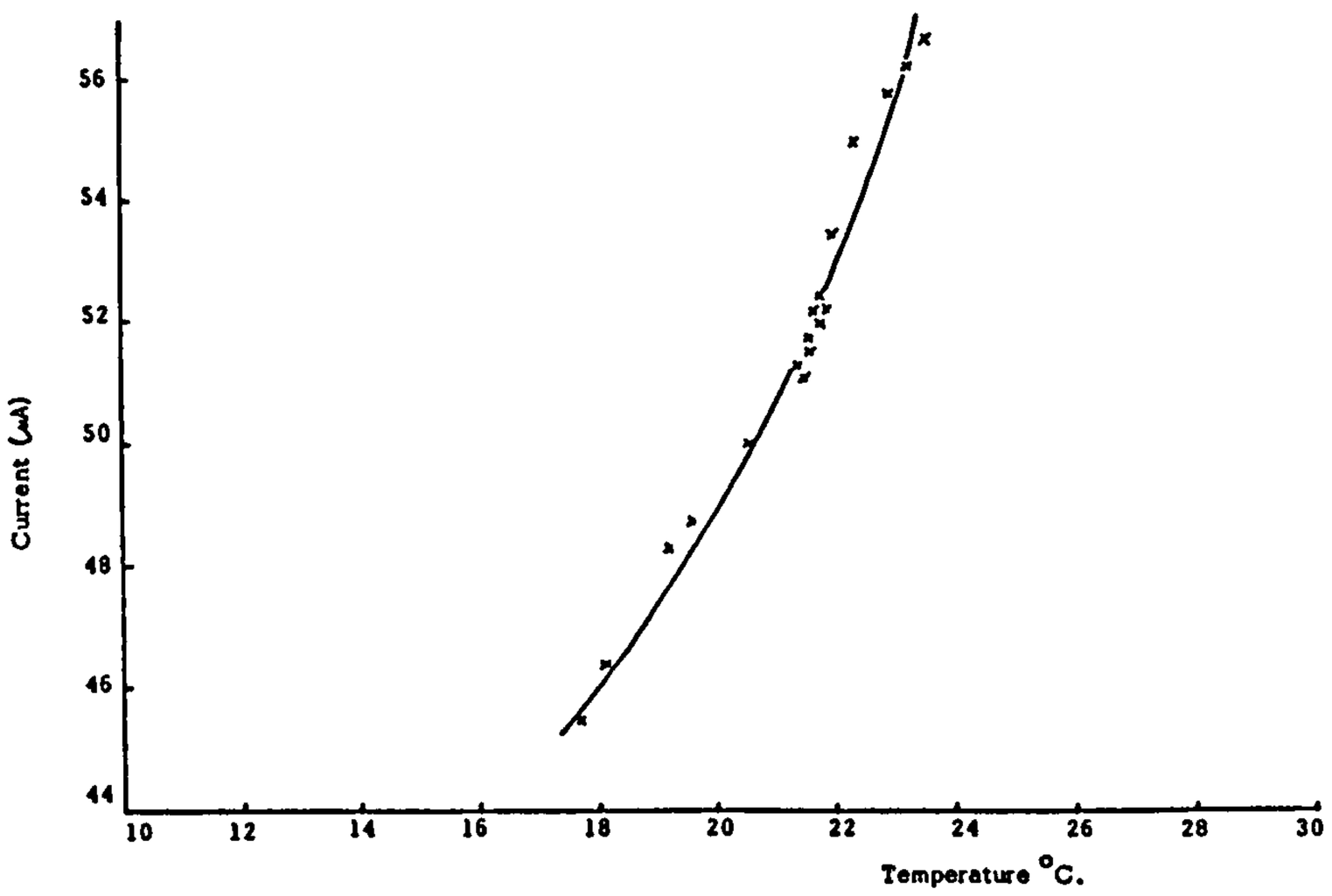

Figure 26 Temperature response of Ecolyser Cell. Load Resistor: 47Ω, gas : 49.2ppm CO/Air flow rate : 100cm^3 min^{-1}, electrolyte : 3.4M H_2SO_4. [After CTL Report No. 79/31/002, (2) 10 Fig. 2.3]

3.3.2 Steady State Potentiostatic i-E curves

Electrode potentials were scanned from 800mV to 1300mV in 50mV steps, allowing sufficient time for currents to reach steady state, typically 10-30 minutes at cathodic potentials and up to 48 hours at anodic potentials, due to oxide film growth (see (1) 2.3.2.2-3).

Net CO oxidation currents were obtained by subtracting the background Pt-O film oxidation currents.

The i-E curves for the sensing electrode in compressed air and the 49.2ppm CO/Air test gas are shown in (1) Fig. 27. The total CO oxidation current as a function of potential, obtained by subtracting the curves in (1) Fig. 27, tended to a limiting value of 130μA above about 900mV vs. DHE (see (1) Fig. 28). Considering the cell geometry and the above temperature coefficient measurement, this limiting current very likely arose from a controlling process of diffusion through an electrolyte film within the electrode (see (2) 10 2.1.2). Any diffusion control through gaseous barriers such as the PTFE backing tape would result in much lower temperature coefficients as for the CTL oxygen sensor.

With the air-cathode counter electrode arrangement used in the Ecolyser and YRL cells, the sensing electrode operating potential was cathodic relative to its OCV. Measured potentials on the DHE scale in (1) 3.3.1 were 1050mV in air and 930mV with a 49.2ppm CO/Air mixture. Under the latter conditions the sensing electrode supported both CO oxidation and oxygen reduction reactions and these coupled to form a parasitic local cell which consumed a significant proportion of the total CO oxidation current (see (2) 10 App.1). Thus the Ecolyser cell signal measured in (1) 3.3.1 was only about 49μA (49.2ppm CO/Air, 47Ω load, 20°C) instead of the 122μA indicated in (1) Fig. 28 at the operating potential of 930mV.

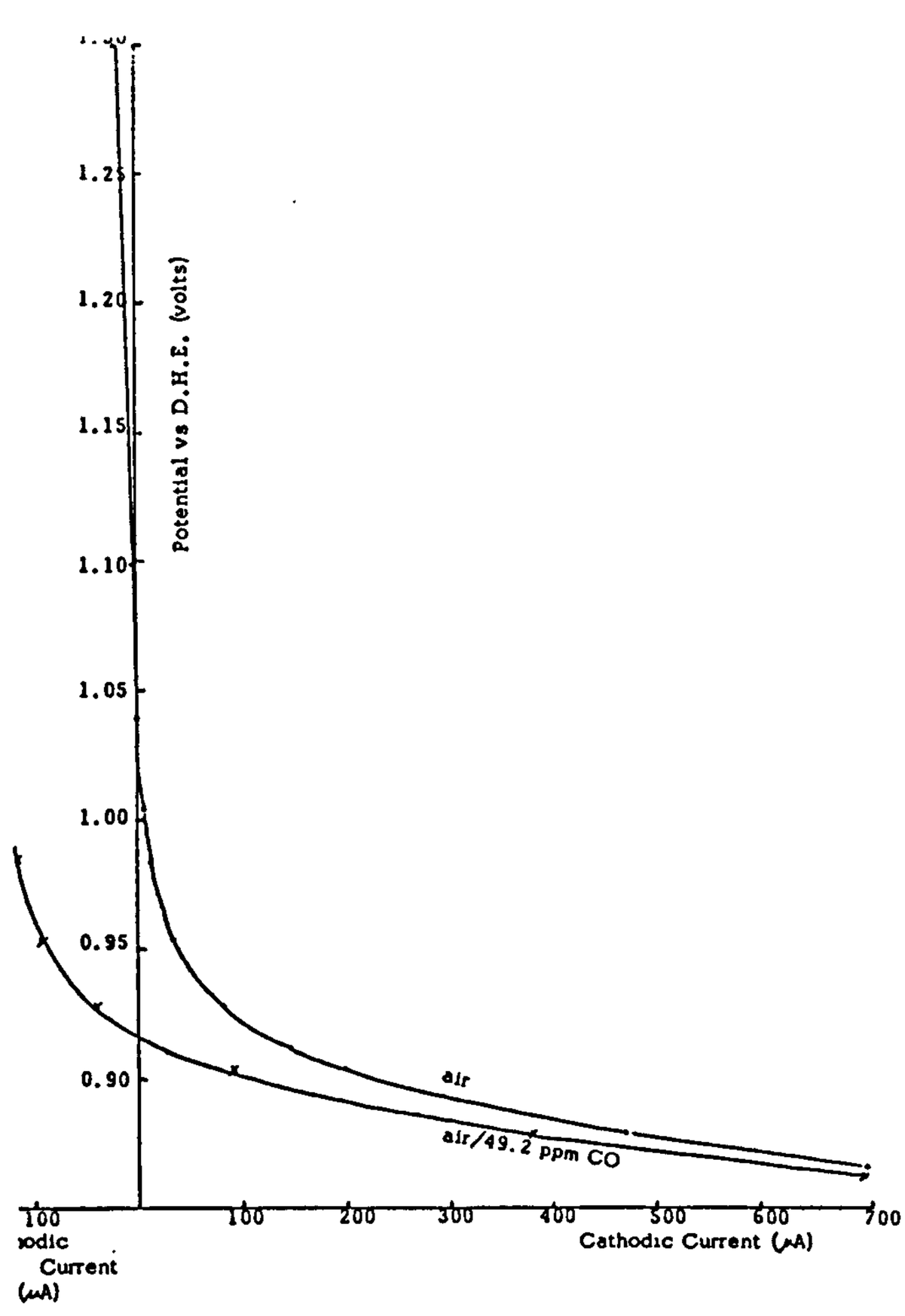

Figure 27 i-E curves for Ecolyser Cell. Gases : Air and 49.2ppm CO/Air, flow rate : 100cm^3 min^{-1}, reference electrode : DHE, temperature : 20°C, electrolyte : 3.4M H_2SO_4.

[After CTL Report No. 79/31/002, (2) 10 Fig. 2.4]

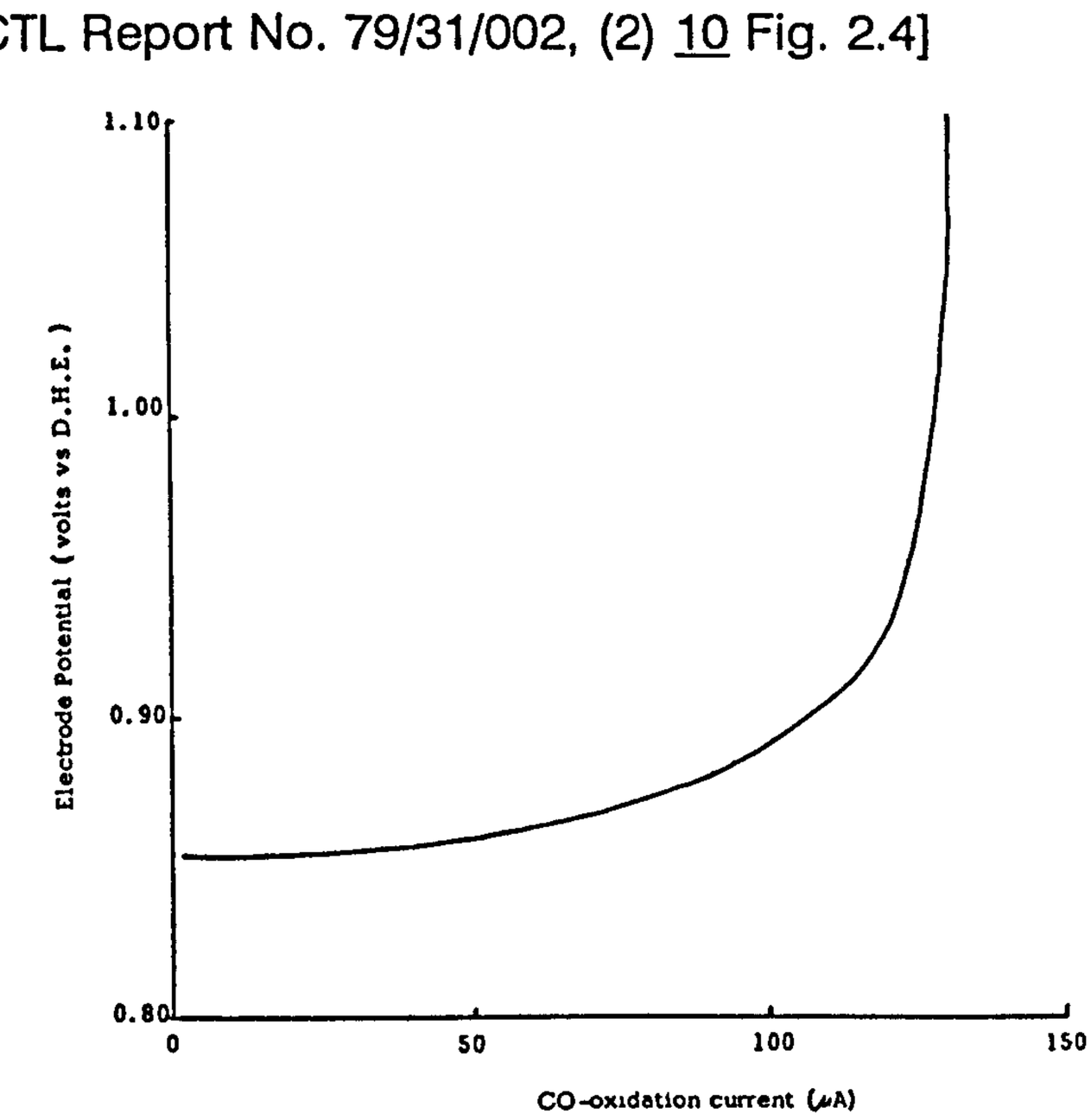

Figure 28 Derived CO oxidation i-E curve for Ecolyser Cell. Electrolyte 3.4M H_2SO_4, gas 49.2ppm CO/Air, flow rate : 100cm^3 min^{-1}, temperature : 20°C.[After CTL Report No. 79/31/002, (2) 10 Fig. 2.5]

An estimated cell signal at 930mV can be obtained from the data in (1) Figs. 27 and 28 and compared with the measured value of 49μA from (1) 3.3.1 as follows:

The sensing electrode rest potential in the CO/Air test gas is 920mV which corresponds to the intersection point of the CO-oxidation i-E curve ((1) Fig. 28) and the air/oxygen reduction curve ((1) Fig. 27), as redrawn in (1) Fig. 29. The current value of 117μA at this intersection

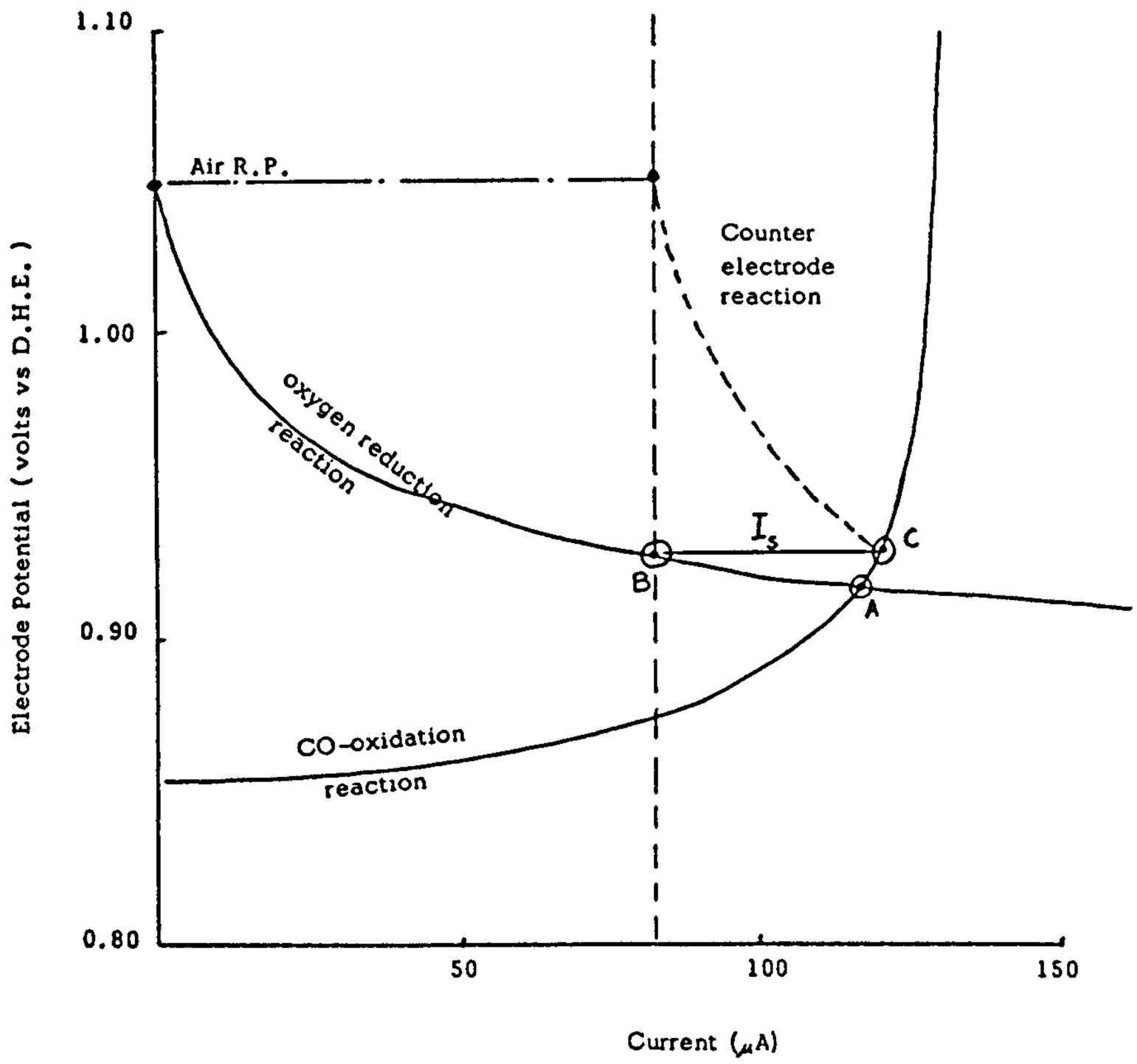

Figure 29 i-E curves for sensing electrode local cell and counter electrode in the Ecolyser Cell. Electrolyte : 3.4M H_2SO_4, flow rate : 100cm^3 min^{-1}, gases : compressed air and 49.2ppm CO/Air, temperature : 20°C.

[After CTL Report No. 79/31/002, (2) 10 Fig. 2.6]

is the local cell current at open circuit in the test gas. An air counter electrode connected via an external load causes the potential of the sensing electrode to rise from 920 to 930mV. The local cell oxygen

reduction current reduces to 83μA (point B, (1) Fig. 29), the total CO oxidation current increases slightly to 121μA (point C, (1) Fig. 29) and the difference of 38μA appears as a cathodic, oxygen reduction current on the counter electrode which represents the sensor signal (I_s). The correlation between this value and the measured value of 49μA is quite good, considering the errors expected in deriving the curve in (1) Fig. 28 (see (1) 2.1.2).

The i-E curve of the counter electrode was not measured, but it is evident that polarisation is greater than for oxygen reduction at the sensing electrode. (A likely curve is sketched in (1) Fig. 29). This originates from a greater contribution from oxygen diffusion resistance through the cell electrolyte at this electrode compared to the sensing electrode.

The use of a non-polarisable counter electrode such as battery cathode materials to hold the sensing electrode near the OCV would suppress the local cell at the sensing electrode and the total CO flux would appear as current in the sensor signal thus increasing sensitivity (see (2) 10 App.1). Alternatively, a third, unpolarised reference electrode could be included to hold the sensing electrode at or above OCV by means of a potentiostatic control circuit; a provision for this is included in the Ecolyser cell design which incorporates a split counter electrode arrangement.

3.3.3 Summary

The Ecolyser, platinum black electrodes exhibited a high, stable activity towards carbon monoxide oxidation and oxygen reduction in 3.4M sulphuric acid electrolyte.

- the CO oxidation current was probably controlled by diffusion through an electrolyte film within the electrode structure and had a limiting value under the conditions tested (20°C, 100cm^3 min^{-1} flow rate) of about 0.5μA per ppm CO per cm^2 electrode area.

- with the YRL 2-electrode arrangement, the sensing electrode operated at about 930mV vs. DHE in a test gas containing 49ppm CO in air. At this potential part of the electrode output was consumed by a local cell involving CO oxidation coupled with O_2 reduction. Consequently the cell sensitivity to CO under the test conditions was only 0.2μA per ppm per cm^2.

- PTFE bonded platinum electrodes were produced by foil transfer techniques as for the silver electrodes used in the CTL oxygen sensor. Some studies of alternative catalysts could be productive, particularly gold and supported gold which possessed poorer activity towards hydrogen oxidation than platinum.

- A more dilute acid electrolyte was desirable, being less corrosive, but YRL work has shown that this results in increased interference from hydrogen.

- Future development work would involve designing suitable corrosion resistant plastic hardware and assembly methods.

3.3.4 Conclusion

3.3.4.1 Sensor Electrochemistry

The carbon monoxide electrode reaction is represented by the equation:

$$CO + H_2O \rightarrow CO_2 + 2H^+ + 2e^- \qquad \text{Equ. (2)}$$

The open circuit potential, relative to a standard hydrogen electrode (arbitrary zero) at 25°C is given by the relationship[112]:

$$E = -0.103 - 0.0591\ pH + 0.0295 \log \frac{P_{CO_2}}{P_{CO}} \qquad \text{Equ. (19)}$$

Where P_{CO_2} and P_{CO} are the partial pressures of CO_2 and CO respectively and negative signs indicate potentials which are cathodic to the hydrogen zero potential.

The potential relative to a hydrogen electrode in the same electrolyte is then given by:

$$E = -0.103 + 0.0295 \log \frac{P_{CO_2}}{P_{CO}} \quad \ldots . (55)$$

If a true equilibrium was established at the electrode, the theoretical potential, relative to a hydrogen electrode in the same electrolyte, in the presence of a gas mixture of 1 atmosphere pressure, containing 50ppm CO, 0.03% CO_2 and the balance nitrogen (or some such electrochemically inert gas) would be -80mV (see (2) 10 App.1). Under these conditions CO is thermodynamically unstable towards water which it would tend to decompose with the evolution of hydrogen:

CO rn.	$CO + H_2O \rightarrow CO_2 + 2H^+ + 2e^-$	$E = -80mV$
H_2 rn.	$2H^+ + 2e^- \rightarrow H_2$	$E = zero$
Overall rn.	$CO + H_2O \rightarrow CO_2 + H_2$	$\ldots . (56)$

However, the carbon monoxide electrode reaction is highly irreversible and approaches equilibrium infinitely slowly at room temperatures, even with precious metal electrocatalysts or relatively high activity. Consequently measured rest potentials of carbon monoxide electrodes are invariably anodic (positive values) relative to a hydrogen reference electrode, ie. water decomposition ((1) Equ. 56) is not observed.

The anodic oxidation of carbon monoxide proceeds via a 'reactant pair' mechanism[21] in which electrode transfer occurs between the electrode and a surface intermediate composed of CO and H_2O molecules adsorbed on adjacent surface sites(see (1) 2.3.3). Precious metal surfaces such as platinum or gold which are normally used as electrocatalysts for the CO reaction, at potentials near or more cathodic to the normal hydrogen electrode, adsorb carbon monoxide strongly with high coverage. Under these conditions the reaction is severely inhibited by the low availability of surface sites for water molecule adsorption to form the reactant pairs. At more anodic potentials the noble metals form surface films of oxides or adsorbed oxygen which have much lower catalytic activity towards the CO reaction but act as adsorption sites for water molecules. CO-H_2O reactant pairs then form at the metal-oxide interfaces and the electrode can sustain CO oxidation currents at these potentials.

The onset of surface oxidation occurs at about 0.8 volts on the hydrogen scale for platinum (see (1) 2.3.2.2) and about 1.30 volts for gold[22], in sulphuric acid electrolyte. These potentials do not vary to any extent with solution pH, but in alkaline electrolyte adsorption films containing hydroxyl ions form at more cathodic potentials and may modify the kinetics of an electrode reaction (see (1) Ref. 22, p.29).

The surface coverage of a precious metal electrode with oxide increases with potential in the anodic direction (see (1) 2.3.2.3). Complete coverage only occurs at considerably more anodic potentials than those quoted above, but when such a condition is reached then the CO reaction will become inhibited by the low availability of suitable adsorption sites for the CO molecule and the electrode is said to be 'passivated'.

Platinum/gold powders, intimately mixed, might provide a more

active catalyst for CO oxidation than either alone. Gold surfaces are essentially free of oxide up to potentials of 1.3 volts (hydrogen scale) and would provide CO adsorption sites. Platinum surfaces above 0.8 volts are extensively covered with oxide for water adsorption. The Pt-Au interfaces would then provide a high number of reactant pair sites. Alternatively gold, supported on corrosion resistant oxides (eg. Fe_2O_3 in alkali electrolytes) could prove a suitable alternative to pure Pt.

3.3.4.2 Two-Electrode Mechanism

Oxygen is an electroactive gas and sets up an electrode reaction on platinum or gold electrodes which can be represented by the following equation in acid electrolytes:

$$2H_2O \rightarrow O_2 + 4H^+ + 4e^- \qquad \textbf{Equ. (14)}$$

The electrode potential relative to a normal hydrogen electrode in the same electrolyte is given by the relationship[28]:

$$E = 1.228 + 0.0148 \log Po_2 \qquad \textbf{Equ. (20)}$$

The theoretical potential for an electrode in contact with air (Po_2 = 0.20 atm) then becomes about 1.22 volts. This electrode reaction is also irreversible and measured values of air electrode rest potentials are about 1.05 volts in acid electrolytes (see (1) 2.3.1) and about 1.15 volts in alkaline media. The potential of a gas sensing electrode, exposed to air containing carbon monoxide, therefore sets up a mixed potential resulting from a local cell between the carbon monoxide and oxygen electrode reactions on the electrocatalyst surface:

Oxygen reduction	$O_2 + 4H^+ + 4e^- \rightarrow 2H_2O$	
CO oxidation	$2CO + 2H_2O \rightarrow 2CO_2 + 4H^+ + 4e^-$	
Local cell rn.	$O_2 + 2CO \rightarrow 2CO_2$	**Equ. (7)**

This can be represented schematically in the following diagram of the current-potential curves for the two electrode reactions - see (1) Fig. 30.

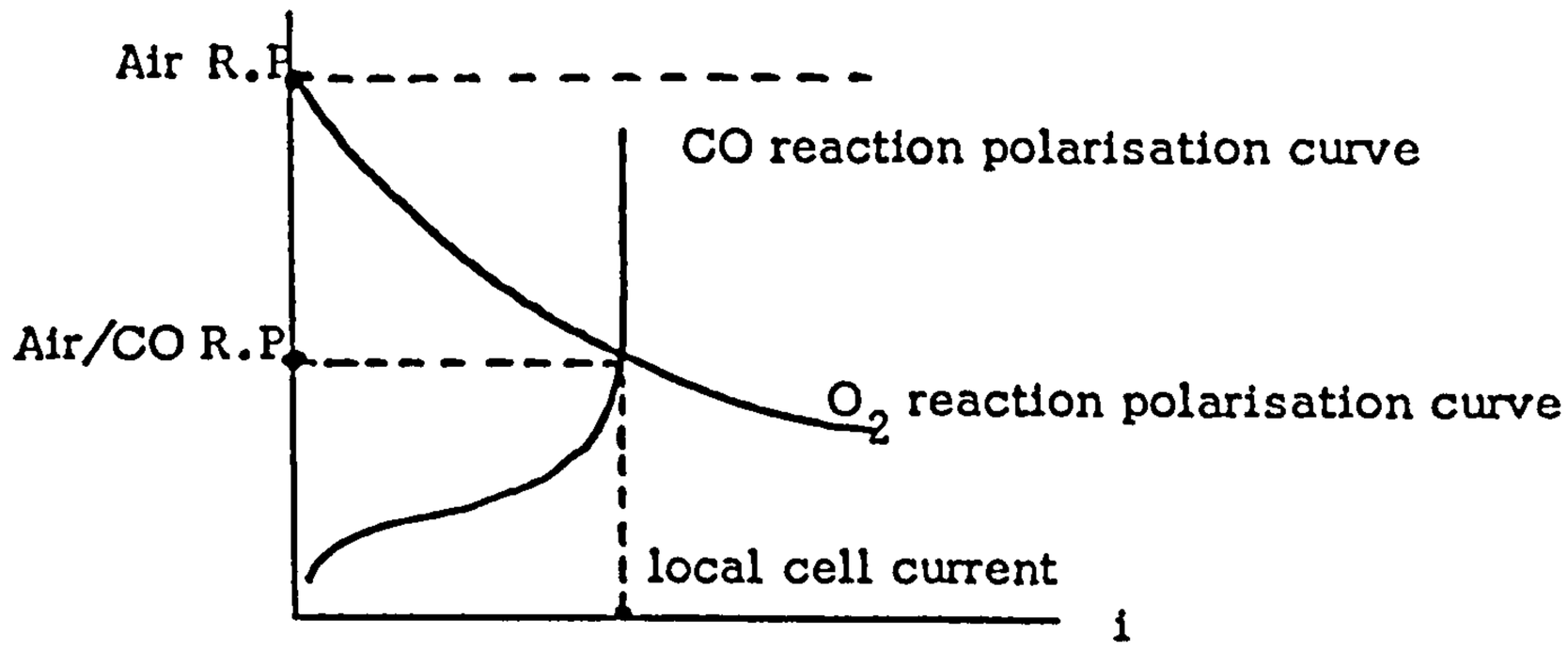

Figure 30 Schematic diagram showing the localised i-E curves for CO oxidation and parasitic O_2 reduction.
[After CTL Report No. 79/31/002 (2), 10 App.1 (iv)]

The mixed potential sensing electrode is connected via an external load circuit to an oxygen reduction counter electrode. In the YRL and Ecolyser cells this is an oxygen electrode located inside the cell so that it is not exposed to the CO in the atmosphere. The cells are designed to oxidise completely any carbon monoxide as it reaches the sensing electrode, but excess oxygen in the air dissolves in the electrolyte and diffuses to the counter electrode where it sets up an oxygen potential; since there is no carbon monoxide in the vicinity of the counter electrode, its potential will be higher than the mixed potential of the sensing electrode. With the load circuit closed, electrons flow from the sensing to the counter electrode and provide the 'signal' of the sensor. The sensor current in the external circuit causes the counter electrode to polarise to a steady potential, slightly above the sensing electrode depending on the load resistance. The counter effectively presents a larger area for the local cell oxygen reduction current at the sensing electrode

which therefore depolarizes. The situation at a fixed CO concentration in air is depicted schematically in (1) Fig. 31.

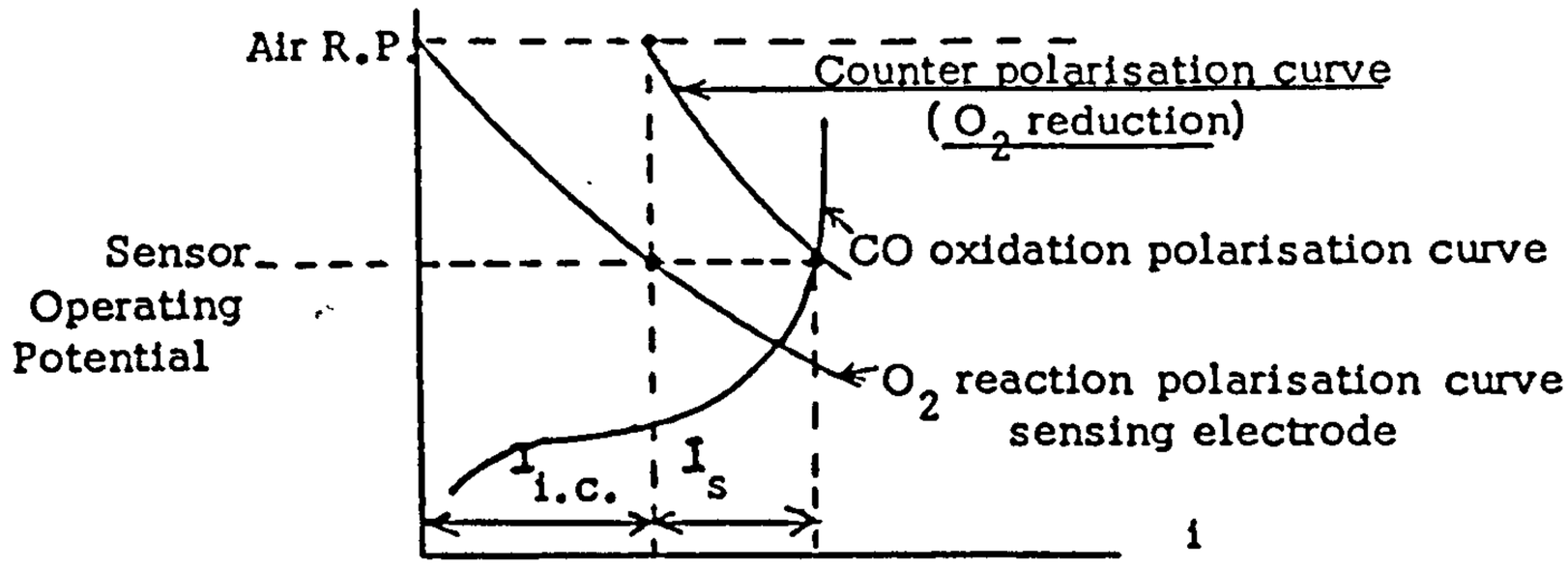

Figure 31 Schematic diagram showing the mixed potential (parasitic) anode and oxygen reduction cathode i-E curves.

$I_{i.c.}$ = local cell current, I_s = sensor signal

[After CTL Report No. 79/31/002, (2) 10 App.1 (v)]

In the YRL cell only part of the total CO-oxidation current appears as a signal in the instrument load circuit. The parasitic signal losses caused by the oxygen reduction reaction at the sensing electrode could be eliminated by employing either 2-electrode bias, or 3-electrode potentiostatic control as follows:

3.3.4.3 Two-Electrode Bias

An external circuit can be used to hold the sensing electrode at a fixed anodic potential difference with respect to the counter electrode (see (1) Fig. 32).

If the applied potential difference is greater than the counter electrode polarisation at the maximum CO-signal, then the sensing electrode will never polarise down to oxygen reduction potentials and the full CO signal will always be obtained,even under maximum sensor load. However this will be at the expense of a higher baseline.

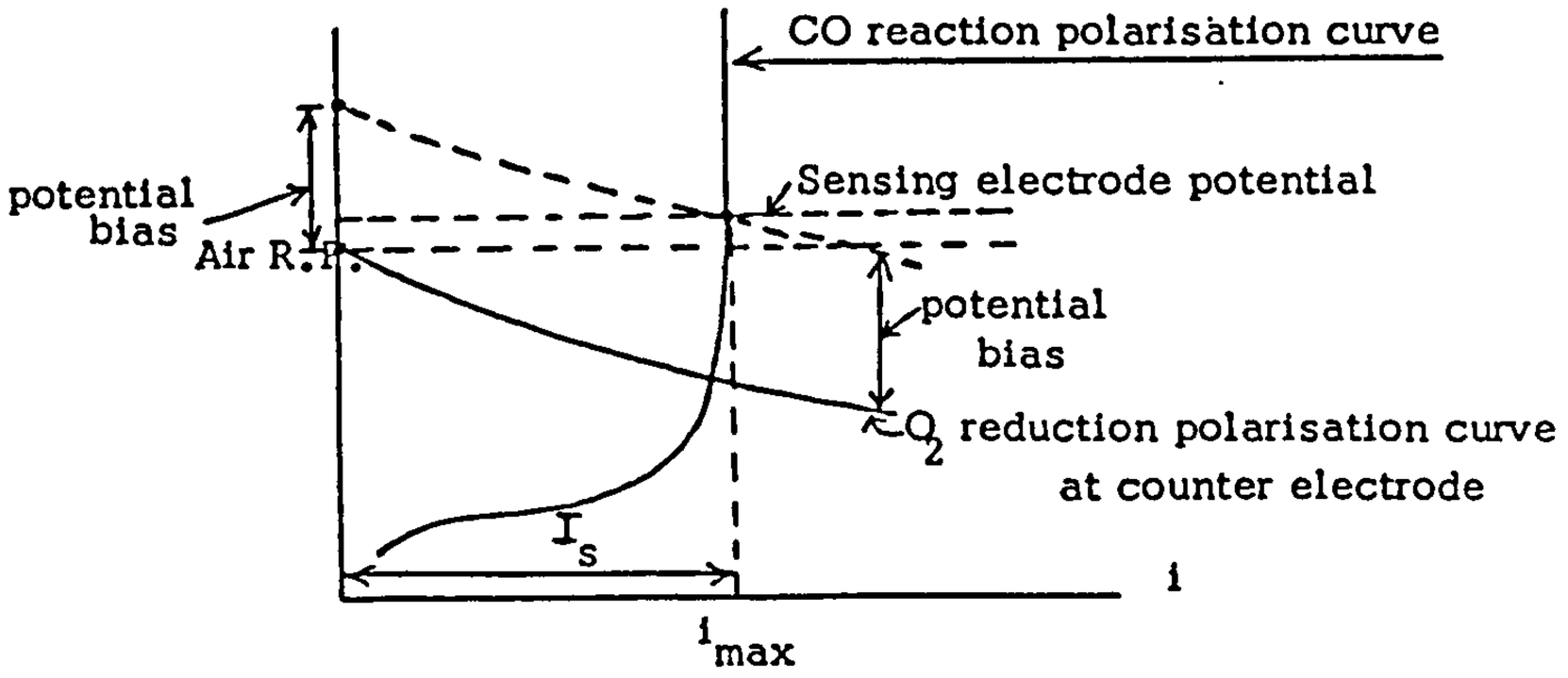

Figure 32 Schematic diagram showing 2-electrode potential bias application. I_s = sensor signal, i_{max} = maximum likely sensor current

[After CTL Report No. 79/31/002, (2) 10 App.1 (v)]

The potential bias should not be so great as to drive the sensing electrode into a 'passive' region, or to cause oxygen evolution.

3.3.4.4 Three Electrode Potentiostatic Control

A third unpolarised reference electrode, in conjunction with a potentiostatic control circuit, can be used to hold the sensing electrode at or above the air rest potential and thereby avoid O_2 reduction. The Ecolyser cell has provision for this mode of operation by employing a split cathode; one side functions as the reference electrode, the other acts as the cell counter electrode.

3.4 HALF CELL OPEN ELECTRODE MEASUREMENTS

3.4.1 Electrolyte : Selection of Acid Type and Concentration

Initially, four options were considered:

(a) concentrated sulphuric acid (3.4 - 6M)

(b) Dilute sulphuric acid (0.05-0.5M) with additions of magnesium sulphate (approx. 2M) to lower the electrolyte vapour pressure and reduce water loss.

(c) Dilute sulphuric acid with about 4M sodium perchlorate in place of magnesium sulphate as above.

(d) Perchloric acid/sodium perchlorate mixtures.

The dilute acids containing dissolved salts proved unsuitable; their vapour pressures and hence water evaporation rates were still high, electrode activity was much lower than with the pure acid and sensors gave erratic signals. Perchloric acid media were also rejected on the basis of possible fire hazard if a cell dried out (see (2) 11 4.1).

Sulphuric acid (5M) was selected for most of the work, having an equilibrium water vapour pressure equivalent to 63% relative humidity. This is roughly in balance with average ambient humidity in temperate climates; other acid concentrations could be selected to be in equilibrium with higher or lower average humidities, without affecting the sensor performance significantly (see (2) 11 3), eg. 2M, RH 92% and 7M, RH 39%. The variation of solution RH with sulphuric acid concentration is shown in (1) Fig.33 - this relationship is essentially unaffected by operating temperature.

3.4.2 Electrode Manufacture

Electrode manufacturing techniques, suitable for volume production without sacrificing performance, were examined. All techniques were based on the 'foil transfer' method whereby the catalyst layer was formed on aluminium foil and then transferred by pressing onto a porous PTFE backing tape to give the completed electrode (see (2) 10 3.1.1 and (2) 11 3.1). The fabrication methods can be classified as follows:

(i) Spray method

(ii) Drop method

(iii) Solvent extraction

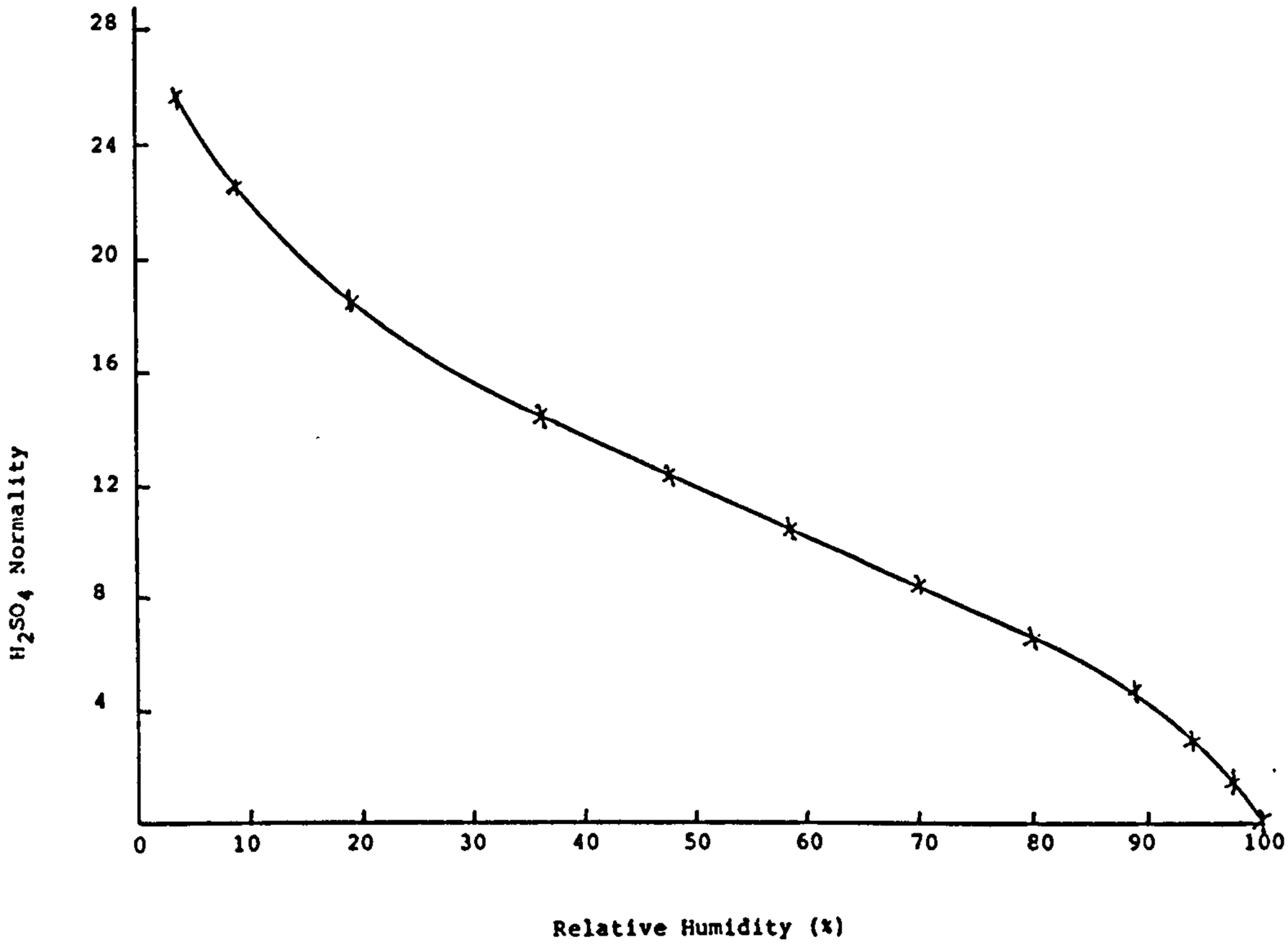

Figure 33 Relationship between relative humidity and concentration of aqueous sulphuric acid mixtures
[After CTL Report No. 80/31/003, (2) 11 Fig. 4.1]

The spray method was originally developed for silver catalysed electrodes, used in the CTL oxygen sensor. It is ideally suited to large scale production and results in good electrode characteristics. However, material wastage was very high due to overspray, offcuts, etc. and overall catalyst transfer efficiency was at best 40 to 50%.

Similarly, the solvent extraction method was considered too hazardous, using 2-propanol and much too labour intensive (see (2) 12 4.1).

The drop method, although quite labour intensive, achieved near 100% Pt utilisation efficiency and was adopted for production. With this method a free flowing slurry of platinum and PTFE dispersion in aqueous acetone was prepared, which was capable of being measured out in

aliquots with a graduated teat dropper into aluminium foil moulds. The procedure was as follows:

Platinum black was weighed out and mixed with an appropriate volume of diluted aqueous PTFE dispersion (ICI, GPI, Fluon dispersion) in an ultrasonic bath. A measured amount of acetone was added to produce a slurry having the required flow characteristics. An homogeneous suspension was maintained by transferring the slurry to a rotating cup, from which aliquots were taken by means of a teat dropper pipette and put into moulds lined with aluminium foil (see (2) 10 3.1.1 and (2) 11 3.1). When using standard Johnson Matthey platinum black, the catalyst moulds were allowed to dry overnight in ambient air. However, the more active Engelhard No. 4 black was dried by forced air circulation at room temperature for 20 minutes to minimise the contact time between foil and wet catalyst mix. This was necessary as prolonged drying resulted in excessive corrosion of the aluminium, due to formation of an oxygen/metal corrosion cell (see (2) 12 4.1).

After drying, the moulds were cured in a circulated air oven according to the following cycle:

- 5 minutes 50°C
- 5 minutes 100°C
- 45 minutes 280°C
- Removed from oven and cooled in ambient air.

The temperature was raised in stages in order to progressively drive off residual acetone before the mix became too hot. This avoided the possibility of local overheating of the catalyst surface by catalytic burning of any organic vapour. The high temperature stage was necessary to achieve the correct wetting properties of the catalyst by removing a surfactant used to stabilise the PTFE dispersion. After cooling, the catalyst castings were transferred from the foil substrate by pressure bonding on to porous PTFE tape.

3.4.3 Test Method

To ensure a stable sensor signal over long periods of time, with minimal temperature dependence, it is essential that the capillary holes present the principal diffusional resistance barrier to the incoming carbon monoxide reactant gas. In particular the electrode reaction polarisation resistance and diffusional resistance through the electrolyte should be at least 1/10th to 1/15th that of the gaseous diffusional barriers, ie. the electrocatalyst activity reserve should be at least 10 to 15 times the sensor signal (see (1) 2.5.3.1).

Early open electrode activity tests had been conducted with catalyst layers, pressure bonded to standard Gore porous PTFE tapes as used in the CTL oxygen sensor. However, diffusibility measurements (see (2) 11 App.1) indicated that this tape would limit at a carbon monoxide current of about 0.9μA/ppm/cm^2, equivalent to a CO signal of about 150μA, on the sensor electrode area of Π cm^2 in a 54ppm CO in air test gas. Measured electrode currents in fact limited at about 70 to 80μA in this test gas. Whilst this test method suffices to establish whether the electrode activity is above or below the target level of 10 to 15 times the corresponding sensor signal of 5.4μA on the 54ppm CO in air test gas, Π cm^2 area, it cannot distinguish between electrodes having different activities above the 70-80μA level and therefore cannot be used to optimise electrode activity as a function of catalyst type and catalyst/PTFE ratio. The electrode optimisation work therefore was conducted with thinner, more porous Gore tapes, having measured diffusibilities greater than 2.5μA/ppmCO/cm^2, i.e. signals in 54ppm CO in air test gas, and Π cm^2 area, of 430μA, or above an 80X factor over the sensor signal.

A new test cell was designed to accomodate the thinner backing tape (see (2) II Fig. 3.1). Electrode testing was restricted to measuring currents in aerobic conditions, using a 54ppm CO in air test gas, at potentials between the air rest potential and up to 100mV anodic overpotential (between about 1000 and 110mV vs. DHE) at ambient

temperature. Potentials were controlled by means of a potentiostat and a Pt/air electrode In this way no contamination by H_2 from the DHE occurred (see (2) II 3.2.1).

The tests were conducted by allowing the test electrode to settle for about half an hour at the air rest potential in static air. The steady background current was noted and test gas admitted to the electrode at a flow rate of about 200ml per minute. The response was monitored on a recorder and the difference between background and the steady test gas signal taken as the CO response of the electrode. This procedure was then repeated at 50 and 100mV anodic polarisation steps.

The following parameters were evaluated using the above procedure:

- effect of platinum/PTFE ratio, using standard Johnson Matthey platinum black in 5M H_2SO_4.
- effect of platinum loading using the standard J.M. black and a near optimum Pt/PTFE ratio.
- effect of platinum black grade and admixture with gold, using a near optimum metal/PTFE ratio.
- effects of ageing various electrode compositions in contact with 5M H_2SO_4.
- effect of H_2SO_4 concentration on various electrode compositions.

3.4.4 Open Electrode i-E Curves

(2) II Fig. 3.3 shows the effect of electrode potential on the signal obtained from the test gas, over the range 1000 to 1100mV vs. DHE, in 5M H_2SO_4, using freshly prepared, standard J.M. Pt black electrodes. A similar trend exists for aged electrodes and with other grades of Pt black.

The virtual independence of signal with potential indicates that the currents are diffusion controlled, either by the PTFE tape or the electrolyte film, or both. The range of currents measured, 155 to 295μA,

was well above both the standard tape and the sensor limits of 70 and 5.4μ respectively in the 54ppm CO in air test gas.

3.4.5 Effect of Pt/PTFE Ratio

(2) II Fig. 3.3 shows the variation of signals obtained at 1000mV vs. DHE, in 5M H_2SO_4, with freshly prepared standard J.M. Pt electrodes, at different Pt/PTFE ratios between 2:1 and 10:1.

Although there is a hint of an activity maximum at about a 6:1 Pt/PTFE ratio, considering the spread between replicate electrodes, there is little to choose between the measurements between 8:1 and 3:1 (see (1) 2.6.3).

The high spread between replicates could have been due to either variations in the very thin, porous, Gore PTFE tape used, or inherent variations introduced by the electrode preparation method.

The 2:1 electrode had a very sluggish response and was obviously too hydrophobic. A 10:1 replicate electrode was virtually inactive and may have flooded with electrolyte. The preferred range chosen was therefore, 6:1 to 4:1 for the standard J.M. grade of platinum black. Sensor tests conducted within this composition range to define more precisely the desired ratio indicated that the 4:1 electrodes gave a slightly faster sensor response than 6:1, but further work on other parameters, in particular temperature coefficient and long term signal stability, favoured 6:1 electrodes.

3.4.6 Grades of Platinum Black and Gold Admixtures

Production of Johnson Matthey, fuel cell grade platinum black, used in the initial development phase, ceased so two other grades of platinum were examined, Johnson Matthey standard black and Engelhard No. 4 black.

Standard J.M. black had a larger particle size (lower specific surface area) than J.M. fuel cell grade. Although this resulted in slightly reduced activity, response time was better (see (2) II 5.2).. On balance, the standard grade was selected on the basis of availability, cost and response time; the slight loss of activity was not important since the activity reserve was still adequate. However, both materials were assessed for long term performance in sensors.

Engelhard black has a particle size nearer to J.M. fuel cell grade. Its activity was about 20% higher than standard J.M. black in a 3:1 Pt:PTFE electrode, 5M H_2SO_4. Response times were longer than an equivalent standard J.M. electrode, particularly with higher load resistors. This material was considered as a fall-back option to J.M. fuel cell grade black.

A 1:1 mechanical mixture of platinum and gold was found to be less active than a similar plain, J.M. standard Pt electrode (2.8 compared to 4.3μA ppm^{-1} respectively, using 0.5M H_2SO_4 with catalyst : PTFE ratio 4:1). Although synergism may be obtained with the correct Pt/Au admixture, corrosion of gold in stronger acid ruled it out as a viable option (see (2) II 3.2.5).

3.4.7 Electrode Ageing Effects

A number of electrode variants were stored in 5M H_2SO_4 and periodically retested. The activities of these electrodes over a 30 day period are shown in (2) II Fig. 3.4. All electrodes showed an initial decline over the first week or two of between 18 to 32%, depending on composition, but stabilised thereafter (see (2) II 3.2.5).

3.4.8 Effect of Acid Concentration

The effects of H_2SO_4 concentration on the activity of 20-30 day aged, standard J.M. electrodes, and a fresh Engelhard No. 4 electrode, are shown in (2) II Fig. 3.5. Activity decreased linearly with increasing acid concentration up to 10M with all electrodes tested. The gradient of each

line was practically the same for all electrodes. Even at 10M the electrode signal was above 100μA with electrodes of Pt/PTFE ratio between 6:1 and 4:1, which is within the target specification of 10 to 15 times the sensor signal (5.4μA) (see (2) II 3.2.6).

3.5 TWO-ELECTRODE DESIGN

In its simplest form a fuel cell electrochemical sensor consists of the following basic elements (see (1) Fig. 34).

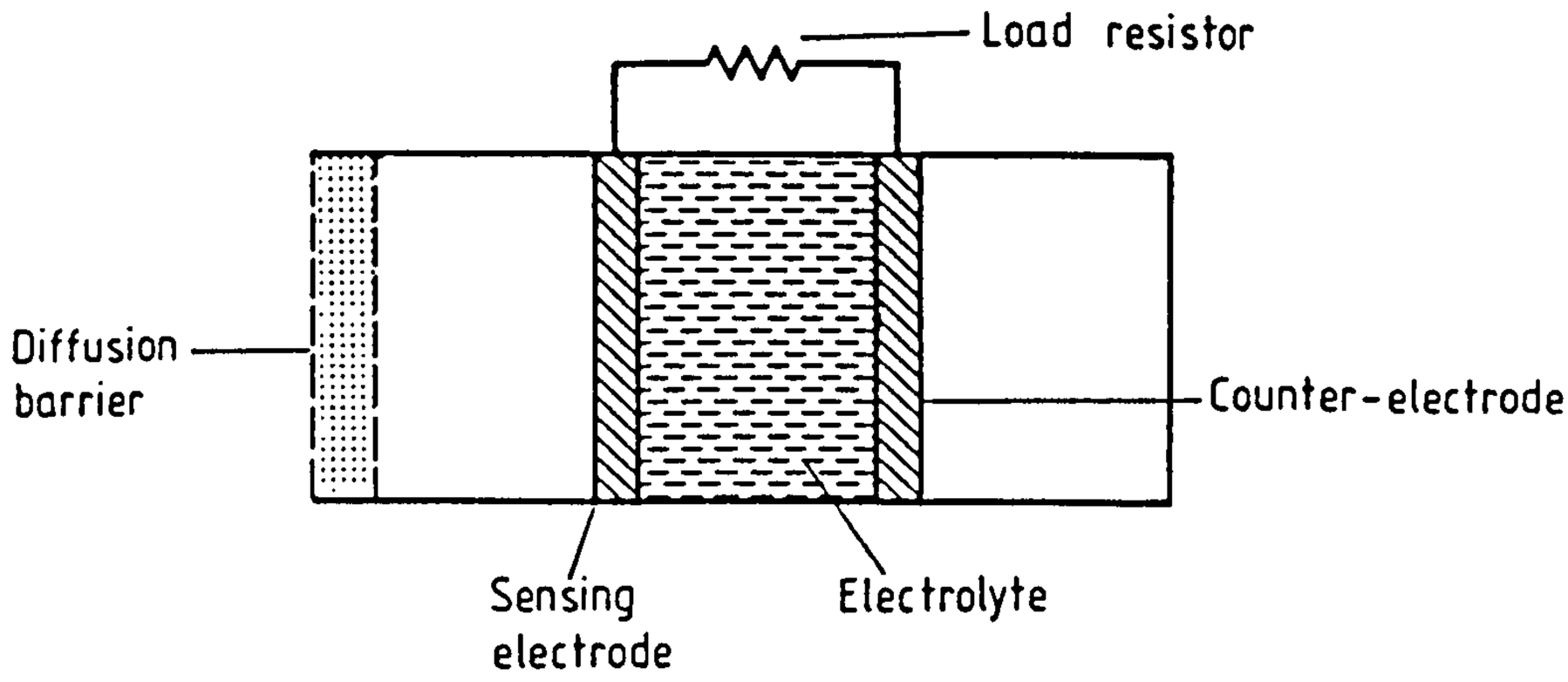

Figure 34 Schematic diagram of the basic elements of a fuel cell gas sensor [After Ref. 8 Fig. 6.1]

(a) Two similar gas diffusion, fuel cell electrodes. The sensing electrode has relatively easy access to external gases via the diffusion barrier. Conversely, the O_2 reduction counter electrode is located deep within the cell interior to provide controlled gas access, ensuring adequate supply of O_2 yet severely restricting CO access to the counter. How this is achieved is described in (1) 3.5.1.3.

(b) A concentrated, ionically conducting aqueous electrolyte separating the two electrodes, eg. a solution of sulphuric acid or alkaline solutions of sodium hydroxide or potassium hydroxide.

(c) A low-impedance external electrical circuit connecting the sensing electrode and counter electrode and providing a voltage output across a load resistor to measure the current output of the cell.

(d) A diffusion barrier controlling diffusion of reactant gases to the sensing electrode.

In clean ambient air, when reactant gases are absent, oxygen diffuses into the cell via the diffusion barrier and adsorbs on both electrodes to set up the air rest potential. Using a platinum electrocatalyst on the electrodes, this potential will be about 1V on the normal hydrogen electrode (NHE) scale and the electrode process is:

$$O_2 + 4H^+ + 4e^- \rightarrow 2H_2O \qquad \text{Equ. (3)}$$

The thermodynamic (or Nernst) potential of this process is about 1.2V in air at 20°C versus NHE. The oxygen reaction, however, is highly irreversible, even on platinum electrodes, and observed potentials are somewhat below this value (see (1) 2.3.1).

In clean air, when reactant gases are absent, both electrodes will assume the same potential and no current will flow in the external circuit. Actually a small baseline current is observed, involving oxide - oxygen reactions[22] on the electrocatalyst as a result of minor differences in the potentials of the two electrodes due to variations in the electrodes and their geometrical environments. With suitable electrode design the baseline current can be limited to below 0.1μA, representing less than one part per million equivalent of the reactant gas. Such baseline currents, and their associated temperature dependence (see (1) 4.3.1), are one of the principal factors establishing the lower limit of resolution of such electrochemical gas sensors. Cross-interferences are the other principal limitation.

If an electrochemically oxidizable gas (reducing gas), such as carbon monoxide, is present in the ambient air, it will diffuse to the sensing electrode and cause its potential to shift in a cathodic direction. The resulting potential difference between the sensing electrode and counter-electrode will then cause a current to flow in the external circuit, sustained by electrochemical oxidation of the reactant gas at the sensing electrode, matched by an equivalent amount of oxygen reduction at the counter-electrode. This is represented for a carbon monoxide sensor, with an acid electrolyte, by the following equations:

sensing electrode	$2CO + 2H_2O$	$\rightarrow 2CO_2 + 4H^+ + 4e^-$	
counter electrode	$O_2 + 4H^+ + 4e^-$	$\rightarrow 2H_2O$	
cell reaction	$2CO + O_2$	$\rightarrow 2CO_2$	**Equ. (7)**

In producing current during active sensing of carbon monoxide, the following dynamic conditions prevail.

(1) Carbon monoxide diffuses via the diffusion barrier to the sensing electrode where it is oxidised to carbon dioxide, consuming water, producing protons and releasing electrons to the external circuit.

(2) The carbon dioxide product is rejected by the acidic electrolyte and diffuses out of the cell via the diffusion barrier; the acidic electrolyte also prevents absorption of carbon dioxide from the external environment, which can cause spurious signals from pH gradients and carbonation in alkaline or near-neutral electrolytes.

(3) Protons produced at the sensing electrode migrate to the counter electrode and, together with electrons from the external circuit and oxygen, react to form water.

An oxygen supply must be provided to the counter electrode to sustain the current. Most applications are concerned with monitoring small concentrations of a gas in ambient air where a high concentration of oxygen is present (about 21%). Under these conditions an adequate oxygen supply to the counter electrode can readily be achieved, even though access is severely restricted and reactant diffusion to the counter electrode is negligible. When measurements need to be conducted with gas mixtures of very low oxygen content, a separate access of air to the counter electrode must be ensured.

The electrochemical power source is converted to a sensor by the inclusion of the diffusion barrier at the sensing electrode of the cell. The nature of this barrier is fundamentally important to the operation of the sensor and is designed to restrict access of the reactant gas so severely that it becomes completely oxidized as it arrives at the sensing electrode (see (1) 2.1.1). Under these conditions the concentration of reacting gas at the sensing electrode approaches zero; not only does this condition prevent reactant gas from accessing the counter-electrode and setting up a reverse reaction, but also the sensing-electrode reaction and resultant current become limited solely by the rate of gas diffusion through the barrier. The sensing electrode is then under mass transfer control and limiting current is observed (see (1) Fig. 35).

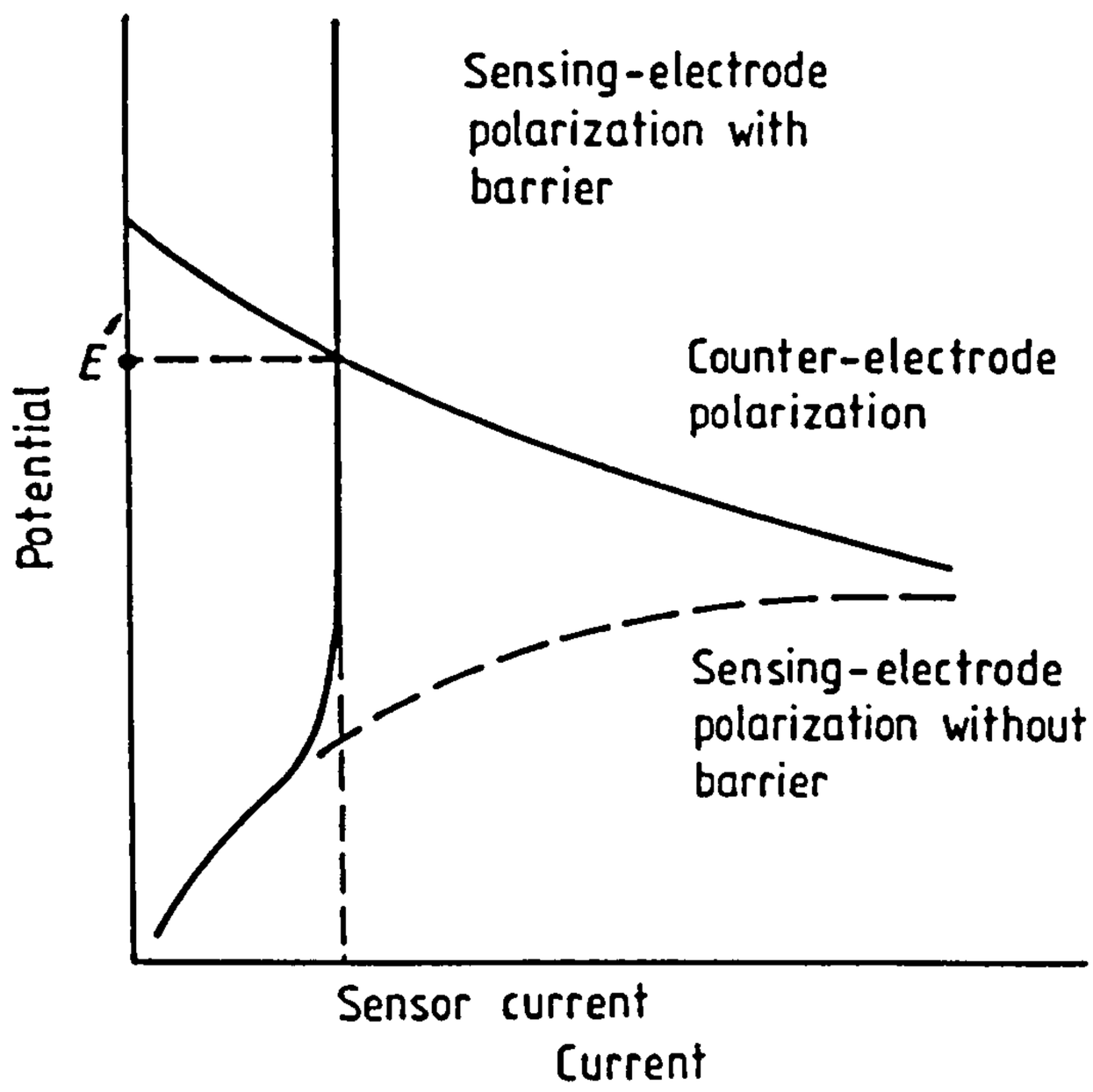

Figure 35 Schematic *i-E* polarisation characteristics for a two-electrode gas sensor. E' is the operating potential. [After (1) Ref. 8, Fig. 6.2]

3.5.1 Hardware Design

3.5.1.1 Materials Selection

Electrode/electrolyte investigations established a strong preference for acid electrolyte systems (see (1) 3.3.1). Early prototype sensors were machined out of perspex and sealed with neoprene O-rings (see (2) 10 6, (2) 11 2.3).

Electrodes consisted of PTFE-bonded Pt black catalyst, cured on aluminium foil and transferred by pressure bonding on to 25.4mm ø discs of porous PTFE backing tape (see (1) 3.4.2). Pt ribbon current collectors were used to lead the signal out of the sensor. Initially polyamide felt (Webril) separator and wicking material was used, but this was not acid stable in the long term and was replaced by glass filter mat material supplied by Whatman (see (2) 11 2.3).

The electrode stacking arrangement comprised a sensing and counter electrode envelope sandwiching some separator material (see (1) Fig. 36).

There are many novel features to this design which are subject to patent[113].

The electrode 'sandwich' construction (see (1) Fig. 36) with a communicating wick (part 4) threaded through a hole in the counter electrode (part 3) provided electrolyte contact with the expansion reservoir. This conferred the following advantages over existing designs such as the Ecolyser sensor.

- eliminated the problem of gas bubbles forming in the electrode compartment, due to water evaporation, which would otherwise cause severe orientation instability as the bubbles tracked across the electrode face.

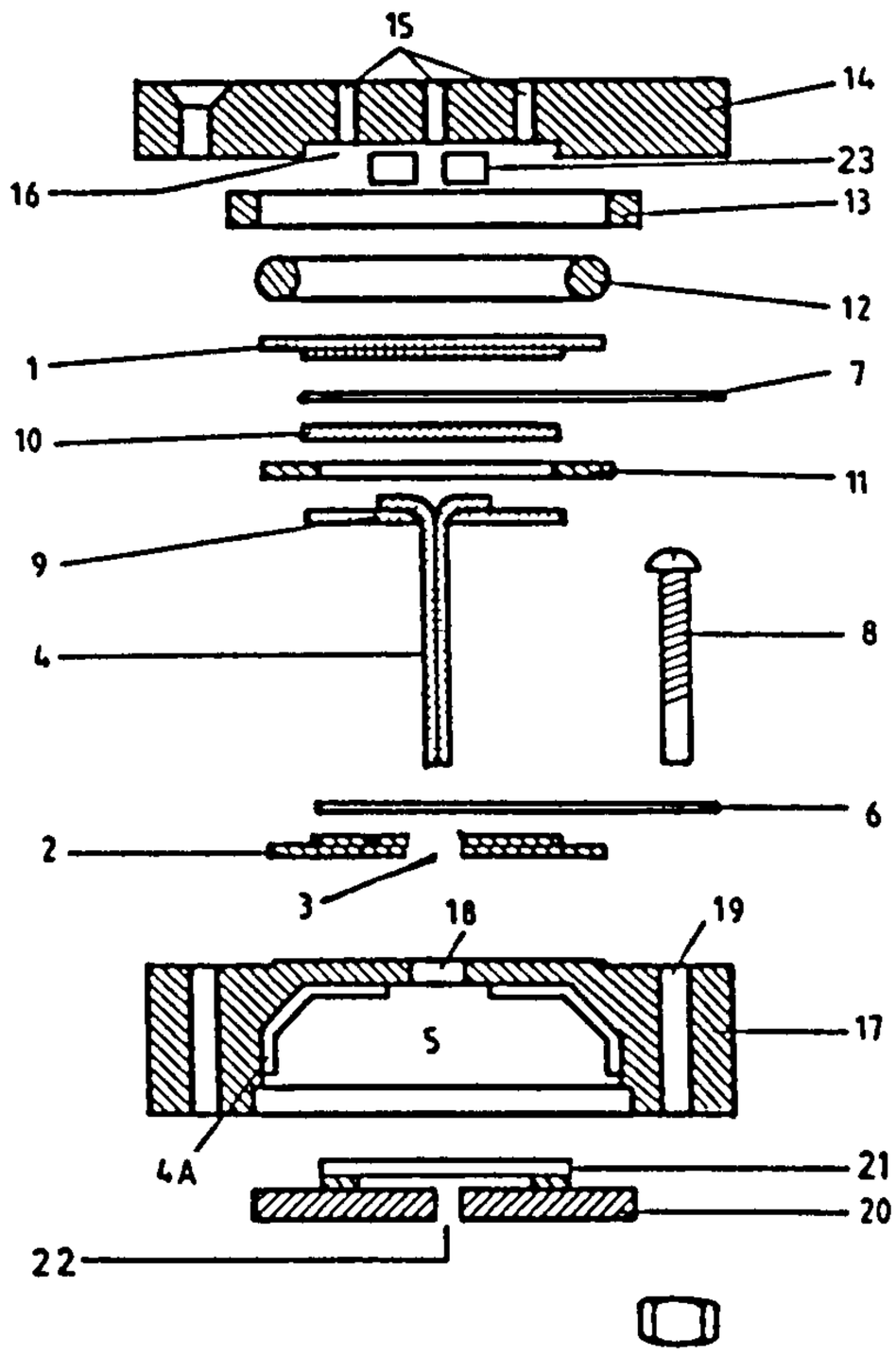

Figure 36 Schematic diagram of fuel cell acid-electrolyte sensor: (1) sensing electrode (2) counter electrode (3) counter electrode wick hole (4) wick (4A) wick extension (5) electrolyte reservoir, expansion chamber (6,7) contact (8) terminal bolts (9,10) separators (11) gasket (12) O-ring (13) retaining ring (14) top plate (15) capillaries (16) cavity (17) bottom plate (18) wick hole (19) terminal post holes (20) cover plate (21) PTFE tape (22) vent (23) electrode support [After (1) Ref.8 Fig. 6.13]

- provided direct O_2 gas access paths to the counter electrode by radial diffusion through the edge of the counter electrode backing tape, which ensured an adequate supply of O_2 and hence minimised cathode polarization under load (see (1) 3.5.1.5).

- the electrode 'sandwich' construction minimised the number of electrolyte sealing areas and therefore made sealing easier and more reliable.

Components not in direct contact with the electrolyte, eg. external electrical connectors, clamping bolts etc. were made from nickel or nickel plated steel. However, even minor electrolyte leaks (or tracking) corroded the bolts and solder tags and caused erratic and drifting signals.

In the latter stages of phase 3 development, an injection moulded polycarbonate version of the sensor was introduced (see (2) 12 3.2) in which the body components, base plate, floor and 'O' ring retainer were incorporated into a single base plate unit (see (2) 12 Fig. 3.4) and current collector tags were relocated to the clamping bolt pressure points to provide maximum sealing pressure and leak resistance.

3.5.1.2 Capillary Plate Modelling

Early machined prototype sensors using a 9-hole capillary pattern evenly distributed round an area of diameter 20mm and using a webril/mesh spacer to provide a 0.25mm gap between the capillary plate and the electrode, had measured sensitivities of 0.10μA/ppm CO, much lower than the calculated sensitivity of 0.51μA/ppm (see (2) 10 6.3.1). This was confirmed in later work, when capillary control was found to be only 20-25% (see (2) 11 2.4). Since sensor temperature coefficients were found to be 0.2-0.4% of signal per °C (see (2) 10 6.2) the additional diffusion resistance was most likely gaseous (0.17% per °C) rather than a liquid film barrier (3% per °C) such as one would find in the electrode structure.

Detailed analysis (see (2) 12 App.1) of the relative contributions to diffusion resistance of capillary and spreading resistance, ie. air gap between capillary and electrode, showed that the webril diffuser

(0.25mm air gap equivalent) accounted for 75% of the diffusion resistance control (see (2) 12 Fig. A1.1). Consequently, the moulded capillary plate diffusion gap was set at 2.5mm, so that the capillaries were at least 95% in control (see (2) 12 Fig. A1.2).

3.5.1.3 Counter Electrode Oxygen Access Calculation

A supply of oxygen to the counter electrode is essential in order to minimise cathode polarisation. There are two main gaseous O_2 feed paths for the counter electrode, namely via the sensing electrode cavity, across the perimeters of the electrode tapes which are in contact with each other and side access via the current collector gates (see (1) 3.5.1.5). Both these paths rely on radial diffusion along the backing tape to reach the cathode.

At one extreme, if the oxygen flux to the counter is insufficient to maintain the sensor current, then the counter electrode will limit rather than the sensing electrode and the sensor will effectively saturate. Even before this limit is reached any diffusion resistance, sufficient to lower the oxygen partial pressure at the counter electrode, will produce added polarisation and contribute to non-linearity.

The limiting flux of oxygen to the counter electrode therefore, needs to be equivalent to many times the sensor current.

At the other extreme, and in the case where the whole sensor is exposed to the atmosphere under test, if there is too much gas access to the counter electrode, an appreciable amount of carbon monoxide will reach the counter electrode, resulting in loss of signal. For example with identical sensing and counter electrodes, having identical gas access, the signal would be zero. The diffusibility to the counter therefore needs to be many times less than that to the sensing electrode.

It is possible to calculate the oxygen supply requirements to the counter electrode, making various assumptions (see (2) 11 2.2). The treatment below assumes that the sensor is completely diffusion limited, which is not necessarily the case. However, it can still be of some value in setting approximate guidelines.

Take: **sensor signal (μA) = fx** **. . . . (57)**

where x is the CO concentration in ppm

f is sensitivity in μA per ppm

Assuming diffusion limiting conditions, the sensor signal in ambient air (21 x 10^4 ppm of O_2) is given by:

i_L (O_2 to sensing in μA) = 42 x 10^4f **. . . . (58)**

(the factor of 2 appears because 1 mol of O_2 is electrochemically equivalent to 2 mols of CO).

If the gas flux to the counter electrode is much less than that to the sensing electrode, say at least by a factor b, so:

$$i_L (O_2 \text{ counter}) \leq \frac{42 \times 10^4}{b} f \qquad \text{. . . . (59)}$$

The other condition is that the oxygen flux to the counter electrode should be much greater compared to the sensor current, say at least by a factor 'a':

i_L (O_2 counter) ≥ afx **. . . . (60)**

(in μA)

Equating (1) Equ. (59) and (1) Equ. (60) gives:

$$ax \leq \frac{42 \times 10^4}{b} \quad \ldots\ldots (61)$$

$$\text{or} \quad x \leq \frac{42 \times 10^4}{a \times b} \text{ ppm} \quad \ldots\ldots (62)$$

Note that these equations are independent of the sensitivity factor f.

The counter electrode will be at its ultimate limit when a = 1, so that the ultimate sensor saturation point is given by:

$$x = \frac{42 \times 10^4}{b} \quad \ldots\ldots (63)$$

eg. if b = 84 the limit would be 5000ppm.

In practice the sensor will suffer appreciably before the ultimate limit is reached, ie. with a > 1, particularly with the balanced pair mode of operation where relatively small increases in counter electrode polarisation can affect the signal, since the sensing electrode is not truly into a limiting current region because of local cell effects (see (1) 3.3.4.2).

Gas supply to the counter electrode via the sensing electrode by dissolution and transport across the electrolyte sandwich is negligible because diffusion rates of gases in solution are four to five orders of magnitude slower than that in the gas phase.

All designs of carbon monoxide sensor, based on this principle therefore, need a specially designed air access to the counter electrode. The access must of course be restricted so as to deny any significant access of carbon monoxide in the atmosphere to the

counter electrode. The porous PTFE tape, supporting the catalysed electrode, projects beyond the cell seal into the atmosphere; this tape then presents a diffusion path for gases to the electrode (see (2) 13 2.3). The diffusion path is highly restrictive relative to the sensing electrode access - measurements indicated oxygen diffusibility rates in air were about 80 times lower relative to the sensing electrode access but, because oxygen is present in much higher concentrations than carbon monoxide, the oxygen supply rate can satisfy the counter electrode without any significant interference from carbon monoxide.

3.5.1.4 Pressure Release Vent

Water uptake and/or heating pressurises the gas in the electrolyte reservoir which, if not vented adequately, can cause electrolyte leakage through the sensor current collector seal (see (1) 5.1.3). This was alleviated by a pinhole of 0.2mm ø, 1mm length in the back coverplate (see (2) 13 2.2.1), protected from electrolyte leakage by a porous PTFE membrane, shown schematically in (1) Fig. 37.

The PTFE membrane also provides a gas diffusion pathway to the pinhole, even when the hole becomes obscured by electrolyte. However, venting is not possible if the membrane is totally obscured eg. if operating in a horizontal position with capillaries facing upwards. In this position, any free liquid in the reservoir, resulting from excessive moisture pick-up, can form a continuous film over the PTFE and thereby prevent venting.

A gas access path to the electrode sandwich may be traced via the pressure release pinhole, into the electrolyte reservoir and through the wick hole. Carbon monoxide entering through the pin hole, particularly during prolonged and/or high concentration exposures, could interfere with the sensor signal and cause prolonged hysteresis during recovery, since the reservoir would provide a large store of carbon monoxide.

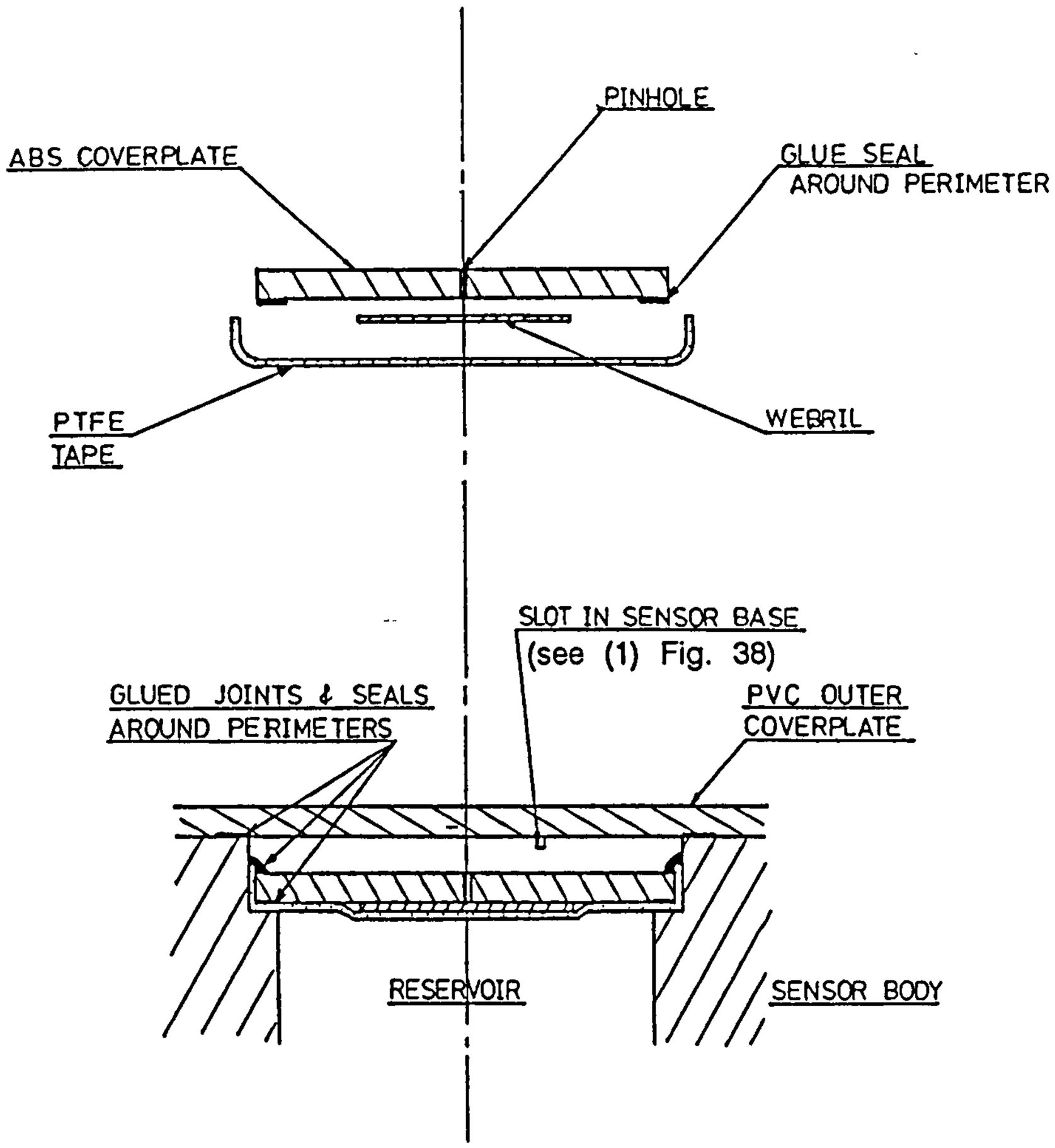

Figure 37 Schematic drawing of the Pressure Release System & Rear Coverplate Seal Design [After CTL Report No. 82/09/007, (2) 13 Fig. 2.5]

In practice however, total exposure tests and tests conducted by exposing only the pinhole, using 500ppm CO in air, showed no measurable signal even after 30 minutes exposure (see (2) 13 2.2.2). Presumably, the wick hole is flooded with electrolyte.

3.5.1.5 Gate Gas Access Control

The principal gas access routes to the sensor interior are:

(a) front access, through the sensor capillaries, directly onto the sensing electrode, where carbon monoxide is immediately oxidised, dropping its partial pressure substantially to zero. However, oxygen is not consumed and can therefore further diffuse from the sensing electrode cavity, across the perimeters of the electrode tapes where they are in contact with each

other, and then radially inwards to the counter electrode (see (2) 13 2.3).

(b) side access, through the current collector gates in the sensor counter plate (see (1) Fig. 38) and diffusion through the sensing and counter electrode PTFE tapes which protrude beyond the 'O' ring seal area.

(c) rear access from the electrolyte reservoir (see (1) 3.5.1.4).

The latter, by inference from the tests described (1) 3.5.1.4 above, is highly restricted, since no measurable diffusion of carbon monoxide could be detected.

Early attempts to assess these gas access routes using machined sensors (see (2) 13 2.3) indicated that front and side access routes provided ample oxygen supply to the counter electrode when measuring up to 500ppm CO in air. Therefore the gates of the injection moulded sensor were raised to limit the side gas access to the sensor in order to give closer agreement in reading between capillary only and total exposure, the enhancement being less than 2%.

Further confirmation of access routes was obtained when oxygen access routes were measured directly by using silver electrodes in 4M NaOH (see (2) 14 3). This showed that the front oxygen access signal in air is 1.8mA, which is equivalent to measuring 1.8% CO in air at a sensitivity of 0.1μA/ppm CO and is clearly quite adequate. A small rear access route also exists, giving 12μA oxygen signal in air.

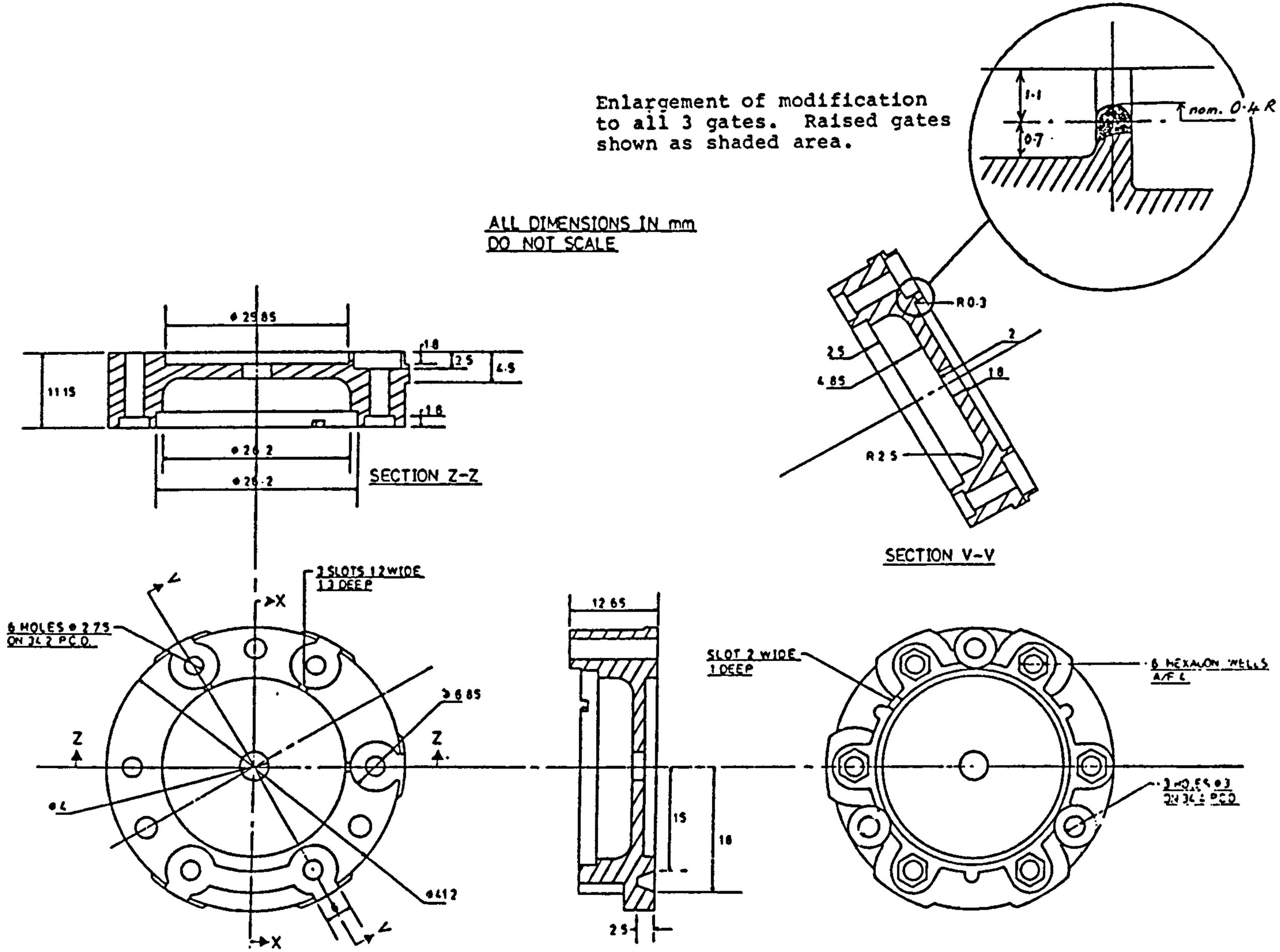

Figure 38 Drawing of gate modification to sensor baseplate

[After CTL Report No. 83/09/008, (2) 14 Fig. 2.4]

3.5.1.6 Water Transfer Rate Determination

Residence times under extreme RH conditions are governed by the water transfer rate capability of the sensor geometry and are temperature dependent. The expression for water transfer may be derived in terms of the sensor oxygen limiting diffusion current, assuming that the sensor capillaries represent the only factor controlling water access (see (2) 11 4.3). An equation of the same form may be obtained by direct consideration of water vapour diffusion through the capillaries (see (2) 12 5.1). Thus, the water flux according to Fick's Law is:

$$\text{Water Flux} = \frac{N \Pi d^2}{4\ell} D_{H_2O} (C_1 - C_2) \quad \ldots . (64)$$

N is the number of identical capillary holes.

d is the capillary diameter (cm).

ℓ is the capillary length (cm).

D_{H_2O} is the diffusion coefficient of water in air at 1atm pressure.

C_1 and C_2 are the water concentrations on either side of the capillaries. C_1 will be the ambient air concentration and C_2 the equilibrium water vapour concentration above the sensor electrolyte.

The water concentration differential may be restated in terms of partial pressures at 20°C :

$$(C_1 - C_2) \text{ (moles cm}^{-3}\text{)} = \frac{\Delta P_{H_2O}}{22.4 \times 10^3 \times 760} \times \frac{273}{293} \quad \ldots . (65)$$

The diffusion coefficient of water at 25°C is 0.256 $cm^2\ s^{-1}$ (see (1) Ref.105, p.562). This changes in proportion to the 3/2-power of absolute temperature and at 20°C has the value 0.25$cm^2\ s^{-1}$.

Substituting values into (1) Equ. (64) and expressing the water flux in g day^{-1} gives :

$$\text{Water Flux (g day}^{-1}\text{)} = \left(\frac{\partial W}{\partial t}\right)_{20°C} = 16.713 \times 10^{-3}\, N\, \frac{d^2}{\ell}\, \Delta P_{H_2O} \quad \ldots\ldots (66)$$

The sensors contain silicone rubber capillary inserts in a perspex top, designed to temperature compensate the span signal (see (1) 3.5.1.8). Assuming this achieves perfect compensation, then (1) Equ. (66) holds at any temperature provided the correct values of water vapour pressure are used, thus:

$$\Delta P_{H_2O} = P_{H_2O}\,(RH - RH_\circ) \quad \ldots\ldots (67)$$

where P_{H_2O} is the saturated vapour pressure of water at the operational temperature (T) and RH , $RH_\circ$ are the relative humidities on the ambient air and electrolyte sides of the capillaries respectively.

Substitution of (1) Equ (67) into (1) Equ. (66) and rearranging gives:

$$\int_0^t (\partial t)_T = \frac{\ell}{16.713 \times 10^{-3} N\, d^2\, P_{H_2O}} \int_0^W \frac{\partial W}{(RH - RH_\circ)} \quad \ldots (68)$$

Integration of (1) Equ. (68) gives the variation of water content with time (days) at a fixed temperature (T) and ambient humidity (RH). $RH_\circ$ is a function of electrolyte concentration and hence water uptake (or loss). The relationship is complex and integration of the right hand term is not easily accomplished.

In practice, a stepwise method may be used in which average values of $RH_\circ$ are taken for a number of small volume increments (∂ W) and the estimated times summed separately (see (2) 11 4.3).

Water uptake experiments were conducted with sensors primed with 0.5cm^3 5M H_2SO_4 and stored in a chamber at 40°C and 100% humidity (RH=1 and P_{H_2O} = 55.324mm Hg) (see (2) 12 5.1). A theoretical water uptake curve was calculated from (1) Equ. (68) for comparison, using 0.4cm^3 volume increments, when:

$$\text{t (days)} = \sum_{o}^{W}\left(\frac{1.805}{1 - RH_{av}}\right)_{T = 40°C} \quad \ldots . (69)$$

where RH_{av} is the mean electrolyte relative humidity for each 0.4cm^3 volume increment.

The theoretical and experimental data points are compared in (1) Fig. 39. The experimental water diffusion rates were about 20% greater than those predicted by (1) Equ. (68), but the general curve shapes were identical. In addition to the capillary access, it was estimated from sensor span measurements that 'side access' through the sensor seal is at least 10% of that through the capillaries. For example, using a 50ppm CO in air span gas mixture, sensor signals on the capillaries alone were about 5μA compared with about 0.2 to 0.5μA on the totally immersed sensors in the gas, with blocked capillaries; the latter, side access, signal represents the difference between cathode and anode side access for CO, which appears as a net sensor signal. The total access would be higher than that indicated by these measurements and could approach 15 to 20% of the capillary diffusibility. Within these uncertainties therefore, the correlation between measured and calculated water transfer rates was very good.

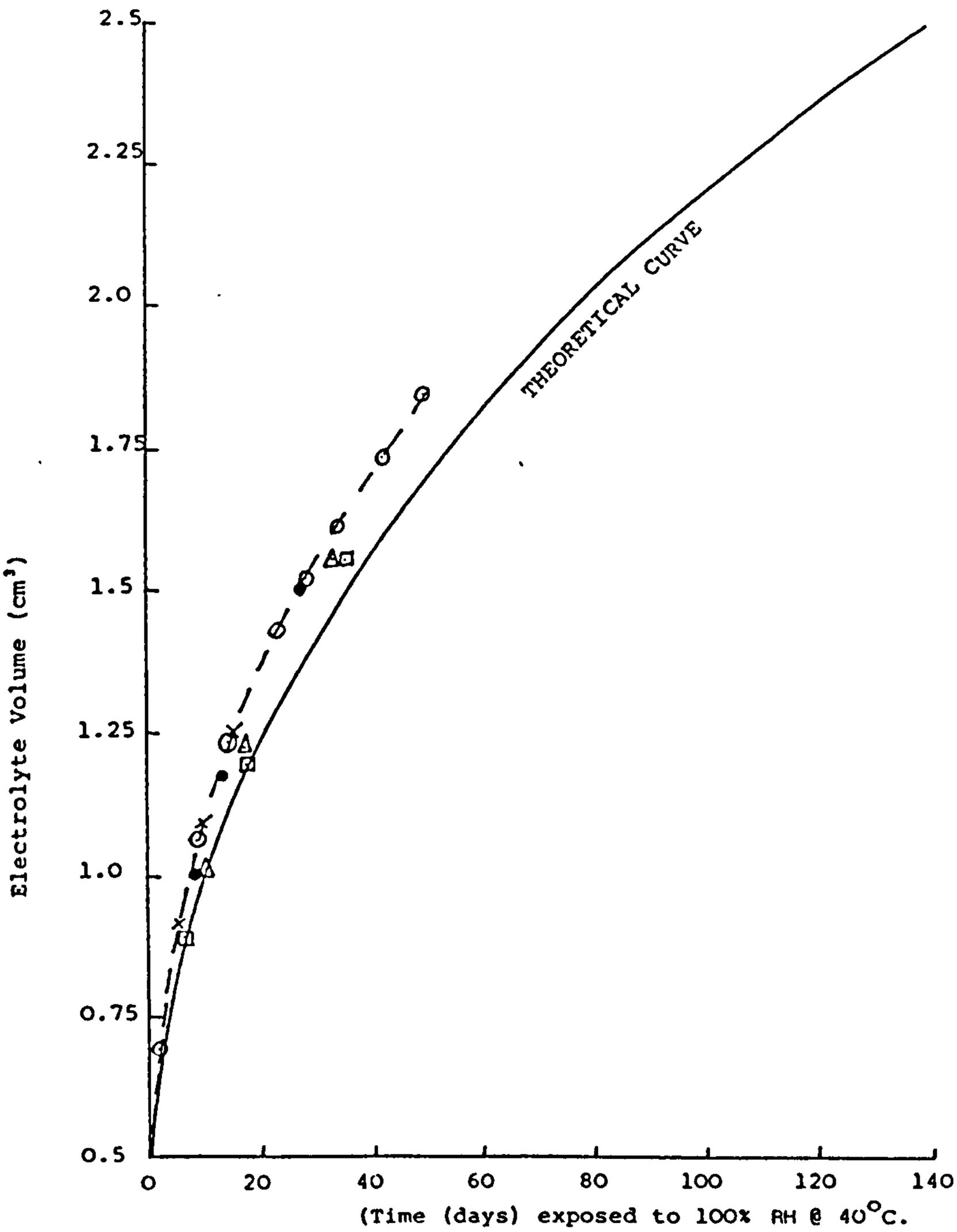

Figure 39 Water Uptake Measurements of Various Sensors in 100% RH, 40°C. All sensors have 5 capillary holes (10.5mm ø x 2.3mm length) and are primed with 0.5cm^3 10M H_2SO_4
[After CTL Report No. 81/31/006, (2) 12 Fig. 5.1]

3.5.1.7 Electrolyte Working Volume

Having chosen 5M H_2SO_4 as the electrolyte for the sensor (see (1) 3.4.1), it was empirically established that the minimum operating volume for the close-wicked sandwich design was 0.5cm^3 (see (2) 11 2). This represented the minimum priming volume at which sensor parameters such as response time, baseline and span stability started to suffer (see (1) Table 3).

Sensor	T19	T20	T21	T22	T23	T24
Electrolyte Volume (cm^3)	1.0	0.9	0.8	0.7	0.6	0.5
Anode Loading (mg Pt cm^{-3})	27	27	29	31	31	27
Cathode Loading (mg Pt cm^{-3})	37	37	39	41	41	37
80% Response Time (s)	19.5	22.0	24.5	22.0	23.4	40.8
90% Response Time (s)	28.0	32.2	39.0	32.2	35.6	76.8
Average baseline @ 20°C (ppm)	0.6	1.0	0.9	0.6	0.9	2.6
Span stability (%)	98.6	93.9	102.0	98.8	100.0	79.5

Table 3 Performance characteristics of Mark 6 sensors with varying electrolyte volumes
[After CTL Report No. 21/31/006, (2) 12 Table 5.1]

The maximum working volume of the injection moulded design (see (1) Fig. 38) was calculated to be 3.5cm^3.

Thus if the cell was initially primed with 1cm^3 5M H_2SO_4 (63% RH), it could sustain continuous exposure to relative humidities in the range equivalent to 10M H_2SO_4 to 1.5M H_2SO_4 , ie. 14 to 94% RH (see (1) Fig. 33).

The upper and lower humidity limits for continuous exposure can be extended by adjustments to the priming electrolyte volume and concentration. For example, by using 0.5cm^3 of 5M H_2SO_4 initially, the sensors can absorb up to 3cm^3 additional water, when the concentration reduces to 0.7M. In this way continuous exposure to high humidities up to 98% is possible, but the sensor will have little tolerance at low RH. Larger volumes of more concentrated acids could be employed where dry atmospheres are likely to be encountered. However, the decline in electrode activity with acid strength above 10M could affect sensor calibration and some doubt exists over the stability of plastic hardware and platinum corrosion resistance in very strong sulphuric acid (see (2) 11 4.2).

3.5.1.8 Span Temperature Compensation

A sensor with 100% capillary diffusion control will have a temperature coefficient near theoretical, ie. about 0.17% signal per °C at 20°C (see (1) 2.5.1.1).

In practice, the 2-electrode CO sensors have finite electrode activity so that the capillary is not fully limiting and some of the diffusion control resides in the electrode, which has a very high temperature coefficient ~ 3% of signal per °C. Sensors therefore have much larger temperature coefficients than expected, nearer 0.5% of signal per °C (see (1) 2.5.3.2).

The span signal may be compensated by differential thermal expansion. This is achieved by lining the capillary with silicone rubber tubing, which has a much higher thermal expansion coefficient than perspex, viz. 3 x 10^{-4} per °C and 10^{-4} per °C respectively.

The degree of compensation is proportional to the ratio of silicone rubber to capillary cross sectional areas, so that a wall to bore ratio of 1.5 should fully compensate an intrinsic sensor temperature coefficient of 0.58% of signal per °C (see (2) 12 App. 2). In fact, a substantial part of the differential expansion is taken up by distortion of the ends of the tube rather than by changing the capillary diameter, which reduces the compensator efficiency. Loss in compensation efficiency accelerates rapidly as silicone rubber wall thickness increases.

Two factors are probably relevant here:

1. The radii of curvature of the silicone rubber surfaces. One would expect that the smaller the radius of curvature the more difficult it will be to distort. So distortion of the flat ends of the tube would tend to be favoured over the interior capillary wall with its small radius of curvature.

2. The relative surface areas of the interior capillary wall and the ends of the silicone rubber. One would expect that the higher the ratio of capillary wall area to end area, the more the differential expansion would be taken up by a change in the capillary as opposed to end distortion.

For a simple capillary tube insert eg. 3mm long, 1mm bore and 1.6mm wall, the surface area ratio is 0.36:1, ie. the relative areas favour end distortion. The fraction of interior wall area to total exposed area is 0.26. This is roughly in line with the measured compensation efficiency (see (2) 13 5.2).

On this basis, compensation efficiency was improved by building in greater interior wall area of higher radius of curvature by splitting the silicone tube lengthwise and inserting a solid core (see (1) Fig. 40).

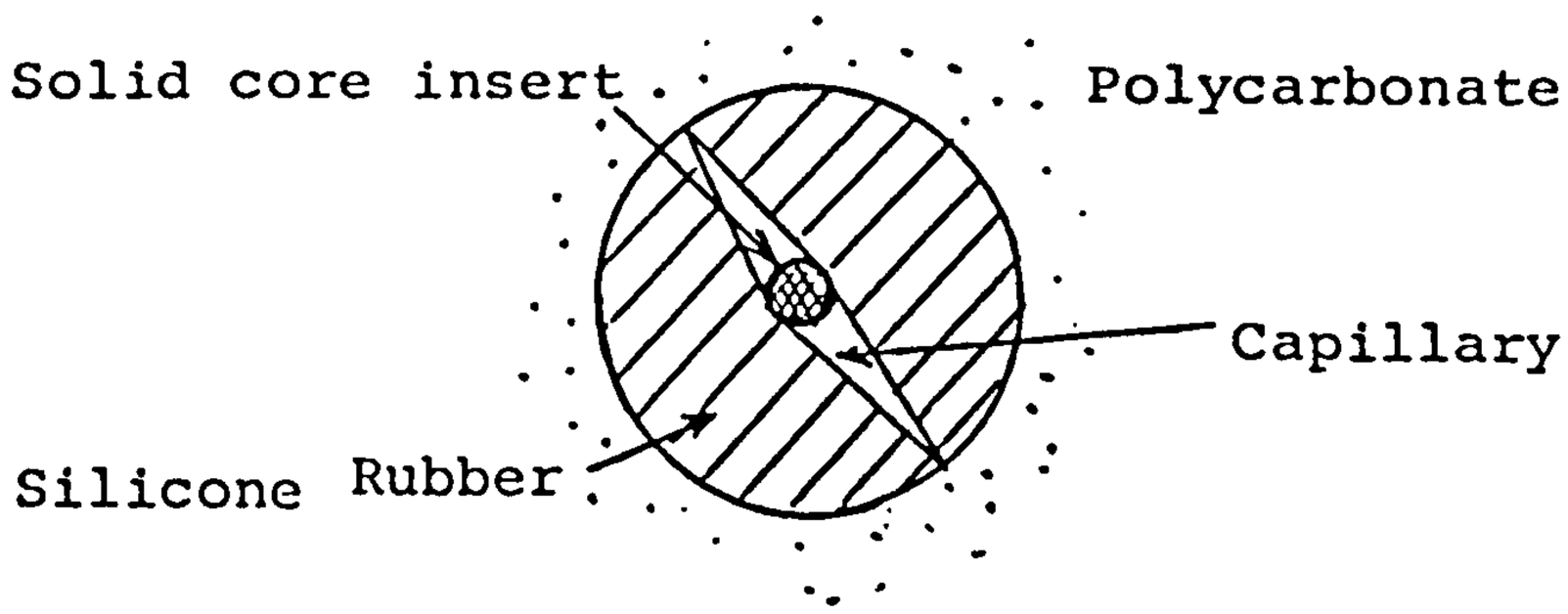

Figure 40 Capillary temperature compensation by split silicone rubber tube inserts [After CTL Report No. 82/09/007, (2) 13 5.2]

A double, cross-split was found to be even more efficient (see (1) Table 4):

Silicone Rubber Capillary Tube Configurations	Area Ratio (Capillary:Total)	Compensation Efficiency
Simple Tube	0.26	26%
Split Tube	0.42	42%
Cross-Split Tube	0.60	60%

Table 4 Comparison of calculated compensation efficiency with various silicone rubber capillary tube configurations [After CTL Report No. 82/09/007, (2) 13 5.2]

3.5.1.9 Inboard Filters

Sensor selectivity can be improved by using chemical filters to remove interfering constituents from the gas stream. Ideal filter materials are those which undergo spontaneous regeneration, for example by catalytic oxidation in aerobic conditions, thus reducing the need for maintenance. However, since most materials are non-regenerative, it would be advantageous to locate the filter downstream of the diffusion barrier of the sensor where the cumulative total exposure to reactants is considerably lower than in the main gas stream.

This concept of "inboard" chemical filtering has been demonstrated with CTL capillary - limited carbon monoxide sensors, particularly for the removal of acid gases such as SO_2 and is covered by patents[114].

3.5.1.9.1 Formulation of Filter Materials

The fine filter materials are blended with PTFE powder (10:1) in order to bind the loose powders, giving a spongy, porous matrix with good diffusibility and which does not settle out and densify in use.

3.5.1.9.2 Sulphur Dioxide Filter

Filters comprising MnO_2 as the active element can remove SO_2 and H_2S by oxidation and salt formation (see (2) 14 6.3.2). A number of chemical reactions are possible:

(i) Formation of Mn(III) oxide and sulphate

$$3\,SO_2 + 6\,MnO_2 \rightarrow 3\,SO_3 + 3Mn_2O_3$$

$$\underline{Mn_2O_3 + 3\,SO_3 \rightarrow Mn_2(SO_4)_3}$$

$$3\,SO_2 + 6\,MnO_2 \rightarrow Mn_2(SO_4)_3 + 2\,Mn_2O_3 \quad \ldots\ldots (70)$$

(ii) Formation of Mn(III) oxide and sulphite

$$SO_2 + 2MnO_2 \rightarrow SO_3 + Mn_2O_3$$

$$\underline{Mn_2O_3 + 3SO_2 \rightarrow Mn_2(SO_3)_3}$$

$$4SO_2 + 2MnO_2 \rightarrow Mn_2(SO_3)_3 + SO_3 \quad \ldots\ldots (71)$$

(iii) Participation of aerial oxygen

$$8\,SO_2 + 4\,MnO_2 + 3\,O_2 \rightarrow 2SO_3 + 2Mn_2(SO_4)_3$$

$$\text{or } 3\,SO_2 + 2\,MnO_2 + O_2 \rightarrow Mn_2(SO_4)_3 \quad \ldots\ldots (72)$$

(iv) Catalytic oxidation via Mn(III) compounds

$$2Mn_2O_3 + 2SO_2 \rightarrow 4MnO + 2SO_3$$

$$\underline{4MnO + O_2 \rightarrow 2Mn_2O_3}$$

$$2SO_2 + O_2 \rightarrow 2SO_3 \quad \ldots\ldots (73)$$

On the basis of the first 3 reactions above, filter capacity would be determined by an SO_2 : MnO_2 stoichiometric ratio of between 0.5 and 2 to 1. If the latter catalytic reactions occur to any significant extent, filter capacity would be considerably greater in aerobic conditions.

A 3F sensor was assembled with a top-plate cavity filter, containing 0.45g of 10:1 mixture of MnO_2 and PTFE (i.e. 4.7 millimoles MnO_2) and subjected to continuous exposure to a 1000 ppm SO_2 in air gas stream. The theoretical capacity based on 100% MnO_2 utilisation, according to (1) Equ. (70) above, was 244 days in 1000 ppm SO_2 (calculated capillary current for SO_2 at this concentration was 22μA). Considerably longer filter life would be expected if any of the other reactions were involved to any significant extent. By the end of the report period, the sensor had completed 63 days at 1000ppm SO_2 without any significant signs of SO_2 breakthrough.

3.5.1.9.3 Ethene Filter

In-board filtration can be used to selectively remove ethene with brominated carbon cloth (see (2) 13 App. 2). Ethene produces a cross-interference at platinum electrodes in carbon monoxide sensors where it undergoes a 2-electron oxidation to 1,2-ethanediol:

$$C_2H_4 + 2H_2O \rightarrow C_2H_4(OH)_2 + 2H^+ + 2e^- \quad \ldots\ldots (74)$$

The diffusion coefficient of ethene in air is 0.157cm^2s^{-1} @ 25°C, 1 atm. pressure, compared to 0.203 for carbon monoxide. Since both gases undergo 2-electron oxidations, the theoretical cross-sensitivity should be 77ppm CO. equivalent per 100ppm ethene.

YRL have found that bromine-impregnated carbon cloth can remove ethene interference without affecting the carbon monoxide signal to any great extent. Presumably the unsaturated double bond reacts to form the relatively stable brominated adduct:

$$C_2H_4 + Br_2 \rightarrow C_2H_4Br_2 \quad \ldots\ldots (75)$$

With a brominated carbon filter the sensor's ethene response was very low and stable, indicating significant removal of hydrocarbon on the filter and complete reaction of the residue as it reached the sensing electrode. However, the efficiency of ethene filtration gradually decreased with time when the sensor was left in ambient air and the ethene cross-sensitivity of the test sensor increased from 0.09ppm CO equivalent per ppm ethene to 0.236, over a 3 week period. One filter left out on the laboratory bench was almost completely deactivated over the same period.

3.5.2 Anode Design

The choice of anode and cathode compositions was complicated because of the need to satisfy a number of conflicting requirements and the final selection involved a number of compromises.

High electrode activity was an important criterion for both anode and cathode. 'Activity' in this context refers to both the intrinsic electrocatalytic activity of the platinum black (kinetic factor) and the diffusibility of the electrolyte film in the thinly wetted region between solid catalyst surface, liquid electrolyte and gas phases within the electrode structure (mass transfer factor) (see (1) 2.6). Such electrode activities may be measured and compared by experimental determination of the currents generated at a given reactant concentration and polarisation (ie. difference between rest and operating potentials of an electrode), in the absence of other controlling factors such as capillary barrier or low diffusibility backing tapes (see (2) 11 Appendix 1). Experimental methods, using thin, Gore backing tapes to support the catalyst layer, are described elsewhere (see (2) 11 3.2.1).

Generally electrode activity was promoted through the use of higher specific surface area (smaller particle size) platinum black, lower

electrode curing temperatures and higher platinum loadings. Thus solvent extracted, 100°C dried, Engelhard No. 4 catalysts produced the most active electrodes at a given platinum loading, and J.M. Standard black, 280°C cured, the least active. Platinum/PTFE ratio also influenced activity, producing broad maxima between about 3:1 and 8:1 for all platinum black types tested; ratios of 4:1 and 6:1 were generally chosen with J.M. Standard and Engelhard No. 4 blacks respectively (see (1) 2.6.3).

With anodes, an unrestricted (open) electrode activity towards CO oxidation of at least 10 times the capillary diffusion barrier sensitivity (ie. activity reserve > 10) was considered desirable to ensure a signal governed predominantly by the capillaries and which is therefore, both stable and of low temperature coefficient (see (2) 11 5.3). However, an upper limit on the anode activity reserve was imposed because of two other considerations:

(i) Sensor response time, being a function of interfacial contact area between anode catalyst and electrolyte, generally increased with steps taken to improve anode activity.

(ii) Parasitic, local cell consumption of carbon monoxide at the anode causes loss of signal sensitivity and may reduce linearity (see (2) 11 5.8). Suppression of parasitic reactions can be accomplished by enhancing the oxygen reduction capability of the cathode relative to that of the anode. However, measures taken to limit the anode oxygen reduction capability may also affect the CO oxidation reaction and hence the activity reserve.

Thin tape anodes produced limiting CO oxidation currents above air rest potentials (ie. in the absence of oxygen interference) which were apparently insensitive to the fabrication technique but increased fairly linearly with platinum loading in the range 7.5 to 35mg cm^{-2} (see (2) 12 Table 4.1 and figs 4.1 and 4.4). This probably reflected the fact that

diffusion of CO through the thinly wetted area was the dominant controlling mechanism under these conditions. Below 4 to 5mg cm^{-2} platinum catalyst coverage was incomplete and activity decreased dramatically with loading. Above 35mg cm^{-2} platinum, CO oxidation currents became more comparable with the thin tape diffusibility and mixed control set in with an apparent decrease in current per unit platinum loading.

Oxygen reduction activity similarly increased with platinum loading but currents were very sensitive to fabrication technique (particularly curing temperature) and prehistory of the electrode (see (2) 12 Table 4.1). This suggested electrocatalytic activity as the controlling factor, rather than film diffusion.

The final choice of anode composition, prepared from J.M. Standard black by the Drop Method and cured at 280°C, achieved an acceptable compromise between the requirements of CO oxidation activity reserve on the one hand and response time and oxygen reduction activity on the other. Anodes prepared in this way, with platinum loadings between 7.5 and 35.0mg cm^{-2} , on thin Gore PTFE tape, supported limiting CO oxidation currents which represented between 10 and 45 times respectively, the 0.1 μA ppm^{-1} sensitivity of the capillary hole barrier used with BCC trace CO sensors.

3.5.3 Cathode Design

The correct balance of oxygen reduction activity between anode and cathode proved to be the single, most important feature in the trace CO sensor design and had important inter-relationships with sensor characteristics such as signal stability and hysteresis, baselines, response times and hydrogen sensitivity.

In a two-electrode galvanic CO sensor, the sensing electrode controls the current whilst the counter electrode determines the operating potential. Platinum is a versatile catalyst, supporting both CO oxidation

and oxygen reduction, so that if the sensing electrode polarises appreciably below its air rest potential, some of the CO signal is lost due to local cell action (see (2) 12 2 and 4.2). It is therefore necessary to bias the oxygen activity in favour of the cathode. This can be achieved by increasing the cathode surface area using:

(a) high platinum loading.
(b) high surface area platinum black, eg. Engelhard No. 4.
(c) solvent extraction with 2-propanol and drying at 100°C to avoid loss of surface area.

Judicious application of these measures provided a means of controlling sensor properties such as signal stability and baseline hysteresis.

3.5.3.1 Influence on Signal Stability

Because the sensors have a large activity reserve (see (2) 12 4.2) hysteresis behaviour probably does not involve saturation of the catalyst per se. Rather, as there is a potential dependent, equilibrium oxide coverage on the electrode (see (1) 2.3.2.3), cathodic polarisation during CO exposure induces an oxide reduction reaction. Sensors in which the anode/cathode surface areas are heavily biased such that the anode operates well into the current limit, where no oxygen scavenging occurs (see (1) Fig. 11), will then exhibit a 'creep-up' effect due to a transient offsetting signal as the oxide coverage readjusts to the new potential conditions (see (1) Fig. 12, shaded area).

The extent of the signal loss is largely governed by the degree of polarisation and to a lesser extent by the anode loading (see (2) 12 7.1(a)).

If the sensor anode/cathode surface areas are only marginally biased, the signal may stray off the current limit (see (1) Fig. 13) and further signal loss would occur due to oxygen scavenging (see (1) Fig. 14, cross-hatched area).

The extent of this signal decay depends not only on the degree of polarisation but also on the operating potential.

3.5.3.2 Influence on Baseline Hysteresis

Biasing anode/cathode oxygen activity unfortunately results in increased baselines, see (2) 12 Fig. 7.1 and Table 7.1; these results represent the long term average, settled baselines of different sensors, monitored at ambient temperatures close to 20°C.

Baselines increased almost linearly up to a loading bias of about 10mg Pt cm^{-2}. Between 10 and 20mg cm^{-2}, baselines showed signs of levelling out, although there was a large scatter in behaviour, and no further increase was found at a 25mg cm^{-2} loading bias.

All sensors, despite large disparities in platinum morphology and loading bias, exhibited similar baseline temperature sensitivity, with an average energy of activation of 16.5 ± 2.5 kcal mol^{-1} (see (2) 12 Table 7.1).

Baseline hysteresis after CO exposure was the reverse of the signal effects observed during exposure, as the surface oxide underwent readjustment back to the quiescent condition (see (1) Figs. 12 and 14).

Unlike the anode, cathode interfacial area did not influence sensor response time. However, an upper limit was imposed on the differential oxygen reduction activity between cathode and anode

due to the need to ensure a minimal sensor baseline in CO-free air (see (2) 12 7.1(b)).

The final choice of cathode, therefore was Engelhard No. 4 Pt (loading 20mg cm^{-2}) prepared by the 'drop method' and cured at 280°C.

3.6 THREE-ELECTRODE DESIGN

Hysteresis problems in 2-electrode sensors derive primarily from the voltage swing resulting from significant cathode polarisation (see (1) 3.5.4), since the sensing electrode potential closely follows that of the counter.

These problems may be overcome by including a third, reference, electrode from which negligible current is drawn. Using a potentiostatic circuit enables the potential of the sensing electrode to be held at any desired potential with respect to the reference electrode, quite independently of the potential of the counter electrode as this changes with polarisation.

In the past, one could not operate the sensing electrode at a fixed potential without running the risk of infringing the Energetics Science patents[115].

However, an earlier, now lapsed, patent[116], achieved something very close to the desired effect by using a potentiostatic circuit to tie the sensing electrode to ground via a fixed load resistor R_L , using the voltage drop across R_L as the sensor signal (see (1) Fig. 41).

When the sensing electrode is exposed to CO its potential drops by an amount:

$$\Delta V = E_c = i_c R_L \qquad \ldots\ldots (76)$$

where i_c is the cell current generated. The change in potential ΔV is effectively used as the output signal.

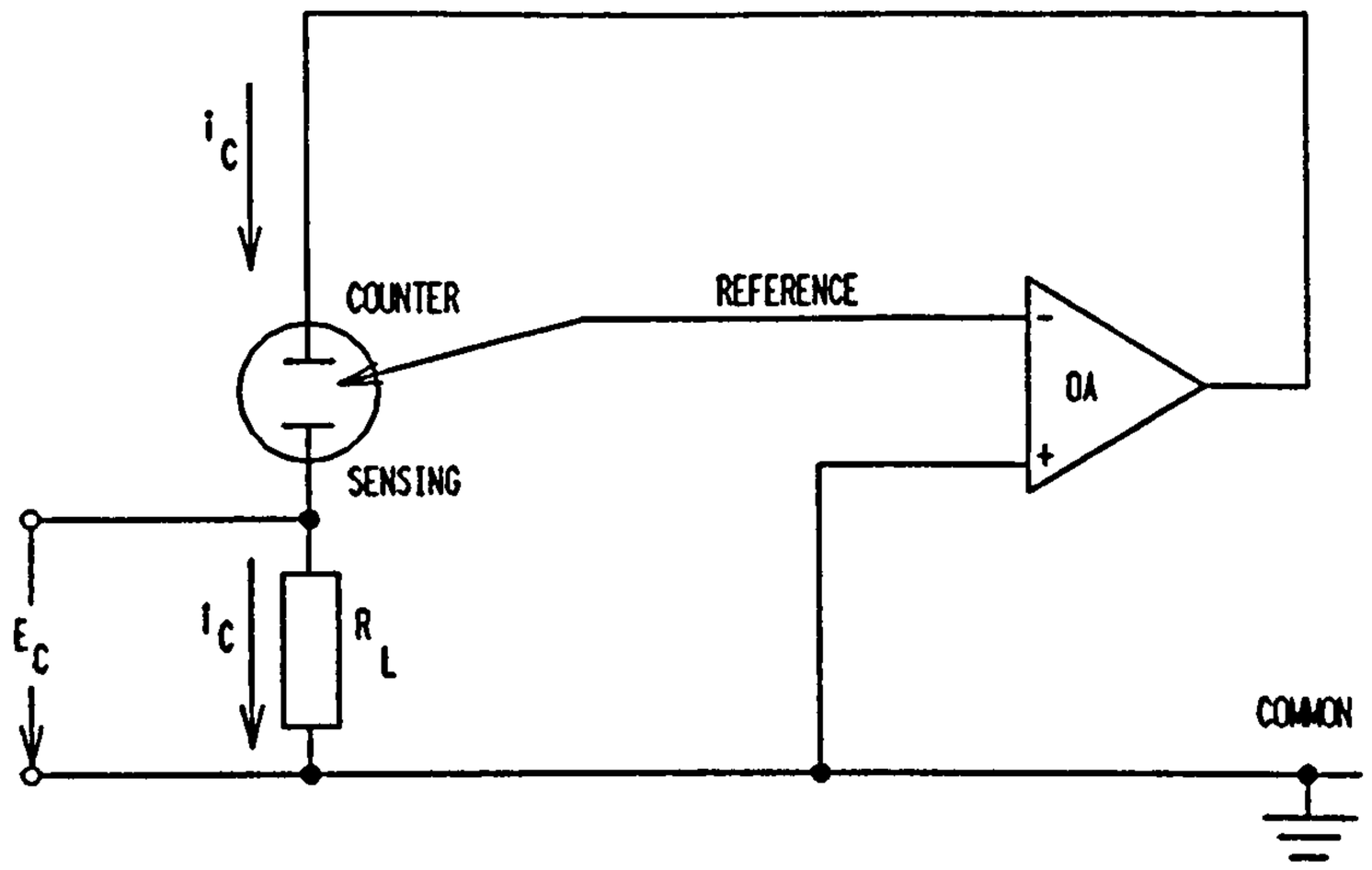

Figure 41 Potentiostatic control circuit for 3-electrode sensors.
[After CTL Report No. 81/03/006, (2) 12 Fig. 8.1]

The movement in electrode potential is only 1% that of 2-electrode sensors at R_L = 51Ω and hence hysteresis is correspondingly less.

Commercially available CO sensors are usually biased 100-200mV above their air rest potential to decrease H_2 cross sensitivity, but this generates large baselines (~10ppm CO≡) with long warm up times when the circuitry is switched on.

By controlling the reference electrode at ground potential (zero bias), the sensing electrode is effectively held at OCV if the sensing and reference electrodes are matched and warm up time is reduced to about 60 seconds and baselines are similar to those of the 2-electrode sensors.

The reference and sensing electrodes may be shorted out when not in use to help maintain stability and to keep start up times to a minimum.

The main advantage of the 3 electrode sensor is the tolerance to very much higher CO concentrations without showing significant hysteresis.

The higher complexity of sensor manufacture is offset by the need to take less care in selecting and manufacturing the electrodes and the Pt loading on the counter electrode can be reduced to a minimum, thereby saving money.

On the other hand 3-electrode sensors require more complicated circuitry and are not self-powered, whereas 2-electrode sensors are.

3.7 AUXILIARY ELECTRODE DESIGN

One of the major problems with electrochemical CO sensors is H_2 cross interference. Three electrode sensors are often run at 200mV bias to reduce H_2 cross interference to under 10% ie. 100ppm H_2 < 10ppm CO≡.

However, the two electrode CO sensor run in self-powered mode with a fixed load resistor has much higher sensitivity to H_2(< 40%). An auxiliary sensing electrode may be placed beneath the primary sensing electrode and arranged so that there is a gas diffusion path to it via the sensing electrode. CO, which reacts completely at the sensing electrode, will not be transmitted to the auxiliary. On the other hand, H_2 , which only partially reacts, will be transmitted. The resulting signal from the auxiliary (or a fraction or multiple thereof) can then be electronically subtracted from the primary sensing electrode (CO + H_2) to null out the H_2 interference. Baselines can also be offset by this method.

The auxiliary electrode principle can be used in both 2- and 3-electrode sensors and is subject to patent[117].

CHAPTER 4 - SENSOR PERFORMANCE

The main criteria which ultimately dictated the choice of design for a two-electrode trace CO sensor for BCC's needs revolved around parameters such as long-term signal stability, baselines (ie. resolution) and CO tolerance at the upper measuring range, namely 200ppm CO in air.

Tolerance was measured using a regime agreed with BCC, based on a 20 minute exposure to 200ppm CO in air and a 1, 2 and 5 minute recovery in clean (CO-free) air (see (2) 12 7.2).

During Phase 3 development, the electrode configuration was narrowed down to:

Sensing Electrode (Anode)	Johnson Matthey Std. Pt Black
	Pt : PTFE ratio 4:1
	Cured at 280°C
	Loading 26-34mg cm^{-2}
Counter Electrode (Cathode)	Engelhard No. 4 Pt Black
	Pt : PTFE Ratio 6:1
	Loading 36-44mg cm^{-2}

These sensors were able to measure up to 500ppm CO and were designated 2E (environmental) sensors (see (2) 12 7.2). However, by Phase 4 development, it was evident that the 2E baselines, as judged on mature sensors, were still too large (1-3ppm CO equivalent at ambient temperature) to meet BCC's specification on accuracy.

The final choice of electrodes therefore necessitated trading off CO tolerance (ie. lowering the upper measuring range from 500 to 200ppm) for the sake of lower baselines (0-2.0ppm CO equivalent). This was achieved by decreasing the anode Pt loading and by using less active catalyst on the counter electrode:

Sensing Electrode (Anode)	Johnson Matthey Std. Pt Black
	Pt : PTFE ratio 4:1
	Cured at 280°C
	Loading 20 - 25mg cm^{-2}
Counter Electrode (Cathode)	Johnson Matthey Std. Pt Black
	Pt : PTFE ratio 8:1
	Cured at 280°C
	Loading 40 - 48mg cm^{-2}

These sensors were designated 2T (Trace) sensors (see (2) 13 4). In general, the 2T sensor represented the best compromise between low baseline and CO tolerance to achieve the overall design objectives set out for an incipient combustion detector to meet BCC's needs (see (1) 1.3), which are discussed in detail below.

4.1 SERVICE LIFE

There was insufficient time to establish any significant long-term service life history on the final version of the 2T sensor, but earlier work on the prototype designs (see (2) 11 5.1) indicated an initial settling in period of about 2 months, with a 4-7% loss of output. In the next 2 months, output loss was much less, averaging 0.7-0.8% and reaching a stable output between 4-6 months. On this evidence, it should be possible to achieve at least 1 year service life, with the prospect that the sensors could actually last 2 years in service.

4.2 OUTPUT SENSITIVITY

A total of 42 2T sensors were made up in 3 batches and monitored over a period of 2 weeks for sensitivity and baseline.

The sensors were gassed with a nominal 50ppm CO in air mixture and a mean sensitivity of 0.100 $\pm$ 0.01μA ppm^{-1} was obtained. There was no significant batch-to-batch variation in sensitivity (see (2) 13 4.2).

4.3 TEMPERATURE RANGE

The baseline and span signals have different temperature characteristics and are therefore best discussed under separate headings as follows:

4.3.1 Baseline Temperature Stability

The baseline temperature dependence (0-40°C) follows an Arrhenius law (see (2) 11 fig. 5.7), with a mean energy of activation of 16.4 ± 2.5 kcal mol^{-1} (see (2) 12 Table 7.1). This means that baselines would roughly double per decade increase in temperature.

The first 3 batches of prototype 2T sensors supplied to BCC for evaluation comprising 42 sensors in total, had a mean baseline of 1.2 ± 0.6ppm CO equivalent with spread 0.3-3.4 ppm CO equivalent. No significant batch-to-batch variation in baselines was found and only three baselines were higher than 2.0, viz. 2.1, 2.5 and 3.4ppm CO equivalent (see (2) 13 4.2).

A further batch of 12 sensors averaging 0.6 ± 0.5ppm CO equivalent subsequently confirmed that 2T sensors could be manufactured with baselines less than 2ppm (see (2) 14 4.3).

4.3.2 Span Temperature Stability

The intrinsic span temperature coefficient of the 2T sensor is so large that sensors would not meet the accuracy specification of ±10% of signal at 0°C, so the sensors were temperature compensated by lining the capillaries with fine bore silicone rubber tubing with a wall : bore ratio of 2.00 (see (2) 12 3.1 and appendix 2). Subsequently, it was discovered that the compensation efficiency could be further improved by using split tubing, as this reduced 'end-loss' effect (see (2) 13 5.2).

Comparison of compensated and uncompensated sensors may be made by obtaining best linear fit values of temperature coefficient between 10 and 40°C (see (2) 14 4.2 and (1) Table 5):

Sensor Type	No. in Batch	Temp. Coefficient (% signal at 20°C per °C)	Standard Deviation
Split Sleeves	12	0.27	0.17
Uncompensated	4	1.20	0.13

Table 5 Temperature Coefficients on Compensated and Uncompensated 2T sensors.

Clearly the split sleeve compensation is very efficient.

4.4 CALIBRATION FREQUENCY

For fixed point monitoring, calibration frequency would depend on 3 main factors:

(a) Long-term stability

(b) Baseline temperature stability

(c) Span temperature stability.

Using the characteristics of these factors as discussed in (1) 4.1 and (1) 4.3 above, it is possible to compute the maximum errors generated over a 3 month period, assuming initial calibration at 20°C using 200ppm CO in air.

4.4.1 Drift Calculation

As discussed in (1) 4.1 above, the maximum drift would occur over the first calibration period, ie. in the first 3 months it would be <8% and subsequently <1%, say. Assuming calibration with 200ppm CO, this would translate to a maximum drift in calibration of -16ppm CO on initial calibration, and -2ppm CO on subsequent recalibration.

4.4.2 Baseline Shift Calculation

Assuming the baseline is nulled out when the instrument is set up at 20°C, the maximum baseline shift with temperature would be incurred with the largest permissable baseline, namely 2.0ppm CO equivalent (see (1) Table 6).

Temp (°C)	0	20	40
I_B (ppm CO equiv.)	0.5	2.0	8.0
ΔI_B (ppm CO equiv.)	-1.5	0	6.0

Table 6 Calculation of Maximum Baseline Shift with Temperature on 2T Sensors.

4.4.3 Span Shift Calculation

Assuming the span is calibrated with 200ppm CO in air at 20°C and a span temperature coefficient of 0.27% per °C (see (1) 4.2.2 and (1) Table 7).

Temp (°C)	0	20	40
Span Calibration (%)	94.6	100.0	105.4
Span Reading (200ppm CO)	189	200	211
Error (ppm CO)	-11	0	11

Table 7 Calculation of Maximum Span Shift with Temperature on 2T Sensors.

4.4.4 Maximum Error Calculation

Assuming 3-monthly calibration with 200ppm CO in air at 20°C, the maximum error in service at 0°C and 40°C may be calculated as shown in (1) Table 8.

Time (months)	Temp. (°C)	Maximum Errors In Service (ppm CO equiv.)			
		Drift	Baseline	Span	Total
3	0	-8	-2	-11	-21
	40	-8	6	11	9
6	0	-2	-2	-11	-15
	40	-2	6	11	15
9	0	-1	-2	-11	-14
	40	-1	6	11	16
12	0	-1	-2	-11	-14
	40	-1	6	11	16

Table 8 Maximum Error Calculation Considering Temperature and Long-Term Drift on 2T Sensors.

Because of the large initial drift, the maximum total error occurs over the first 3 month calibration period (-10% of FSD reading) and subsequent errors are less than 8% of FSD reading.

4.4.5 Baseline Effect on Error Calculation

For genuine trace level monitoring (0-10ppm CO), baseline shift with temperature is the single largest source of error, as shown (see (1) Table 9).

Baselines	PPM CO Equivalent				
@ 20°C	2.0	1.5	1.0	0.5	0
@ 40°C	8.0	6.0	4.0	2.0	0
Baseline Shift	6.0	4.5	3.0	1.5	0

Table 9 Calculation of Baseline Shift with Temperature at Various Ambient Baselines.

The maximum baseline error of 6ppm CO equivalent may be compared with the span calibration error at 40°C using 10ppm CO in air of <0.1ppm CO and a long term calibration drift of -0.1ppm CO.

However, most sensors have baselines <1ppm CO equivalent at 20°C, which limits the baseline shift error at 40°C to 3ppm CO equivalent.

4.5 ATTITUDE STABILITY

On inverting the sensor, the baseline stability is better than ±0.2ppm CO equivalent.

4.6 SHOCK AND VIBRATION SENSITIVITY

This test is rather subjective, but nevertheless shows how stable the sensors are - the sensors may be tapped on the bench surface, at all faces and all corners, without inducing a baseline disturbance of more than ±0.2ppm CO equivalent.

4.7 LINEAR MEASURING RANGE

Two sensors were calibrated with 55ppm CO in air and then exposed to 9.5ppm CO in air. Sensor P9 read 10.1ppm (+6%) and sensor P18 read 9.7ppm (+2%) (see (2) 10 6.2.3).

Similarly, four other 2T sensors were calibrated at 50ppm and exposed to 209ppm CO in air for 5 minutes, when a mean reading of 205± 6ppm CO was obtained (see (2) 13 table 4.1).

However, a comparison at 1000ppm CO level showed that the 2T sensor read low at 864ppm CO but the 3E sensor coped very well, reading 991ppm CO (see (2) 13 table 7.1).

4.8 RESPONSE TIME

The 2T sensor 90% response times, measured on a load resistance of 50Ω, ranged from 23 to 35 seconds (see (2) 13 4.3).

The 90% response time dependence on load resistance (measured on sensor 2T 158) was linear up to 100Ω RL, with a slope of 0.32 $s\Omega^{-1}$ and an intercept of 16s at zero RL (see (2) 13 fig. 6.5). Further work on a batch of 5 2T sensors indicated that the response time dependence was near-linear up to 50Ω and started deviating above linearity up to 100ΩRL. The deviation from linearity was thought to be related to the sensors being relatively fresh at the time - approximately 1 month old (see (2) 14 fig. 4.2). These results yielded a slope in the range 0-50Ω of 0.30 $S\Omega^{-1}$ and an intercept at zero RL of 16 s (see (2) 14 4.4) which is in good agreement with the earlier findings on sensor 2T 158 above.

4.9 PRESSURE COEFFICIENT

The pressure coefficients of a batch of 12 2T sensors were measured using 49.3ppm CO in air test gas in the range 764-1100 torr.

Output increased linearly with pressure, giving a mean pressure coefficient of 0.030 ± 0.01% per torr (see (2) 14 4.5).

The small but finite pressure coefficient stemmed from partial electrode control - ie. low activity reserve (see (1) 2.5.3).

4.10 CARBON MONOXIDE TOLERANCE

Four 2T sensors were subjected to a standard tolerance test by exposure to 200ppm CO for 20 minutes and monitoring the recovery in clean air (see (2) 12 7.2).

Signal decay after 20 minute exposure averaged 4 ± 2ppm CO and baseline hysteresis after 5 minutes recovery in clean air averaged 0.9 ± 1.2ppm (see (2) 13 table 4.1).

A 2T sensor (no. 158) and a 3E sensor (no. 120) were compared using 1000ppm CO in air. Although stability during exposure was good, the 2T sensor read low - 856ppm on average compared to 991ppm for the 3E sensor (see (2) 13 table 7.1). The 2T sensor also suffered negative hysteresis, reading -12ppm CO at the

5 minute recovery stage. Clearly the 2T sensor was not capable of handling 1000ppm overload conditions, whereas the 3E sensor managed much better, registering 4ppm CO equivalent hysteresis at the 5 minute recovery stage.

4.11 MOISTURE TOLERANCE

During the 2 electrode design stage, the following facts regarding water balance were established:

(a) Water transfer rates closely follow the theoretical relationship for control by diffusion through the sensor capillaries (see (1) 3.5.1.6).

(b) The limits of workable electrolyte volume for the trace sensor are between 0.5 and 3.5cm^3, corresponding to acid concentrations of 10M and 1.4M respectively, when primed with 1cm^3 5M H_2SO_4 (see (1) 3.5.1.7).

The remaining aspects of moisture tolerance that needed to be empirically established were the residence times at zero and 100% RH during which sensors still functioned normally and the impact of prolonged operation at the upper and lower humidity limits on sensor performance.

Note:

The humidity work was carried out on nominal 2E sensor designs. In comparison, the 2T design, finally adopted by BCC for trace CO measurement, had the same nominal sensitivity of 0.1μA per ppm, but had larger capillaries to compensate for the fact that, due to the electrode design, it only operated at about 55% theoretical signal, compared to 2E operation nearer 95% theoretical signal. Thus the 2T sensor was capable of correspondingly greater water transfer rates.

The 2E electrode composition also gave baselines that were generally higher than the 2T and this was reflected in the experimental sensors studied in this work.

4.11.1 Residence Times in Zero and 100% RH

Sensor E4 was primed with 1cm^3 5MH_2SO_4 and stored in a desiccator over silica gel.

The sensor was periodically removed and weighed to determine water loss. Baseline and span signals were also recorded.

The sensor ran satisfactorily for about 4 weeks in zero humidity, during which time the acid concentration increased to 11.6M representing a final volume of 0.45cm^3. There were few signs of performance decline at this point due to electrolyte deficiency (see (2) 13 Table 5.1).

Water loss rate followed the theoretical relationship closely, taking an estimated 27 days to reach 11.6M H_2SO_4 (assuming a mean laboratory ambient temperature of 20°C) compared to 29 days actually measured.

During the 5th week the ABS coverplate and perspex base of the sensor fractured and the test was discontinued. The acid concentration had by then reached 12.7M which was the most probable reason for the plastics failure. The sensor continued to operate reasonably, albeit at a somewhat enhanced baseline and decreased span, although the response time was normal. The final electrolyte volume was 0.4cm^3 (see (2) 13 5.12).

Three sensors, equipped with a pressure release vent (see (1) 3.5.1.4) were primed with 1cm^3 5M H_2SO_4 and stored in a desiccator over water. Similar measurements were made as for sensor E4 above.

Sensor PR1 leaked at the cover plate seal after 3 weeks but sensors E6 and E8 had stable performance at ambient temperature, 100% RH for 250 and 175 days respectively, without leakage. This represented about 80% utilization of the expansion reservoir capacity.

4.11.2 Humidity Limits

Early experiments, running the sensors at low humidity and hence at high acid concentrations for prolonged periods, established that perspex material was unstable above acid strengths of 7.5M H_2SO_4 (see (2) 13 5.1.2).

A comparison of sensors moulded out of Noryl, ABS and polycarbonate material, run at 10M H_2SO_4, identified the latter material as the most acid compatible.

Moulded polycarbonate sensors, primed with 0.5cm^3 10M H_2SO_4 and stored in a desiccator over the same electrolyte, gave stable, normal performance at ambient temperature for over 200 days, when tests were terminated (see (2) 13 5.1.2).

At the other extreme, sensors primed with 2cm^3 0.86M H_2SO_4 and stored in a desiccator over the same electrolyte, also gave stable, normal performance for over 200 days, when tests were terminated (see (2) 13 5.1.3).

4.11.3 Conclusion

Although the sensor can function normally down to an electrolyte volume of 0.4cm^3 before catastrophic loss of signal sets in, at 0.5cm^3 (10M H_2SO_4) the concentrated acid starts attacking glued joints and seals.

However, the practical limit is really determined by long-term span stability considerations, as the electrode activity deteriorates below 0.6cm^3 (8.5M H_2SO_4) due to Pt corrosion.

Within these limits the standard sensor can operate continuously in relative humidities down to about 20%, without incurring any water balance problems. Excursions of several weeks at zero humidity can be sustained, but special measures may be necessary to cope with the

cumulative water loss when operating for frequent and/or extended periods in very dry conditions. Operating times in dry conditions could be extended by priming with greater volumes and/or using more concentrated electrolyte, but at some point sensors will need to have their water restored by exposure to a moist atmosphere, before any permanent damage occurs through degradation of the plastic hardware, joints, seals, etc.

The upper limit of acid volume is determined by the free space within the sensor reservoir, which is about 2.5cm^3 in current standard sensor designs. Acid concentration in a standard sensor, primed with 1cm^3 5M H_2SO_4, at the limit of water uptake, would be about 1.5M. No measurable changes in sensor performance characteristics (baseline or span) resulted from acid dilution to this extent. The increase in liquid volume however, made it essential to have a pressure release vent. This was also necessary to release pressures caused by thermal cycling. The pressure release system achieved better than 80% space utilization for water uptake and thermal cycling between 20 and 40°C, provided the back of the coverplate was not completely obscured by electrolyte.

Standard sensors incorporating the pressure release vent are capable of continuous operation in relative humidities up to about 93%, without incurring any water balance problems. Excursions of several months (depending on temperature) at higher humidities are possible but, as with very dry conditions, special measures may be necessary to cope with any cumulative water gain when operating frequently or for any extended periods in very moist conditions. Operating times may be extended by priming with smaller volumes of less concentrated electrolyte, but at some stage it will be necessary to restore the water balance by drying out, before permanent damage from leakage occurs.

4.12 CROSS INTERFERENCE

The 2 electrode trace CO sensor is sensitive to various gases arising from processes in mines, such as ethene, NO, NO_2, SO_2 and H_2 (see (1) 1.3.9). These are discussed under separate headings:

4.12.1 Hydrogen Response

Cross interference on a CO sensor at trace level may be expressed in terms of the CO equivalent response per 100ppm test gas.

For example, if a CO sensor with sensitivity 0.100μA ppm^{-1} CO is exposed to 100ppm H_2 and gives a signal of 2μA, the CO equivalent response would be $\frac{2}{0.100}$ = 20ppm.

This may be defined in terms of a percentage cross interference, θH_2:

$$\theta H_2 = \frac{\$H_2}{\$CO} \times 100\%$$

Thus for the above example:

$$\theta H_2 = \frac{2}{100} \times \frac{1}{0.100} \times 100 = 20\%$$

All cross interferences may be expressed in the same way.

Hydrogen sensitivity has been very variable not only from one design to the next, but also within the same sensor design (see (2) 12 table 7.3).

Although the mechanism of hydrogen response is incompletely understood, several trends are apparent. Platinum in its zero valent state is an extremely active catalyst for hydrogen fuel cell anodes operating at low overpotential ~100 to 200mV vs. DHE (see (1) 2.3.2).

On the other hand, platinum operated near its open circuit potential in ambient air ~1050mV vs. DHE gives only a partial response to several hundred ppm H_2 and it is quite likely that the surface oxide at these potentials (see (1) 2.3.2.3) in some way passively obscures, or more likely actively inhibits, the reaction. One would therefore expect hydrogen sensitivity to be potential dependent, decreasing in some fashion as counter electrode loading and hence potential, increases. Also, since the hydrogen response is not capillary-controlled, it should be sensitive to anode loading.

In order to deconvolute the cathode contribution, the product of the hydrogen sensitivity and the cathode loading was plotted against the anode loading (see (2) 12 fig. 7.5 and table 7.4). Although there was some scatter, the hydrogen sensitivity generally increased linearly with anode loading up to ~30mg Pt cm^{-2} and then reached a plateau, suggesting that it had become diffusion limited.

This is borne out by the H_2 cross interference on 2T sensors, which range from 10-30% CO equivalent at 20°C and have a large temperature coefficient, indicating diffusion and electrode kinetic control (see (2) 13 4.6 and (1) Table 10).

Temperature (°C)	Hydrogen Cross Interference (% equivalent CO signal)			
	2T130	2T129	2T128	2T127
-30	4	2	5	4
20	17	15	27	15
30	28	25	47	24
40	41	34	74	37

Table 10 Hydrogen Cross Interference Variation with Temperature on 2T Sensors.

Hydrogen cross interference may be further reduced by anodisation (see (2) 14 5.4) or by biasing the sensing electrode during operation (see (2) 14 5.2) but both of these methods are unsatisfactory, anodisation blunting CO activity and bias operation leading to large baselines.

4.12.2 NOX and SO_2 Response

The only method of reducing the sensitivity to these gases is to use inboard chemical filters (see (1) 3.5.1.9) such as MnO_2 (see (1) 3.5.1.9.2), which proved very effective for SO_2 removal in flue gas analysis, surviving 63 days exposure at 1000ppm SO_2 without any significant SO_2 breakthrough (see (2) 14 table 6.2). There was also some indication that MnO_2 could remove NO_2 by adsorption and NO by oxidation to NO_2 and subsequent adsorption of the NO_2 product.

Use of MnO_2 filters in 2T sensors was highly desirable in view of its efficiency in removing SO_2 cross interference, but was only implemented after phase 5 development.

4.12.3 Ethene Response

Ethene gives a partial, sluggish response on a 2T sensor, with a great deal of baseline hysteresis on recovery (see (2) 13 fig. A2.2). Theoretical cross interference is 77%, compared to the measured response of 64% (see (2) 13 table A2.1).

Work done at YRL showed that brominated carbon cloth can remove ethene, presumably by forming a stable brominated adduct across the unsaturated double bond (see (1) 3.5.1.9.3):

$$C_2H_4 + Br_2 \rightarrow C_2H_4Br_2 \qquad \text{Equ. (75)}$$

Brominated carbon cloth was supplied by YRL and incorporated into inboard filters in 2T sensors and tested at CTL.

Although these filters dropped the cross interference to 5% initially (see (2) 13 table A2.1), shelf life was rather short, deteriorating to 24% after 3 weeks (see (2) 13 table A2.2). This was probably due to the Br_2 desorbing from the carbon cloth with time, as evidenced by the slightly negative baselines, indicating Br_2 reduction.

No further work was done on ethene cross interference.

CHAPTER 5 - CONCLUSIONS AND FURTHER DEVELOPMENT

The main thrust of this thesis has been concerned with the incipient combustion detector, the objectives for which were set out in (1) 1.3. In general most of these objectives such as compactness, seal integrity, long life, maintenance free robust operation with freedom from shock, vibration and orientation stability, have been achieved in the 2T sensor design. These sensors have been used widely and successfully in coal mines throughout the world.

Other CO sensors were developed in parallel to cover general environmental monitoring (2E- and 3E-sensors) and flue gas analysis (3F sensors). The performance characteristics of these sensors are compared in (1) Table 11.

Improvements in electronics, both in performance and cost, now mean that three-electrode sensors with their better control are favoured over two-electrode sensors in spite of the latter's intrinsic simplicity.

A number of the innovatory concepts have since been further developed with success. Of particular value have been:

(1) The inboard filter system, which has been used to remove cross interferences from H_2S, SO_2, NO, NO_2, Cl_2, NH_3 and C_2H_4 by chemical reaction/adsorption.

(2) The auxiliary electrode concept using transmission of unreacted H_2 from the sensing electrode to null out hydrogen interference; it is not possible to remove H_2 cross interference by inboard filtration.

(3) The auxiliary electrode principle can also be used to offset baselines; this is especially beneficial where biased sensors generate large baselines.

The basic design concepts described are capable of being applied directly to the detection and measurement of many other gases and this in fact has been done with sensors being produced for H_2S, SO_2, NO, NO_2, H_2, Cl_2, HCN, HCl and PH_3(see (1) App. 2).

Application	Trace	Environmental Monitoring		Flue Gas
CO Sensor Type	**2T**	**2E**	**3E**	**3F**
Linear Measuring	0-200	0-500	> 1000	> 4000
Nominal sensitivity (μA/ppm)	0.1	0.1	0.1	0.03
Baseline, pure air, 20°C (ppm CO equivalent)	+0.5 to +2.0	+1 to +3	-1 to +3	-3 to +10
90% response time @ 20°C, 50Ω load (s)	23 to 35	20 to 30	25 to 35	25 to 35
H_2 cross sensitivity without any preconditioning (CO equivalent %)	10 to 30	10 to 20	15 to 25	20 to 40
Intrinsic temperature coefficient (% signal @ 20°C per °C change)	0.9 to 1.0	0.7	0.7	0.5

Table 11 Comparison of Performance Characteristics of CTL CO Sensors
[After CTL Report No. 82/09/007, (2) 13 p.78]

APPENDIX 1

COMPANY PROFILE

City Technology Limited

Company History

City Technology Limited is the brainchild of Dr A D S Tantram who established the company with three other scientists, Mr J R Finbow, Dr B S Hobbs and Mr R Chan-Henry, in 1977. The company, which is still owned today by London's City University, was formed to apply laboratory technology to the development of a commercially viable oxygen sensor.

The CiTiceL® oxygen sensor was designed initially for personal safety monitoring. Increasing awareness of the importance of safety, spurred on by the Health and Safety at Work Act (1974) had produced a pressing demand for gas sensors. The sensors had to be small, robust, reliable, stable and inexpensive in order to meet the requirements for widespread use in the working environment, often under difficult conditions such as in mines and sewers. One of the most important requirements was for an Oxygen deficiency monitoring sensor.

The CiTiceLs rapidly became established in the safety field and the range was extended to cover a variety of toxic gases. This now includes sensors for the measurement of oxygen (O_2), carbon monoxide (CO), hydrogen sulphide (H_2S), sulphur dioxide (SO_2), nitric oxide (NO), nitrogen dioxide (NO_2), chlorine (Cl_2), hydrogen (H_2), hydrogen cyanide (HCN), hydrogen chloride (HCl), and ammonia (NH_3); in addition, **CITIpeL®** catalytic sensors/pellistors are now available for the detection of combustible gases. In most cases there are several models for each gas to cover different concentration ranges and application requirements. This technical prowess has been rewarded by two of the prestigious Queen's Awards for Technological Achievement; in 1982 for the Oxygen **CITIceL®** and in 1985 for the toxic **CITIceL®** range.

As a measure of City Technology's success, it is worth noting that in 1977 the UK was almost totally dependent on imports for the supply of electrochemical gas sensor equipment. However, by 1984 following entry into the market, City Technology was supplying some 80% of the UK market. Continued international growth means that today City Technology exports 80% of **CITIceL®** production and holds a 1992 Queen's Award for Export Achievement.

Market Information

Gas sensors are mainly concerned with:

a) Environmental monitoring e.g. is it safe to breath?
b) Accident prevention e.g: incipient fire detection, and inerting of tankers.
c) Combustion efficiency

CITIceLs are sold into three main markets:-

i) Combustion Emissions (45% Revenue)

The monitoring of emissions from chimneys, boilers and automotive engines to ensure they meet national legislation e.g. TÜV in Germany and UK MOT requirements.

Also, further to the oil crisis in the 70s, **CITIceLs** are employed to analyse the efficiency of combustion processes i.e. to ensure that fuel consumption is minimised.

ii) Portable Monitors (45% Revenue)

CITIceLs are used in small single or multiple gas detectors designed for individuals to use in their working environment e.g. miners operating underground, workmen entering confined spaces, etc.

iii) Ambient Monitoring (10% Revenue)

The detection of toxic and combustible gases and oxygen deficiency in both industrial and domestic environments. Remote heads are fixed at various points in industrial plants and public places such as underground car parks. Readings are then transmitted back to a central point where measurements can be analysed and appropriate action taken e.g. venting the underground car park.

CITIceLs are supplied worldwide, with exports contributing approximately 80% to sales. The three major geographical markets for **CITIceLs** are:-

North America	40%
Germany	30%
UK	20%

The remaining 10% of sales are exported to: South Africa, Italy, Spain, France, Denmark, Belgium, Switzerland, Netherlands, Austria, Norway, Sweden, Finland, Eastern Europe, Australia, New Zealand, India, Israel, Turkey and the Far East.

This export success was recognised with Queen's Awards for Export Achievement in 1988 and 1992.

The Future

The future looks busy for City Technology.

The increasing concern for the environment and both proposed and pending legislation will challenge our R & D capabilities in anticipating future sensor designs. Consequently, this department is undergoing extensive expansion and investment.

The single European Market and our continued efforts in South Africa, Eastern Europe, the Far East and Pacific Rim offer City Technology the opportunity of extending sales to the whole world. This will be backed by continued investment in both the production facilities and our other support departments.

- City Technology designs and manufactures gas sensors. These are supplied on an OEM (original equipment manufacturer) basis to leading instrument companies who incorporate them in a wide range of advanced gas detection instruments.

- City Technology has its own R & D facility enabling new sensors to be developed and improvements made to existing **CITIceLs**, as market requirements change. An example of this was City Technology's launch of the A3ME/F Carbon Monoxide **CITIceL®** to meet the immediate demand for specific sensors required in emission monitoring, brought about by legislation enacted in Germany.

- Our marketing success is a result of frequent customer visits, overseas exhibitions, freely available technical literature and the provision of a constantly manned after-sales and technical support service. We have exhibited in USA, Germany, France, Italy, Korea, and have participated in a very successful DTI sponsored trade mission to the Far East.

- City Technology has established a rigorous Quality Assurance System and is approved to British Standards BS 5750, Pt 11, International Standards ISO 9002, and European Standards EN 29002.

- City Technology has exhibited in Chicago, Detroit, London, Los Angeles, Milan, New York, Nürnburg, Paris and Seoul in its world wide promotion of **CITIceLs**, and will be exhibiting in Nürnburg and Philadelphia in October 1992.

City Technology consistently exhibits annual growth of between 30-40%. As a result of this in 1990 it was necessary for City Technology to relocate from its London base to a custom made building in Portsmouth, Hampshire. The 66,000 ft^2 City Technology Centre has been designed to streamline the Company's entire operation so maximising production and sales efficiency.

Officially opened in February 1992 by the Right Honourable John Major MP, Prime Minister, the City Technology Centre provides an excellent base from which to respond to the challenges of the years ahead.

TYPICAL APPLICATIONS

	O_2	CO	H_2S	SO_2	NO	NO_2	Cl_2	H_2	HCN	HCl	NH_3	CH_4
Air Quality		●										
Auto Exhausts	●				●							
Battery Rooms								●				
Beer Cellars	●											
Breath Analysis		●						●				
Chemical Industry			●	●		●	●	●	●	●	●	●
Chicken Farms											●	
Chimney Stacks	●	●		●	●	●				●	●	●
Construction Sites	●		●									
Domestic Boilers	●	●		●	●	●						●
Fertiliser Plants											●	
Fire Detection		●										
Food Processing	●			●							●	
Fumigation									●			
Garage Workshops		●										●
Grain Storage	●					●						
Greenhouses	●	●										
Incubators	●											
Inerting	●											
Mining	●	●			●	●						●
Nuclear Industry	●							●				
Oil Rigs	●		●					●				●
Paper Mills				●			●					
PCB Manufacture				●						●		
Refrigeration											●	
Semiconductor Industry								●	●	●	●	●
Sewage Industry	●		●									●
Steel Works		●		●								●
Swimming Pools				●			●					
Tunnels		●	●									●
Underground Car Parks		●										
Water Treatment				●			●					

Gas Type	O_2	CO	H_2S	SO_2	NO	NO_2	Cl_2	H_2	HCN	HCl	NH_3	Grand Total To June 1992
Sensors Made	729,442	306,550	130,215	23,713	21,514	7,475	14,178	3,958	2,044	962	512	1,240,563
Launch Date	1977	1982	1983	1984	1985	1985	1985	1985	1987	1988	1991	1992
Queen's Awards		Technological Achievement			Technological Achievement					Export Achievement		Export Achievement

Sensors manufactured at City Technology Ltd to June 1992, showing new product launch dates and Queen's Award Achievements. The first Queen's Award for Technological achievement was for the oxygen sensor design and the second was for the toxic gas sensor design.

APPENDIX 2

HISTORIC DEVELOPMENT OF SENSORS AT CITY TECHNOLOGY

HISTORIC DEVELOPMENT OF SENSORS AT CITY TECHNOLOGY LIMITED

Essentially, City Technology make sensors of two generic types, namely alkaline electrolyte and acid-electrolyte sensors. The former is housed in the Ever Ready RR size metal crimp can and the latter makes use of injection-moulded polycarbonate.

(1) Oxygen Sensors

The Wolfson Unit for Electrochemical Technology (WUET) was set up in 1971 at City University to undertake Contract Research and Development work. One of the important functions of WUET was to bridge the gap between academia and industry and to translate academic ideas into useful products.

Research and development into gas sensor technology was initiated by an early contract with the Ministry of Defence (MOD) to develop an Air Crew Hypoxia sensor. When initial feasibility was established, the National Coal Board (NCB) sponsored work on the translation of the laboratory model into a practical, working sensor using battery crimp technology. Increasing awareness of the importance of safety, spurred on by the Health & Safety at Work Act (1975), produced a growing and pressing demand for gas sensors, so that in 1977 City University set up its own commercial company, City Technology Ltd, to manufacture oxygen sensors for industry. This has been a tremendous success, culminating in the Queen's Award for Technological Achievement in 1982, for the design of the oxygen sensor. A total of 729,442 oxygen sensors have been manufactured up to June 1992.

(2) Development of Carbon Monoxide Sensors

In 1979, on the strength of the success of the oxygen sensor, NCB jointly funded on an equal basis with CTL, work to develop a 2-electrode CO sensor for incipient combustion detection in mines. The innovative features of the oxygen sensor were retained, namely a capillary limiting barrier and very active fuel cell electrodes, but acid-resistant hardware had to be developed.

This design proved to be so versatile that modification to 3-electrode design extended its application to cover general ambient air monitoring and flue gas analysis.

The ability to reliably measure CO and O_2 with simple, portable and cheap instruments opened up a very large market in flue gas analysis. Since its launch in 1982, more than 306,550 CO sensors have been manufactured.

(3) Other Toxic Gas Sensors

By using different combinations of catalyst, operating potential and electrolyte, the basic CO sensor hardware was adapted to measure H_2S, SO_2, NO, NO_2, Cl_2, H_2, HCN, HCl and PH_3. Of these sensors, H_2S (130,215) and SO_2 (23,713) are the longest running, although chlorine recently introduced also shows tremendous potential.

City Technology was awarded a second Queen's Award for Technological Achievement in 1985, for the design of the Toxic Gas sensor range. The company has also won two Queen's Awards for Export Achievement in 1988 and 1992.

In 1987 Frost and Sullivan [118] acknowledged City Technology as 'World Leaders in Gas Sensor Manufacture'.

APPENDIX 3

LIST OF PUBLICATIONS

OXYGEN SENSORS

MOD REPORTS

1. HYPOXIA - Phase 1 (July 1973)

Key Words : Survey - electrolytes and membranes

2. AIRCREW HYPOXIA WARNING SYSTEM - Phase 2 (June 1974)

MOD Contract No. K/A676/618
ERA Project No. 5047
TCU Project No. 03/91/009
Report to : MOD

Key Words : Breadboard sensor - potassium carbonate electrolyte, fuel cell cathode, Pb anode, capillary barrier.

3. AIRCREW HYPOXIA WARNING SYSTEM - Phase 2 Extension (July 1975)

Tantram ADST
Finbow JR
Palmer AG

MOD Contract No. K/A676/618
ERA Project No. 5047
TCU Project No. 03/91/09
Report to : Dr ED Wall (MOD)

Key Words : Nuclepore porous membranes, PTFE tape Cd-plated Ni mesh, cylindrical sensors, volume changes and gas bubbles.

4. OXYGEN DETECTOR FOR USE IN COAL MINES - Phase 1 (May 1976)

Tantram ADST
Finbow JR
Hobbs BS
Chan-Henry R

NCB Project No. 7B 1350/09/22
ERA Project No. 44-01-2977
TCU Project No. 03195/18
Report to : Dr ED Wall (MOD)

Key Words : Production prototype, capillary barrier, sodium hydroxide electrolyte, porous Pb anode, low temperature and pressure coefficient.

5. OXYGEN DETECTOR FOR USE IN COAL MINES (Sept 1977)

Tantram ADS
Finbow JR
Chan-Henry R
Hobbs BS

CTL Report No. 77-13-010
NCB Project No. YB 1350/09/22
TCU Project No. 03/95/13
Report to : Mr LR Cooper (NCB)

Key Words : Prototype → production sensor, field trials (OTOX 80) 4 M KĀc, Pb wool, temperature coefficient follows $T^{½}$ law.

6. OXYGEN SENSOR FOR USE IN COAL MINES (July 1978)

Tantram ADS
Chan-Henry R
Hobbs BS
Finbow JR

CTL Report No. 78/02/001
NCB Contract No. YB 1350/09/22
CTL Report No. 94/02/00
Report to : Mr LR Cooper (NCB)

Key Words : Mesh-less FS6 electrode, fast response time, pressure sensitivity, exponential response to O_2, discovery of Knudsen Diffusion Barrier (KDB)

7. OXYGEN SENSOR FOR USE IN COAL MINES (Aug 1979)

Partial Pressure Sensor with Knudsen Diffusion Barrier

Tantram ADS
Chan-Henry R

CTL Report No. 79/06/001
NCB Contract No. YB 1350/09/22
CTL Report No. 94.06.00
Report to : Mr LR Cooper (NCB)

Key Words : Knudsen diffusion theory, 'Sandwich Tape' barrier, low negative temperature coefficient, linear 0-21% oxygen.

8. OXYGEN SENSOR FOR USE IN COAL MINES

Partial Pressure Sensor with Knudsen Diffusion Barrier - Phase 2 (Sept 1980)

Tantram ADS
Finbow JR
Hobbs BS
(Chan-Henry R)

CTL Report No. 80/06/004
NCB Contract No. YB 1350/09/22
CTL Project No. 94.06.00
Report to : Mr LR Cooper (NCB)

Key Words : Knudsen barrier measures O_2 partial pressure, signal $\propto T^{1/2}$, production sensors characterised O_2 concentration, pressure and long term stability.

9. OXYGEN SENSOR FOR USE IN COAL MINES

Partial Pressure Sensor with Knudsen Diffusion Barrier - Phase 2

Supplementary Report (June 1981)

Tantram ADS
Finbow JR
Hobbs BS
(Chan-Henry R)

CTL Report No. 81/06/005
NCB Contract No. YB 1350/09/22
CTL Project No. 94/06/00
Report to : Mr LR Cooper (NCB)

Key Words : Previous report covered life testing up to 20 weeks; this report covers end of life.

10. CARBON MONOXIDE SENSORS FOR USE IN COAL MINES - Phase 1

(Sept 1979)

Tantram ADS
Chan-Henry R
Hobbs BS

CTL Report No. 79/31/002
NCB Contract No. Y 135007/09/21
CTL Project No. 94/95/31
Report to : Mr L R Cooper (NCB)

Key Words : NCB cell studied, Au/NaOH system active for CO but prone to CO_2 interference. Pt/H_2SO_4 'sandwich' design established.

11. CARBON MONOXIDE SENSORS FOR USE IN COAL MINES - Phase 2

(April 1990)

Tantram ADS
Chan-Henry R
Hobbs BS

CTL Report No. 80/31/003
NCB Contract No. Y135007/09/21
CTL Project No. 94.95.31
Report to : Mr LR Cooper (NCB)

Key Words : Small reservoir, balanced electrolyte ~63% RH, law $\propto_T$, large Ar, wide range of measurement, wide RH range, baseline study, pre-treatment of components.

12. CARBON MONOXIDE SENSORS FOR USE IN COAL MINES - Phase 3

(July 1980) Final Report

Tantram ADS
Chan-Henry R
Hobbs BS

CTL Report No. 81/31/006
NCB Contract No. Y135007/09/21
CTL Project No. 94.95.31
Report to : Mr LR Cooper (NCB)

Key Words : 2-electrode sensors, improving tolerance and minimising hysteresis, 3E sensor, cavity in capillary plate, Si rubber temperature compensation, injection moulding, minimum operating volume established.

13. CARBON MONOXIDE SENSORS FOR USE IN COAL MINES - Phase 4

(Sept 1982)

Tantram ADS
Chan-Henry R
Hobbs BS

CTL Report No. 82/09/007
NCB Contract No. Y135007/09/21
CTL Project No. 94.09.00
Report to : Mr LR Cooper (NCB)

Key Words : '2T' designation, moulded components, vents, hoods and chambers, diffusion collars, split Si rubber tube compensation, in-board filter, water balance.

14. CARBON MONOXIDE SENSORS FOR USE IN COAL MINES - Phase 5

(July 1983)

Tantram ADS
Chan-Henry R
Hobbs BS

CTL Report No. 83/09/008
NCB Contract No. Y135007/09/21
CTL Project No. 94.09.00
Report to : Mr LR Cooper (NCB)

Key Words : In-board filters for SO_2 and CO, water balance calculations, 'residence time' models.

15. CARBON MONOXIDE SENSORS FOR USE IN COAL MINES - Phase 6

First Progress Report (Oct. 1984)

Tantram ADS
Chan-Henry R
Hobbs BS
Gilby JH
Amabilino GG
Chow T

CTL Report No. 84/09/009
NCB Contract No. Y135007/09/21
CTL Project No. J009
Report to : Dr J Wykes (NCB)

Key Words : Improved 2-electrode performance, H_2 and NOX sensor development, auxiliary electrode sensors, double-headed sensors, temperature compensation by Si rubber and thermistors, instrument performance modelling, 3E sensors, A2E Undergraduate Project (TC).

16. CARBON MONOXIDE SENSORS FOR USE IN COAL MINES - Phase 6

Second Progress Report Volume 1 (Nov 1985) Nitrogen Oxides Sensors

Tantram ADS
Chan-Henry R
Hobbs BS
Gilby JH
Amabilino GG
Chow T

CTL Report No. 85/09/010
NCB Contract No. Y135007/09/21
CTL Project No. J009
Report to : Dr J Wykes (NCB)

Key Words : 3NF sensor at 200mV bias, range 1000ppm NO, 3NT sensor prototype at 5 times 3F sensitivity, prototype NO_2 sensor.

17. CARBON MONOXIDE SENSORS FOR USE IN COAL MINES - Phase 6

Second Progress Report Volume 2 (Jan 1986) Auxiliary Electrode Carbon Monoxide Sensors

Tantram ADS
Chan-Henry R
Hobbs BS
Gilby JH
Stokell N

CTL Report No. 86/09/010
NCB Contract No. Y135007/09/21
CTL Project No. J009
Report to : Dr J Wykes (NCB)

Key Words : Pilot production A2E sensors, H_2 cross-interference and baseline temperature coefficients improved, A2E circuits, A3E sensor prototypes.

18. CARBON MONOXIDE SENSORS FOR USE IN COAL MINES - Phase 7

(Feb 1987) NOX and A2E sensors

Tantram ADS
Chan-Henry R
Hobbs BS
Gilby JH
Smith GN
Chow T

CTL Report No. 87/09/011
NCB Contract No. Y135007/09/21
CTL Project No. J009
Report to : Dr J Wykes (BCC)

Key Words : 3NF flue gas sensor (200mV bias) characterised, 3NT trace NO sensor prototypes (300mV bias), SO_2 enhancement of NO signal studied, silver oxide used to remove SO_2 cross-interference, 3ND (NO_2) sensor characterised. Further development of A2E and A2E/F (split filter) production prototype to final production stage.

19. CARBON MONOXIDE SENSORS FOR USE IN COAL MINES - Phase 7

(June 1987) Supplementary Investigations of A2E Carbon Monoxide Sensors

Tantram ADS
Chan-Henry R
Hobbs BS

CTL Report No. 87/09/012
NCB Contract No. Y135007/09/21
CTL Project No. J009
Report to : Dr J Wykes (BCC)

Key Words : Study of separator diameter/H_2 null, long-term null stability, circuit design for production prototypes have hydrogen null gains set between 1 and 2.

20. CARBON MONOXIDE SENSORS FOR USE IN COAL MINES - Phase 8

(Sept 1988) Part 1 : Auxiliary, 2-Electrode, Carbon Monoxide Sensors

Tantram ADS
Chan-Henry R
Hobbs BS
Hon CSS
Smith GN

CTL Report No. 88/09/012
NCB Contract No. Y135007/09/21
CTL Project No. C009
Report to : Dr J Wykes (BCC)

Key Words : Final design A2E, A2E/F characterised in batches of 10 over 1 year, filter improves performance, baseline, tolerance and hydrogen cross-sensitivity better than 2E.

21. CARBON MONOXIDE SENSORS FOR USE IN COAL MINES - Phase 8 (Sept 1988) Part 2 : Nitric Oxide Sensors

Chan-Henry R
Hobbs BS
Smith GN
Hon CSS
Latif F
Barton S

CTL Report No. 88/09/013
NCB Contract No. Y135007/09/21
CTL Project No. C009
Report to : Dr J Wykes (BCC)

Key Words : 10x3NT, 10xA3NT NO sensors (300mV bias) characterised over 1 year. Auxiliary electrode analogues much better on start-up time and baseline temperature stability, higher sensitivity of 3NT and A3NT have much lower filter capacity than 3NF sensors.

22. CARBON MONOXIDE SENSORS FOR USE IN COAL MINES - Phase 8 (Sept 1988) Part 3 : Nitrogen Dioxide Sensors

Hobbs BS
Chan-Henry R
Smith GN
Latif F

CTL Report No. 88/09/014
NCB Contract No. Y135007/09/21
CTL Project No. C009
Report to : Dr J Wykes (BCC)

Key Words : 3NDH (NO_2) has $ 1 μA/ppm, better baseline and resolution than 3ND, stagnant layer effect and moisture transient studied, 3NDH can measure 1000ppm NO_2 (diesel exhaust).

23. Tantram ADS and Chan-Henry RY (1985) Oxygen Sensors with Knudsen Diffusion Barrier. Paper presented at **Occupational Health and Safety Conference**, London, September 1985.

24. Hobbs BS, Tantram ADS and Chan-Henry RY (1991) Liquid Electrolyte Fuel Cells. In : **Techniques and Mechanisms In Gas Sensing**, EDs. by PT Moseley, JOW Norris and DE Williams. (Adam Hilger : New York).

APPENDIX 4

PORTFOLIO OF PATENTS

City Technology Limited, PATENT PORTFOLIO

TITLE (Informal Title)	Priority No./Date	Applcn Date	Publication Dates (Applcn.)	(Patent)	Patent No.	Status	Expiry Date
Gas Sensor (Capillary Barrier) (GJE)**	76/9843 11/MAR/76	2/MAR/77		9/JUL/80	GB 1,571,282	Granted	2/MAR*/97
		8/MAR/77			DE 2,709,903	Draeger objection	8/MAR/95
				2/JAN/79	US 4,132,616	Granted	2/JAN/96
					HK 717/85	Granted	
		11/MAR/77	4/NOV/77	4/DEC/86	JP 1,387,110	Granted	11/MAR/97
Diffusion barrier Gas Sensor (Knudsen Barrier) (GJE)**	79/17237 17/MAY/79	6/MAY/80	31/DEC/80	30/MAR/83	GB 2,049,952	Granted	6/MAY/00
				13/APR/82	US 4,324,632	Granted	13/APR/99
Gas Sensor (CO_2) (GJE)**	80/14272 30/APR/80	14/APR/81	11/NOV/81	7/MAR/84	GB 2,075,197	Granted	14/APR/01
				2/OCT/84	US 4,474,648	Granted	2/OCT/01

** Note : subject to licence of right from 11/MAR/93 in GB*

** GJE - Gill, Jennings & Every IW - Ian Wishart

TITLE (Informal Title)	Priority No./Date	Applcn Date	Publication Dates (Applcn.)	(Patent)	Patent No.	Status	Expiry Date
Gas Sensor (Inboard Gas Filter) (GJE)	82/15426 26/MAY/82 EU			6/JAN/87	US 4,633,704	Granted	6/JAN/04
Gas Sensor (Auxiliary Electrode Transmission) (GJE)	83/13846	16/MAY/84	28/NOV/84		EP 126 623	(Designated GB,DE,FR) 'B1' spec. published Draeger objection)	16/MAY/04
				6/MAY/86	US 4,587,003	Granted	6/MAY/03
Caliban (IW)	86/10586 26/AUG/86	26/AUG/87	9/MAR/88	6/JUN/90	GB 2,194,639	Granted	26/AUG/07
	86/26941 11/NOV/86	21/AUG/87	16/MAR/88		EP 260,005	(Designated DE,FR,IT, CH,ES,NL,LI) search A2 stage	
				16/MAY/89	US 4,829,809	Granted	16/MAY/06
				23/JAN/90	CA 1,264,808	Granted	23/JAN/07
					JP	Allowed Oct. 89	
					HK	To decide within 3 yrs of 6/JUN/90	

TITLE (Informal Title)	Priority No./Date	Applcn Date	Publication Dates (Applcn.)	(Patent)	Patent No.	Status	Expiry Date
Diffusibility Measurement (IW)	86/26430 5/NOV/86		11/MAY/88		GB 2,197,080	Abandoned, replaced by EP 266,955	
		28/NOV/87	11/MAY/88		EP 266,955	(Designated GB,DE,FR) Examination, B1 specn. due.	28/NOV/07
				28/MAR/89	US 4,815,316	Granted	28/MAR/06
Flammable Gas Detection (IW)	89/28177.8 13/DEC/89	5/DEC/90	19/JUN/91		GB filed EP 0432962 A2 JP 2-415713	Filed 13/12/89 (Designated GB,DE,FR,IT) Filed 12/12/90	5/DEC/10
				10/DEC/91	US 5,070,721	Filed 26/11/90 (Ser.No.617,596)	10/DEC/08
					CA	Filed 30/11/90 (Applcn. 2,031,325)	

Paid up licence from British Coal.

Sandwich Wick (Toxic Design) (GJE)	3/FEB/81 81/3258	29/JAN/82	8/SEP/92	27/SEP/83	GB 2,094,005 US 4,406,770	Granted	29/JAN/02 27/SEP/00
		2/FEB/82			DE 3,203,362		2/FEB/02
		2/FEB/82			FR 2,499,246		2/FEB/02
					JP	Applcn No. 57-15016	

TITLE (Informal Title)	Priority No./Date	Applcn Date	Publication Dates (Applcn.)	(Patent)	Patent No.	Status	Expiry Date
Gas Diffusion Control Assembly (CPO) (GJE)	12/NOV/90 9024521.8					Filed GB 12/11/90	
Gas Diffusion Control Assembly (CPO) (GJE)	27/MAR/91 9106531.8					Filed GB 27/3/91	
f Gas Diffusion Control Assembly	Filed 29/OCT/91		20/MAY/92 (0486179)		EP Applcn. 91309963.6 US Applcn. 783625 JP Applcn. P6474	Designated GB,DE,FR,IT Filed 24/OCT/91 Filed 12/NOV/91	
Ammonia Sensor (GJE)	24/JAN/91 9101643.6		29/JUL/92 (0496527)		EP Applcn. 92300364.4 US Applcn. 824510 JP Applcn. P6528	Filed GB 24/1/91 Filed EU 16/1/92 Filed US 23/JAN/92	

City Technology Limited, LIST OF WITHDRAWN, ASSIGNED, ETC. PATENTS

TITLE (Informal Title)	Patent Nos.	Applcn. Date	Priority No./Date	Publication (Application)	Publication (Patent)	Status
Electrochemical Gas Sensor (Wicked Sandwich Construction) (GJE)	GB 2,094,005 US 4,406,770 FR 2,499.246 DE 3,203,362 JP 147,04882	29/JAN/82 3/FEB/81 2/FEB/82 2/FEB/82	81/03258	8/SEP/82	27/SEP/83	All rights assigned to British Coal. GB Expiry 29/JAN/02
Gas Sensor (Inboard Gas Filter) (GJE)	EP 95 277	82/15426 26/MAY/82				
Gas Sensor (Subtractive Principle) (GJE)	EP 127 387 US 611 832	83/13846 19/MAY/83				
Caliban	ZA 87/05891					

APPENDIX 5

CONVERSION TO SI UNITS

THE INTERNATIONAL SYSTEM OF UNITS (SI)

The International System of Units (SI)[1] comprises the *SI Units* and the *SI Prefixes.*

(119)
The SI Units are of three kinds: *base, derived,* and *supplementary.* There is one and only one SI Unit for each physical quantity. The SI Units all belong to a single coherent system.

The SI Prefixes are used with the help of four simple rules to form decimal multiples and decimal fractions of the SI Units. The decimal multiples and fractions so formed do not in general belong to a coherent system of units but are nevertheless part of the International System of Units or SI.

A) The SI base Units

The names and symbols of the SI base Units are as follows:

Physical Quantity	Name of SI Unit	Symbol for SI Unit
length	metre	m
mass	kilogramme	kg
time	second	s
electric current	ampere	A
thermodynamic temperature	kelvin	K
amount of substance	mole	mol
luminous intensity	candela	cd

The orthography of the *symbols* for the units is international, but the spelling of the *names* of the units depends on the language within which they are used. The spelling given above is the authorised English-language version.

---

[1] The cipher SI is used in all languages to denote what, in the English language, is called the International System of Units. It is written SI and not 'S.I.'

B) **The SI derived Units**

The Si Units for derived physical quantities are those coherently derived from the SI base Units by multiplication and division.

Some of the SI derived Units have special names and symbols as follows:

Physical Quantity	**Name of SI Unit**	**Symbol for**	**Definition of SI Unit**
frequency	hertz	Hz	s^{-1}
energy	joule	J	$kg\ m^2\ s^{-2}$
force	newton	N	$kg\ m\ s^{-2} = J\ m^{-1}$
power	watt	W	$kg\ m^2\ s^{-3} = J\ s^{-1}$
pressure	pascal	Pa	$kg\ m^{-1}\ s^{-2} = N\ m^{-2} = J\ m^{-3}$
electric charge	coulomb	C	$A\ s$
electric potential difference	volt	V	$kg\ m^2\ s^{-3}\ A^{-1} = J\ A^{-1}\ s^{-1}$
electric resistance	ohm	Ω	$kg\ m^2\ s^{-3}\ A^{-2} = V\ A^{-1}\ S^{-1}$
electric conductance	siemens	S	$kg^{-1}\ m^{-2}\ s^3\ A^2 = \Omega^{-1}$
electric capacitance	farad	F	$A^2\ s^4\ kg^{-1}\ m^{-2} = A\ s\ V^{-1}$
magnetic flux	weber	Wb	$kg\ m^2\ m^2\ s^{-2}\ A^{-1} = V\ s$
inductance	henry	H	$kg\ m^2\ s^{-2}\ A^{-2} = V\ A^{-1}\ s$
magnetic flux density (magnetic induction)	tesla	T	$kg\ s^{-2}\ A^{-1} = V\ s\ m^{-2}$

It will be noted that none of the special names and symbols listed above relates to any physical quantity involving either of the dimensionally independent quantities, thermodynamic temperature or amount of substance. In spite of general reluctance to extend the list, there is a strong case for special SI names and symbols at least for some of the following:

Physical Quantity	**Name of SI Unit**	**Symbol for**	**Definition of SI Unit**
molar energy	?	?	$kg\ m^2\ s^{-2}\ mol^{-1} = J\ mol^{-1}$
molar heat capacity molar entropy gas constant	?	?	$kg\ m^2\ s^{-2}\ K^{-1}\ mol^{-1} = J\ K^{-1}\ mol^{-1}$
concentration	?	?	$mol\ m^{-3}$
molality	?	?	$mol\ kg^{-1}$

Some illustrative examples of SI derived Units formed from the SI base Units, and where relevant from the SI derived Units having special names and symbols, are given below.

Physical Quantity	**Name of SI Unit**	**Symbol for SI Unit**
wavenumber	reciprocal metre	m^{-1}
area	square metre	m^2
volume	cubic metre	m^3
speed	metre per second	$m\ s^{-1}$
acceleration	metre per second squared	$m\ s^{-2}$
density (mass density)	kilogramme per cubic metre	$kg\ m^{-3}$
dynamic viscosity	pascal second	$Pa\ s = N\ s\ m^{-2} = kg\ m^{-1} s^{-1}$
kinematic viscosity, diffusion coefficient	square metre per second	$m^2\ s^{-1}$
surface tension	pascal metre	$Pa\ m = N\ m^{-1} = kg\ s^{-2}$
electric field strength	volt per metre	$V\ m^{-1} = N\ C^{-1} = kg\ m\ s^{-3}\ A^{-1}$
magnetic field strength	ampere per metre	$A\ m^{-1}$
electric conductivity	siemens per metre	$S\ m^{-1} = kg^{-1}\ m^{-3}\ s^3\ A^2$
dipole moment	coulomb metre	$C\ m = A\ s\ m$
magnetic moment	ampere square metre	$A\ m^2$
thermal conductivity	watt per metre kelvin	$W\ m^{-1}\ K^{-1} = kg\ m\ s^{-3}\ K^{-1}$
heat capacity, entropy	joule per kelvin	$J\ K^{-1} = kg\ m^2\ s^{-2}\ K^{-1}$
specific heat capacity, specific entropy	joule per kilogramme kelvin	$J\ kg^{-1}\ K^{-1} = m^2\ s^{-2}\ K^{-1}$
molar heat capacity, molar entropy, gas constant	joule per kelvin mole	$J\ K^{-1}\ mol^{-1} = kg\ m^2\ s^{-2}\ K^{-1}\ mol^{-1}$
concentration	mole per cubic metre	$mol\ m^{-3}$
molality	mole per kilogramme	$mol\ kg^{-1}$

C) The SI prefixes

The SI Prefixes and their symbols are as follow:

Fraction	SI Prefix	Symbol	Multiple	SI Prefix	Symbol
10^{-1}	deci	d	10	deca	da
10^{-2}	centi	c	10^{2}	hecto	h
10^{-3}	milli	m	10^{3}	kilo	k
10^{-6}	micro	μ	10^{6}	mega	M
10^{-9}	nano	n	10^{9}	giga	G
10^{-12}	pico	p	10^{12}	tera	T
10^{-15}	femto	f			
10^{-18}	atto	a			

D) Conversion factors to SI Units for Unit Quantities used in CTL Reports

Physical Quantity	Unit Quantities used in CTL Reports	Symbol for SI Units	Equivalent
length	A°	m	100 pm
	μ		1μm
	mm		1mm
	cm		10mm
	m		1m
mass	mg	kg	1mg
	g		1g
	Kg		1kg
time	second (sec)	s	1s
	minute (min)		60s
	hour (hr)		3.6ks
electric current	nA	A	1nA
	μA		1μA
	mA		1mA
electric charge	μC	C	1μC
thermodynamic temperature	°C	K	274.16K
amount of substance	mol	mol	1 mol
concentration	mols cm^{-3}	mol m^{-3}	1Mmolm^{-3}
	ppm	(ppm)*	(1 ppm)
energy of activation	kcal mol^{-1}	J mol^{-1}	4.1868kJmol^{-1}
diffusion coefficient	cm^2 s^{-1}	m^2 s^{-1}	100μm^2 s^{-1}
pressure	cm H_2O	Pa	98.1Pa
	cm Hg		1.333kPa
	Atm		101.325kPa
	mBar		100Pa
	torr		133.3Pa

* This is a ratio and is therefore dimensionless

APPENDIX 6

HYDROGEN REFERENCE ELECTRODE DEFINITIONS

HYDROGEN REFERENCE ELECTRODE DEFINITIONS

$H_2 \rightarrow 2H^+ + 2e^-$ $\quad E_o = 0 - 0.0591pH - 0.0295 \log P_{H_2}$ (volts)

Standard Hydrogen Electrode (SHE)

This is accepted as the absolute zero of potential at all temperatures[120]. It is defined as the potential of the reversible H_2 electrode in unit activity of H^+ (pH = 0) in equilibrium with H_2 at 1 atmosphere pressure.

It can be considered as the primary reference.

Normal Hydrogen Electrode (NHE)

In practice one will usually be working with electrolytes of pH not equal to zero. What is significant is the potential of the electrode under study relative to the potential of the hydrogen electrode in the same electrolyte. This is the Normal Hydrogen Electrode (NHE).

The NHE is formed by bubbling H_2 over a platinised platinum electrode and is connected to the cell under study via a luggin capillary.

Dynamic Hydrogen Electrode (DHE)

The NHE is somewhat awkward to use in practice, requiring a hydrogen cylinder.

The DHE was developed by Giner[18] to provide a much more convenient reference for experimental purposes. Hydrogen is generated at the reference electrode itself (high surface platinum) by passing a current. Because of the small polarisation that results, the DHE is slightly more negative than NHE by an amount depending on the current used.

In the present work the DHE current was selected when calibrating so that the DHE was -30mV with respect to NHE.

LIST OF REFERENCES

1. Health and Safety Executive (1992)
   Occupational Exposure Limits London : HMSO
   (EH 40/92) 15

2. Matheson (1980)
   Matheson Gas Data Book
   (Secaucus, NJ 07094, Eds. Baker W and Mossman AL)

3. Federal Ministry for the Environment, Nature Conservation and Nuclear Safety (1988)
   Air Pollution Control Manual of Continuous Emission Monitoring - 2nd Revised Edn.
   PO Box 120 692
   D5300 Bonn 1
   Federal Republic of Germany

4. Dalla Betta R and Bynum B (1989) 'A New Combustion Control Sensor'
   In : Sensors April 27

5. Harker JH and Backhurst JR (1981)
   Fuel Energy (Academic Press : New York) 155
   Dept. of Chemical Engineering
   University of Newcastle Upon Tyne
   England

6. Sam G Dukelow (1986)
   The Control of Boilers (ISA Press)

7. Davies CW and James AM (1976)
   A Dictionary of Electrochemistry (The MacMillan Press Ltd : London)
   125-126

8. Hobbs BS, Tantrum ADS and Chan-Henry R (1990) Liquid Electrolyte Fuel Cells. In : Techniques and Mechanisms In Gas Sensing (Adam Hilger : New York, Eds. Moseley PT, Norris JOW and Williams DE)

9. The Penguin Dictionary of Physics
(Lawrence Urlang Assocs. Ltd, Ed. Pitt VH) 149

10. Sawyer DT and Roberts JL (1974)
Experimental Electrochemistry For Chemists
(Wiley : New York) 256

11. Oswin HG and Burton KF (1973) US Patent 3776832

12. Oswin HG and Burton KF (1974) US Patent 3824168

13. Oswin HG and Burton KF (1975) US Patent 3925183

14. Bay HW, Blurton KF, Lieb HC and Oswin HG (1972) Am. Lab. 57

15. Oswin HG and Bay HW (1975) US Patent 3909386

16. Tantram ADS and Tseung ACC (1969) Nature 221 167

17. Giner J and Hunter C (1969) J. Electrochem. Soc. 116 1124

18. Giner J (1964) J. Electrochem Soc. 111 376

19. Blurton KF and Sedlak JM (1974) J. Electrochem. Soc. : Electrochemical Science and Technology 121 1315.

20. Shaw M (1979) Proceedings of the Symposium on the Development and Usage of Personal Monitors for Exposure and Health Effect Studies : EPA-600/9-79-032 (June 1979) 413

21. Gilman S (1964) J. Phys. Chem. 68 70

22. Hoare JP (1968) The Electrochemistry of Oxygen (Interscience : New York) 13

23. Bockrins J O'M and Huq AKMS (1956) Proc. Roy. Soc. (London) A237 277

24. Damjanovic A and Bockris J O'M (1966) Electrochim. Acta 11 376

25. Damjanovic A, Dey A and Bockris J O'M (1966) Electrochim. Acta 11 791

26. Hoar TP (1933) Proc. Roy. Soc. (London) A142 628

27. Hoare JP (1965) J. Electrochem. Soc. 112 602

28. Porbaix M (1965) Atlas of Electrochem. Equilibria (Pergamon Press) 541

29. Bowden FP (1929) Proc. Roy. Soc. (London) A125 446 and A126 107

30. Hoare JP (1963) J. Electrochem. Soc. 110 1019

31. Biachi G and Mussini T (1965) Electrochim. Acta 10 445

32. Watanabe N and Devanathan MAV (1964) J. Electrochem. Soc. 111 615

33. Lingane JJ (1961) J. Electroanal. Chem. 2 296

34. Randles JEB (1948) Trans. Faraday Soc. 44 322

35. Sevcik A (1948) Collection Czech. Chem. Commun. 13 349

36. Vogel J (1962) Progress In Polarography (Interscience : New York, Eds. Zuman P and Kolthoff M) 1 429

37. Randles JEB (1948) Trans. Faraday Soc. 44 327

38. Will FG and Knorr CA (1960) Z. Elektrochem. 64 258

39. Bõld W and Breiter MW (1961) Electrochim. Acta 5 145

40. French WG and Kuwana T (1964) J. Phys. Chem. 68 1279

41. Shumilova NA, Zhutaeva GV, Tarasevich MR and Burshtein R Kh (1965) Zh. Fiz. Khim. 39 1012

42. Vielstich W (1963) Z. Instrumentenk. 71 29

43. Lorenz R (1909) Z. Elektrochem. 15 661

44. Lorenz R and Lauber E (1909) Z. Elektrochem. 15 205

45. Lorenz R and Spielmann PE (1909) Z. Elektrochem. 15 293

46. Lorenz R and Spielmann PE (1909) Z. Elektrochem. 15 349

47. Spielmann PE (1909) Trans. Faraday Soc. 5 88

48. Grube GZ (1910) Z. Elektrochem. 16 621

49. Nagel K and Dietz H (1961) Electrochim. Acta 4 141

50. Latimer WM (1952) Oxidation Potential
(Prentice-Hall : Englewood Cliffs, NJ) (2nd ed.) 39

51. de Bethune AJ and Loud NAS (1964) Standard Aqueous Electrode Potentials and Temperature Coefficients (Clifford A. Hampel : Skokie, IU.)

52. Hoare JP (1962) J. Electrochem. Soc. 109 858

53. Foerster F (1909) Z. Physik. Chem. (Leipzig) 69 236

54. Klemenc A (1939) Z. Physik. Chem. (Leipzig) 185 1

55. Naray-Szabo St V (1927) Z. Elektrochem. 33 15

56. Schock EP (1910) J. Phys. Chem. 14 665

57. Tamman G and Runge F (1926) Z. Anorg. Allgem. Chem. 156 85

58. Anson FC and Lingane JJ (1957) J. Am. Chem. Soc. 79 4901

59. Hickling A (1945) Trans. Faraday Soc. 41 333

60. Laitinen HA and Enke CG (1960) J. Electrochem. Soc. 107 773

61. Mayell JS and Langer SH (1964 and 1966) J. Electrochem. Soc. 111 438 and 113 385

62. Sawyer DT and Interrane LV (1961) J. Electroanal. Chem. 2 310

63. Butler JAV and Armstrong G (1932) Proc. Roy. Soc. (London) A137 604

64. Ershler BV (1947) Discussions Faraday Soc. 1 269

65. Frumkin AN and Slygin A (1936) Acta Physicochim. URSS 5 819

66. Giner H (1959) Z. Elektrochem. 63 386

67. Rao MLB, Damjanovic A and Bockris J O'M (1963) J. Phys. Chem. 67 2508

68. Schuldiner S and Warner TB (1965) J. Electrochem. Soc. 112 212

69. Vetter KJ and Berndt D (1958) Z. Elektrochem. 62 378

70. Damjanovic AM, Rao MLB and Genshaw M (1962) ASTIA Rept. No. AD 405675

71. Gilman S (1964) Electrochimica Acta 9 1025

72. Niedrach LW, McKee DW, Paynter J and Danzig IF (1967) Electrochemical Technology 5 318

73. McKee DW, Paynter J and Danzig IF (1967) Electrochemical Technology 5 419

74. Niedrach LW and McKee DW (1967) 21st Annual Proceedings Power Sources Conference (May 16-18)

75. Bockris J O'M and Srinivasan S (1969) Fuel Cells; Their Electrochemistry (McGraw Hill : New York)

76. Vielstick W (1970) Fuel Cells (Interscience : New York)

77. Gilman S (1962) J. Phys. Chem. 66 2657

78. Gilman S (1963) J. Phys. Chem. 67 78

79. Gilman S (1963) J. Phys. Chem. 67 1898

80. Warner TB and Schuldiner S (1964) J. Electrochem. Soc. 111 992

81. Brummer SB and Ford IJ (1965) J. Phys. Chem. 69 1355

82. Brummer SB (1965) J. Phys. Chem. 69 1363

83. Stonehart P (1966) Proc. Fifth Intern. Symp. on Non-Mechanical Power Sources (Brighton) 509

84. Stonehart P (1967) Electrochim. Acta 12 1185

85. Stonehart P (1973) Electrochim. Acta 18 63

86. Hamann CH (1971) Ber. Bunsenges. Phys. Chem. 75 542

87. Hamann CH and Vielstick W (1971) Ber. Bunsenges. Phys. Chem. 75 918

88. Brummer KDN (1967) Journal of Catalysis 9 207

89. Brett J, Kinoshita K, Routsis K and Stonehart P (1973) Journal of Catalysis 29 160

90. Blurton KF and Bay HW (1974) Intern. Lab. 5 60

91. Bergman I and Windle DA (1972) Ann. Occup. Hyg. 15 329

92. Bergman I, Coleman JE and Evans D (1975) Chromatographia 8 581

93. Bergman I (1974) Proc. Inst. Electron. Radio Engs. Conf. on Environmental Sensors 29 67

94. Holleck GL, Bradspies JL, Brummer SB and Nelson LL (1973) Report NAS 8129031

95. McCallum C and Pletcher D (1976) J. Electroanal. Chem. 70 277

96. Gibbs TK, McCallum C and Pletcher D (1977) Electrochimica Acta 22 525

97. Angerstein-Kozlowska H, Conway BE and Sharp WBA (1973) J. Electroanal. Chem 43 9

98. Conway BE and Gottesfield S (1973) J. Chem. Soc. Faraday Trans. 1 1091

99. Tilak BV, Conway BE and Angerstein-Kozlowska H (1973) J. Electroanal. Chem. 48 1

100. Shibata K (1972) Electrochem. Acta 17 395

101. Mancy KH and Okun DA (1962) Anal. Chem. 32 108

102. Briggs R and Viney M (1964) J. Sci. Instr. 41 78

102. Mancy KH et al (1962) J. Electroanal. Chem. 4 65

103. Mancy KH, Okun DA and Reilly N (1962) J. Electroanal. Chem. 4 65

104. Tantram ADS, Kent MJ and Palmer AG (1977) UK Patent GB 1,571,282

105. Foust AS (1960) Principles of Unit Operations (Wiley : New York)

106. Niedrach LW and Alford HR (1965) J. Electrochem. Soc. 112 117

107. Haldeman RC, Barber WP, Langer SH and Barber WH (1965) Fuel Cell Systems. In : Advances in Chemistry Series (American Chemical Society : Washington, Ed. Gould RF 47 106

108. Giner J (1965) Report to US Army Research and Development Labs.

109. Giner J (1967) Proc. Ann. Power Sources Conf. 21 10

110. Giner J, Hunter C and Turkman K (1969) J. Electrochem. Soc. 116 1693

111. Watanabe M, Tomikawa M and Motoo S (1985) J. Electroanal. Chem. 182 193

112. Pourbaix M (1965) Atlas of Electrochemical Equilibria (Pergamon Press) 452

113. Tantram ADS, Finbow JR, Chan YS and Hobbs BS (1982) UK Patent 2094005

114. Tantram ADS and Chan YS (1984) US Patent 4,633,704

115. Oswin HG and Burton KF (1974) UK Patent GB 1,372,245

116. Blazhennova AN, Krukov GI and Saifi RN (1968) UK Patent GB 1,101,101

117. Tantram ADS and Chan YS (1984) European Patent EP0126623

118. Frost And Sullivan (1987) Industrial Gas Sensor Market In Europe (E878). (Frost And Sullivan Inc.: 106 Fulton St., NY 10038)

119. McGlashan MC (1971) Monographs For Teachers. In: Physicochemical Quantities And Units (2nd Edn.) (Royal Institute Of Chemistry: London)

120. Bevan HL (1970) The Preparation and Characterisation of High Surface-Area Semi-Conducting Oxides for Cathodic Reduction of Oxygen in Alkaline Solutions PhD Thesis (City University, Department of Chemistry)